MODELING AND CHARACTERIZATION OF CELLULAR MOBILE CHANNELS FOR 3-D RADIO PROPAGATION ENVIRONMENTS

by

Syed Junaid Nawaz
PE083006

A thesis submitted to the
Department of Electronic Engineering
in partial fulfillment of the requirements for the degree of
DOCTOR OF PHILOSOPHY IN ELECTRONIC ENGINEERING

Faculty of Engineering
Mohammad Ali Jinnah University
Islamabad

February 2012

Dedicated to my beloved grandparents' memories, parents, and brother.

ACKNOWLEDGMENT

All thanks to almighty Allah, the most gracious and the beneficent, who loves and cares us the most.

I would like to express my most sincere gratitude to my supervisor Dr. Noor M. Khan for his support, encouragement, and guidance through every step of this research. His kind efforts contributed greatly to my knowledge, understanding, and enthusiasm for this research. I have not only learnt from his insight, deep technical knowledge, and practical experience, but also a lot of things from him as a person. It has been a real honor for me to work under his supervision and to attend his lectures and talks.

I owe my deepest appreciation to Dr. Mohammad N. Patwary, reader at Staffordshire University, for his valuable guidance and encouragement. I am very grateful to him for his support in all aspects throughout my stay at Staffordshire University, UK, which I attended under his supervision for ten months to conduct a part of this research. I also thank him for his confidence in my abilities. I would also like to thank Prof. Dr. Hongnian Yu for providing me with opportunities to attend various talks and conferences.

I would like to express my gratitude to my supervisor Dr. Noor M. Khan for suggesting and referring me for the scholarships, which I availed during my studies. I wish to thank Prof. Dr. M. Mansoor Ahmed, executive vice president of Mohammad Ali Jinnah University (MAJU), for providing me the scholarship which I availed during my studies at MAJU, Islamabad. I am very grateful to eLink scholarship program (by EU) for sponsoring my study and stay at Staffordshire University, UK. I especially thank Dr. Nayyer Masood, coordinator and organizer of eLink program Pakistan, for considering me for the scholarship.

I would like to thank Prof. Dr. M. Noman Jafri, Dean of Faculty of Engineering, Federal Urdu University of Arts Science and Technology, Islamabad, for his encouragement and support for my Ph.D. research work.

I would like to thank all of my fellow researchers in the Acme Center for Research in Wireless Communications (ARWiC) for creating such a pleasant working environment. I especially thank Mr. Bilal Hasan Qureshi, my fellow researcher at ARWiC, for the useful discussions with me. I owe my thanks to Mr. Muhammad Riaz, my fellow researcher at ARWiC, for his prompt help in various departmental matters. I also owe my deepest appreciation to my colleagues and friends.

I would like to thank my affectionate parents for their unwavering love, moral support, and encouragement. They always prayed for me in my hard times. I also thank my brother for his moral support to conduct this research and also for all the great times we had growing up together.

ABSTRACT

In order to meet the increasing demands of capacity in land mobile radio cellular communication systems, the use of directional antennas has become an integral part of future communication systems. With purpose to gauge the capabilities of systems with directional antennas, it is essential to have a precise knowledge of angular and temporal representation of the dispersion of multipath waves in 3-D propagation environments. Such representation of propagating waves can only be achieved with the use of spatial channel models. Therefore, this thesis focuses on modeling and characterization of cellular mobile channels for 3-D radio propagation environments.

The research work in this thesis consists of three parts. Part-I aims at the physical modeling of cellular mobile channels in 3-D radio propagation environments. Part-II characterizes the impact of mobility on the Doppler spectrum; while, part-III provides a geometrically based performance analysis of handovers in land mobile radio cellular systems.

The thesis begins with an overview of the basics of spatial channel models in different cellular environments and then proceeds towards a detailed and comprehensive survey of spatial channel models. Further, a generalized 3-D scattering model is proposed for macro-cellular land mobile radio cellular systems with a Mobile Station (MS) located at the center of a 3-D scattering semi-spheroid and a Base Station (BS) employing a directional antenna located outside of the semi-spheroid. The effect of directional antenna is thoroughly observed on spatial and temporal characteristics of the proposed model. Closed-form expressions for joint and marginal Probability Density Functions (PDFs) of Angle of Arrival (AoA) seen at MS and BS in correspondence with azimuth and elevation angles are derived. Furthermore, closed-form expressions for propagation path delays and trivariate joint PDFs of Time of Arrival (ToA) seen at MS and BS in correspondence with azimuth and elevation angles are derived. Moreover, the theoretical results along with observations illustrate the effect of directional antenna on the spatio-temporal statistics of the proposed 3-D spatial model. All the statistics are derived for both uniform and Gaussian scatter densities.

The proposed 3-D scattering model for the case of uniform scatter density, is shown to deduce all previously-proposed 2-D and 3-D models that assume uniform distribution of scatters with directional or omnidirectional antennas, found in literature for macro-cell environment. The theoretical results obtained are compared with some notable 2-D and 3-D scattering models to validate the generalization of the proposed model. Obtained theoretical results (for the case of Gaussian scatter density) for spatial statistics at BS are compared with an empirical set of measured data (found in literature), which also demonstrates the validity of proposed model.

In the second part of thesis, the effect of mobile motion on the statistical characteristics of Doppler spectrum is presented. An analytical model to quantify the effect of directivity of the radiated waves from the BS antenna on the Doppler spectrum in 3-D radio propagation environment is proposed. Closed-form expressions for trivariate PDFs of propagation path distance, power, and Doppler shift are derived. Furthermore, general expressions for joint and marginal PDFs of elevation AoA, power, and Doppler shift are established. The obtained theoretical results along with the observations are presented that illustrate the effect of directivity of the antenna beam-width and the direction of MS's motion on the distribution characteristics of power Doppler spectrum. It is established that for motion of the MS in all directions, the spread in distribution of the Doppler shift observed is reduced significantly due to the use of directional antenna at the BS with a narrow beam directed towards the desired user. It is also observed that, for a sharp azimuthal beam of directional antenna, the multipath components corresponding to the scatterers in elevation plane result in the reduction of Doppler shift with an increase in their vertical distance from MS.

In part-III, an analysis for the impact of various channel parameters on the performance of handover in mobile radio cellular systems is presented. Using the proposed analytical model, a mathematical relation for the handover margin with velocity of MS, direction of mobile motion, and propagation environment is derived on the basis of path loss propagation model. Relationship for the ratio between the radius of coverage area and the length of overlapped region between adjacent cells is derived, which guarantees to satisfy the required handover margin. The impact of velocity and direction of MS's motion on the handover margin is comprehensively analyzed. The impact of propagation environment on the handover margin is also analyzed, where it has been observed that, the handover margin decreases significantly with an increase in the path loss exponent. For dense urban areas with higher propagation path loss exponent, the time margin available to perform the handover is less; therefore, quicker decision of handover is required to be made.

LIST OF PUBLICATIONS

[**J01**] Syed Junaid Nawaz, Bilal Hasan Qureshi, and Noor M. Khan, "A Generalized 3-D Scattering Model for Macrocell Environment with Directional Antenna at BS," IEEE Transactions on Vehicular Technology, vol. 59, no. 7, pp. 3193-3204, May. 2010.

[**J02**] Syed Junaid Nawaz, Noor M. Khan, Mohammad N. Patwary, and Mansour Moniri, "Effect of Directional Antenna on The Doppler Spectrum in 3-D Mobile Radio Propagation Environment," IEEE Transactions on Vehicular Technology, vol. 60, no. 7, pp. 2895 - 2903, Jul. 2011.

[**C01**] Syed Junaid Nawaz, Bilal H. Qureshi, Noor M. Khan, and M. Abdel-Maguid, "Effect of Directional Antenna on the Spatial Characteristics of 3-D Macrocell Environment", in Proc. of IEEE, Int. Conf. on future comp. and commun., vol. 1, May 2010, pp. 552-556.

[**C02**] Syed Junaid Nawaz, Bilal Hasan Qureshi, and Noor M. Khan, "Angle of Arrival Statistics for 3-D Macrocell Environment using Directional Antenna at BS", in Proc. of IEEE, Int. Multitopic Conf., vol. 1, Dec. 2009, pp. 1-5.

[**C03**] Syed Junaid Nawaz, M. N. Patwary, Noor M. Khan, and Hongnian Yu, "3-D Gaussian Scatter Density Propagation Model Employing a Directional Antenna at BS," in Proc. of IEEE, 5th Advanced Satellite Multimedia Systems Conf., vol. 1, Sep. 2010, pp. 395-400.

[**C04**] Saif-Ur-Rehman, Syed Junaid Nawaz, Mohammad N. Patwary, and M. Abdul Muguid, "Impact of Terrain Variance and Velocity on the Handover Performance of LTE Systems," in Proc. of IEEE, Int. Conf. on Wireless Commun. and Signal Processing, vol. 1, Nov. 2010, pp. 1-5.

TABLE OF CONTENTS

LIST OF FIGURES

LIST OF TABLES

LIST OF ACRONYMS

1G	First Generation
2G	Second Generation
3G	Third Generation
4G	Fourth Generation
2-D	Two Dimensional
3-D	Three Dimensional
AMPS	Advanced Mobile Phone Services
AoA	Angle-of-Arrival
AoD	Angle-of-Departure
BS	Base Station
CDF	Cumulative Distribution Function
CDMA	Code Division Multiple Access
DAMPS	Digital AMPS
EDGE	Enhanced Data Rates for GSM Evolution
EGPRS	Enhanced General Packet Radio Service
ESM	Eccentric Scattering Model
FDMA	Frequency Division Multiple Access
GBHDS	Geometrically-Based Hyperbolic Distributed Scatterers
GBSBM	Geometrically-Based Single Bounce Macro-cell Model
GoS	Grade of Service
GPRS	General Packet Radio Services
GSDM	Gaussian Scatter Density Model
GSM	Global System for Mobile Communication
ISI	Inter Symbol Interference
LoS	Line-of-Sight
LTE	Long Term Evolution
MIMO	Multiple Input and Multiple Output
MS	Mobile Station
OFDMA	Orthogonal Frequency Division Multiple Access
PDF	Probability Density Function
RS	reference symbols
RSSI	Received Signal Strength Indicator
SDF	Scatter Density function
SNR	Signal-to-Noise Ratio
TDMA	Time Division Multiple Access
ToA	Time of Arrival
UMTS	Universal Mobile Telecommunication Systems
WCDMA	Wideband CDMA
WLANs	Wireless Local Area Networks

LIST OF NOTATIONS

ϕ_m	Azimuthal AoA observed at MS
ϕ_b	Azimuthal AoA observed at BS
ϕ_v	Direction of MS's horizontal motion w.r.t. LoS component
θ_m	Direction of MS's horizontal motion w.r.t. a certain arriving multipath
θ_{HO}	Direction of MS's horizontal motion w.r.t. the line joining two adjacent BSs
β_m	Elevation AoA observed at MS
β_b	Elevation AoA observed at BS
Ψ_i	Azimuthal AoA of LoS component received at i^{th} BS
α	Beam-width of directional antenna at BS
$\alpha_{\max}$	Maximum beam-width of directional antenna at BS that illuminates all the scatterers in the vicinity of MS
I_{Region}	Illuminated scattering region
E_{Region}	Eliminated scattering region
ϕ_{t1}	Azimuth threshold angle 1 to separate among different partitions
ϕ_{t2}	Azimuth threshold angle 2 to separate among different partitions
β_t	Elevation threshold angle to separate among different partitions
ϕ_L	Limit of azimuth angle for a fixed value of β_b
β_{Los}	LoS elevation AoA
d	Horizontal distance of MS from serving BS
d_i	Horizontal distance of MS from i^{th} BS
d_{OR}	Maximum horizontal length of overlapped region between adjacent cells
d_{BS}	Horizontal distance between BSs of adjacent cells
l_p	Path length of a certain multipath component
l_{Los}	Length of LoS path
a	Radius of semi-spheroid along horizontal axis
b	Radius of semi-spheroid along vertical axis
r_c	Radius of a cell
σ_a	Deviation of Gaussian distributed scatterers along horizontal axis
σ_b	Deviation of Gaussian distributed scatterers along vertical axis
h_t	Height of BS's antenna
r_m	Distance of MS from a certain scattering object
$r_{m,\max}$	Distance of MS from the scatterer located at the boundary of scattering region in a particular direction
$N_{m,\max}$	Effective number of scatterers in a particular direction for the case of Gaussian scatter density
r_b	Distance of BS from the scattering object
ρ_b	Projection of r_b on azimuth plane
τ	Propagation delay

τ_o	Propagation delay of LoS component
$\tau_{\max}$	Propagation delay of longest path
$\tau_{\lim}$	Propagation path delay of longest path in a certain direction
A_c	Area of scattering circle region
A_{e,ϕ_b}	Area of a vertical ellipse for a certain ϕ_b
V	Volume of semi-spheroid for uniformly distributed scatterers
E	Number of illuminated scatters for Gaussian scatter density
f_c	Carrier frequency
f_{DS}	Doppler frequency
f_m	Maximum Doppler frequency
γ	Normalized Doppler shift
c	Speed of light
v	Velocity of MS
p_r	Received power level
p_o	Measured power level at some known distance
p_l	Lower bound on power level, associated with longest multipath component
p_u	Upper bound on power level, corresponding to the shortest multipath component
n	Path loss exponent
δ_{RO}	Ratio between the length of overlapping region and radius of cell
$p(.)$	Probability density function
$J(.)$	Jacobian transformation function
$f(.)$	Scatter density function
$f_U(.)$	Uniform scatter density function
$f_G(.)$	Gaussian scatter density function
erf(.)	Standard error function
erfc(.)	Standard complementary error function
exp(.)	Standard exponential function

Chapter 1

INTRODUCTION

This chapter starts with a brief history of capacity demands in wireless communication systems and their respective solutions in the form of various wireless communication systems in Section 1.1, which provides the motivations to work in the targeted research area. Then it proceeds towards the significance of the targeted research area in Section 1.2. A brief summary of research contributions presented in this thesis is given in Section 1.4. Published research articles related to the proposed work included in this thesis are listed in Section 1.5. Finally, a brief layout of the thesis is provided at the end of this chapter.

1.1 History of Capacity Demands in Wireless Communication Systems

Advancements in the field of communications have allowed people to communicate without any physical connection since a century ago when Marconi successfully managed to demonstrate wireless telegraphy. Since the beginning of last decade, the land mobile radio communication industry has been enjoying its fastest growth period in the history. In wireless communication systems, capacity enhancement has always been highly demanded. In this regard, many efforts have been made by the scientists in literature which exploit various features of wireless signals to enhance the capacity. Among initial efforts, the problem of shortage of frequency channels was resolved by making use of high frequency channels available [1] with the invention of frequency modulation (FM). Land mobile radio communication systems are often categorized in different generations with respect to their capacity offerings. As the demands of high capacity began to grow further, the concept of frequency reuse was evolved and the first generation (1G) of cellular mobile systems called the Advanced Mobile Phone Services (AMPS) was deployed in America in 1983 [2,3]. AMPS used frequency division multiple access (FDMA).

AMPS and all other analog communication technologies of the age are categorized as 1G of mobile systems. Mobile systems evolved later in the new era of digital communication systems are classified as the second generation (2G) of mobile systems. 2G systems that were introduced in early 1990s, used digital technology. 2G digital mobile systems achieved an estimated increase of three times in the capacity of communication systems over analog systems [4]. This era of mobile systems included Global System for Mobile Communication (GSM), Digital AMPS (D-AMPS), IS-136, and Code Division Multiple Access (CDMA) based systems (IS-95). These systems mainly offered speech communications. The GSM and IS-136 mobile systems used Time Division Multiple Access (TDMA) scheme. Various new features were provided by GSM, viz: encryption, authentication, short messaging services (SMS), and subscriber identity module (SIM) card. One of the major factors in the enhancement of capacity was the compression of voice data before transmission [5]. The IS-95 and GSM with GPRS (General packet radio services) are some times referred to as 2.5 generation of mobile networks [4], which provide data communication limited to rather low data rates. Technologies to provide improved rate of data services with GSM mobile systems are categorized in 2.75G, which are Enhanced Data Rates for GSM Evolution (EDGE) and Enhanced General Packet Radio Service (EGPRS). EDGE achieved a potential increase of three times in the communication capacity [2] of GSM/GPRS systems. Further demands of increased communication capacity have lead to the development of third generation (3G) of mobile systems [6]. The 3G mobile systems include Universal Mobile Telecommunication Systems (UMTS) (i.e., Wideband CDMA (WCDMA)) and CDMA2000 [7, 8].

With increasing demand of high capacity, the available frequency spectrum became highly precious resource. Thus, these days, researchers are inspecting the possible new ways to enhance the capacity by keeping the frequency band fixed. Multiple antenna systems are thought to be a solution in this regard. The multiple-antenna arrays both with diversity enhancing and beamforming abilities changed

the trends by clearly demonstrating that it can boost all the performance parameters significantly. Therefore, the use of multiple-antenna arrays has become an integral part of future communication systems. Multiple Input and Multiple Output (MIMO) systems have been developed with the use of multiple antenna arrays at both ends of communication link. Apart from the advantage of multiple antenna systems being used as smart antenna systems, they can also be used for spatial multiplexing in MIMO. Therefore, MIMO systems can significantly boost the spectral efficiency by simultaneously transmitting the multiple data streams. Recently, multiple antenna systems are emerging to achieve the targets of fourth generation (4G) of mobile systems such as high data rate, high reliability, and long range communications. The 4G mobile systems are an end-to-end IP solution where voice, data, and streaming multimedia can be communicated at higher data speed. The demand of industry for future generation (4G) networks to improve the speed several times as compared to the speed of existing 3G networks, so that the bandwidth-intensive applications like streaming media can be facilitated. The infrastructure of 4G networks aims to implement all the mobile standards from 2G to 4G networks to provide support for heterogenous environments and for existing users of previous technologies. The commercially available technologies which are being considered to lead to 4G are WiMax and Long Term Evolution (LTE) [9,10].

In a typical propagation environment, the signal emitted from the transmitter faces various physical phenomena (like; reflection, refractions, diffraction, and scattering), that form multiple copies (attenuated, phase shifted, frequency shifted, and delayed) of the transmitted radio signal at the receiver antenna. These multiple copies of the transmitted radio signal are called multipath signal components and usually lead to interference in the received signal. This phenomenon may drastically affects the performance of a communication system. In contrast to the disadvantages inherent in these multipath components, research in recent years has shown several advantages offered by multipath components if utilized appropriately. In this regard, spatial filtering of multipath waves has gathered significant

attention in recent years, as discussed above. Thus, in order to enhance the performance of systems with multiple antennas, it became essential to have a precise knowledge of the radio propagation environment.

1.2 Significance of Research Topic

In recent years, in order to have good understanding of mobile radio channel, more attention has been paid to its spatio-temporal characteristics. In the literature, the spatial and temporal characteristics of mobile radio channel are proven to be useful in performance evaluation of mobile communication systems. The angular characteristics of cellular and mobile channels are useful in determining their shape factors (i.e., angular spread, angular constriction, and direction of maximum fading), which can further be used for second order statistics like level crossing rate, average fade duration, spatial correlation and coherence distance [11, 12]. To serve this purpose efficiently, it is essential to have reliable understanding of radio propagation characteristics of the transmission path between Base Station (BS) and Mobile Station (MS) that leads to the design of effective signal processing techniques [13]. Geometrically based models are typical and adequate solutions in this regard. Therefore, a number of 2-D and 3-D propagation models are presented in the literature [13–26], which describe the nature of spreading of multipath components to characterize channel parameters.

To quantify the effects of directional antenna on the characteristics of angular, temporal, and Doppler spectrum of land mobile radio cellular systems for the case of 2-D scattering models, a number of scattering models have been proposed in the literature [26–30]. However, such analysis for the case of 3-D scattering models is missing in the literature. Although, 2-D models offer low computational complexity but they fail to provide accurate channel characteristics; whereas, 3-D propagation models provide more precise and accurate channel characteristics. The multi-path waves reflected from vertical structures do not often propagate horizontally, hence the waves are seen to spread wide in vertical plane over the

angle of 20^o [22,24]. Therefore, it is more practical and fairly essential to consider the elevation plane in such scattering environments for the derivation of accurate propagation characteristics.

1.3 Research Aims

The main aim of this research is to develop a geometrically based generalized 3-D scattering model, which can be deduced to other 2-D and 3-D scattering models, found in the literature, with an appropriate choice of a few parameters. It is considered to be within the scope of this research to analyze the effects of directional antenna at BS on the angular and temporal statistics of land mobile radio cellular systems.

This is also regarded as one of the aims of this research to characterize the impact of mobility on the performance of cellular communication links. Mobility usually imposes two impacts, viz: the introduction of time-variability in radio fading channel and performance degradation of the handover procedure, in cellular mobile communication systems. Regarding the first impact, we aim to characterize the 3-D propagation channels for Doppler power spectrum. Since, the impact of directional antenna on the distribution characteristics of the Doppler shift in 3-D propagation environments is not discussed in the literature so far. Therefore, it is considered appropriate to develop an analytical model encompassing the effects of directional antennas on the characteristics of Doppler power spectrum for 3-D mobile radio propagation channel for ongoing research in MIMO communications in dynamic downtown urban environments.

Regarding the second impact of mobility, the aim of our research is to provide a geometrically based analysis for the impact of propagation environments on the performance parameters of handover, so that uninterrupted communication links can be maintained with minimum delay for mobile users traveling among different environments. Moreover, the impact of the velocity of MS and direction of MS's

motion on the performance of handover procedures are also considered to be within the scope of this research.

1.4 Research Contributions

The research contributions presented in this thesis consists of the following three major parts:

1.4.1 Physical Modeling of Cellular Mobile Channels in 3-D Radio Propagation Environments

Main research contributions of this part of research can be summarized as follows:

i. A comprehensive comparative analysis of various 2-D and 3-D propagation models found in the literature with uniform and Gaussian scatter densities is presented.

ii. A new geometrically based generalized 3-D scattering model is proposed which can be deduced to any 3-D or 2-D scattering model proposed in the literature for macro-cell environment with an appropriate choice of a few parameters.

iii. An analysis is presented to measure the effects of directional antenna at BS on the angular and temporal statistics of land mobile radio cellular systems.

iv. A study to investigate and establish a realistic choice of distribution for the scattering objects around MS is presented. To serve this purpose, analytical expressions are derived for both uniform and Gaussian scatter densities.

1.4.2 Characterization of 3-D Propagation Channel for Doppler Spectrum

In this part of the research, the main contributions are as follows:

i. The effects of directional antenna on statistic distributions of power, Doppler spectrum, and Angle-of-Arrival (AoA) for 3-D radio propagation environment is intensively analyzed.

ii. An analytical relationship of joint and marginal Probability Density Function (PDF) of azimuth and elevation AoA with Doppler shift is derived.

iii. A study to gauge the impact of direction of MS's motion and velocity of MS on the characteristics of Doppler shift distribution for uniform and Gaussian scatter densities is presented.

iv. Comparative analyses of the proposed Doppler characteristics with those provided in literature for both 2-D and 3-D propagation models with uniform and Gaussian scatter densities are presented.

1.4.3 Performance Analysis of Handover Procedures in Cellular Environments

The following are the contributions of this part of research thesis:

i. Author provides a geometrically based analysis for the performance of handover procedures in cellular networks.

ii. A study is presented to analyze the effects of propagation environments on the performance of Handover process.

iii. An analysis is presented to measure the impact of direction and velocity of MS's motion on the performance of handover margin in cellular networks.

1.5 Research Publications

The research work contained in this thesis consists of the following publications.

1.5.1 Journal Publications

[**J01**] Syed Junaid Nawaz, Bilal Hasan Qureshi, and Noor M. Khan, "A Generalized 3-D Scattering Model for Macrocell Environment with Directional Antenna at BS," IEEE Transactions on Vehicular Technology, vol. 59, no. 7, pp. 3193-3204, May. 2010.

[**J02**] Syed Junaid Nawaz, Noor M. Khan, Mohammad N. Patwary, and Mansour Moniri, "Effect of Directional Antenna on The Doppler Spectrum in 3-D Mobile Radio Propagation Environment," IEEE Transactions on Vehicular Technology, vol. 60, no. 7, pp. 2895 - 2903, Jul. 2011.

1.5.2 Conference Proceedings

[**C01**] Syed Junaid Nawaz, Bilal H. Qureshi, Noor M. Khan, and M. Abdel-Maguid, "Effect of Directional Antenna on the Spatial Characteristics of 3-D Macrocell Environment", in Proc. of IEEE, Int. Conf. on future comp. and commun., vol. 1, May 2010, pp. 552-556.

[**C02**] Syed Junaid Nawaz, Bilal Hasan Qureshi, and Noor M. Khan, "Angle of Arrival Statistics for 3-D Macrocell Environment using Directional Antenna at BS", in Proc. of IEEE, Int. Multitopic Conf., vol. 1, Dec. 2009, pp. 1-5.

[**C03**] Syed Junaid Nawaz, M. N. Patwary, Noor M. Khan, and Hongnian Yu, "3-D Gaussian Scatter Density Propagation Model Employing a Directional Antenna at BS," in Proc. of IEEE, 5th Advanced Satellite Multimedia Systems Conf., vol. 1, Sep. 2010, pp. 395-400.

[**C04**] Saif-Ur-Rehman, Syed Junaid Nawaz, Mohammad N. Patwary, and M. Abdul Muguid, "Impact of Terrain Variance and Velocity on the Handover Performance of LTE Systems," in Proc. of IEEE, Int. Conf. on Wireless Commun. and Signal Processing, vol. 1, Nov. 2010, pp. 1-5.

1.5.3 Additional Contributions

[**C05**] Syed Junaid Nawaz, Khawza I. Ahmed, Mohammad N. Patwary, and Noor M. Khan, "Superimposed Training Based Compressed Sensing of Sparse Multipath Channels", to submit in IET Communications.

[**C06**] A. Kamar, Syed Junaid Nawaz, M. N. Patwary, and M. Abdel-Maguid, "Optimized Algorithm for Cellular Network Planning Based on Terrain and Demand Analysis," in Proc. of IEEE Int. Conf. on Comp. Technol. and Development, vol. 1, Nov. 2010, pp.359-364.

[**C07**] N. Satti, Syed Junaid Nawaz, M. N. Patwary, and M. Abdul Muguid, "Dynamic Subcarriers and Power Allocation Algorithm for OFDMA Cellular Systems," in Proc. of IEEE Int. Conf. on Comp. Technol. and Development, vol. 1, Nov. 2010, pp.359-364.

1.6 Organization of Thesis

The rest of this thesis is organized as follows:

In Chapter 2, basics of multipath propagation phenomena, overview of land mobile radio cellular environments, and an introduction of geometrically based channel modeling is presented. Channel models are classified with respect to the targeted scattering environments. A comprehensive survey of some notable channel models found in the literature along with the statement of problems is presented, these problems are addressed later in this thesis.

Chapter 3 presents a generalized 3-D scattering model for macro-cellular land mobile radio cellular systems, in which MS is assumed to be located at the center of a 3-D scattering semi-spheroid and a BS employing a directional antenna is located outside of the semi-spheroid. The proposed model is derived for both uniform and Gaussian scatter densities.

In Chapter 4, the effects of the directional antenna on the spatial and temporal characteristics of the channel are thoroughly observed in proposed scattering environment. Closed-form expressions for joint and marginal PDFs of the AoA seen at the MS and the BS in correspondence with azimuth and elevation angles are derived. Further, closed-form expressions for propagation path delays and trivariate joint PDFs of the Time-of-Arrival (ToA) seen at the MS and the BS in correspondence with azimuth and elevation angles are also derived. Moreover, theoretical results along with observations are shown, that illustrate the effects of the directional antenna on the spatio-temporal statistics of the channel in proposed 3-D scattering environment. The proposed 3-D scattering model is shown to deduce all previously proposed 2-D and 3-D models that assume a uniform distribution of scatters with directional or omnidirectional antennas found in the literature for a macro-cell environment. The obtained theoretical results are compared with some notable 2-D and 3-D scattering models to validate the generalization of the proposed model.

In Chapter 5, an analytical model is proposed for land mobile radio cellular systems with a directional antenna at BS to quantify the effects of directivity of the radiated waves from antennas on the Doppler spectrum in 3-D radio propagation environment. The impact of antenna beam-width and motion of MS is thoroughly investigated on the statistical distribution of power Doppler spectrum. Closed-form expressions for trivariate PDFs of propagation path distance, power, and Doppler shift are derived. Furthermore, general expressions for joint and marginal PDFs of elevation AoA, power, and Doppler shift are established. Finally, the obtained theoretical results along with the observations are presented that illustrate the effects of directivity of the antenna beam-width and the direction of MS's motion on the distribution characteristics of power Doppler spectrum.

In Chapter 6, an analysis for the impact of various channel parameters on the performance of handover in mobile radio cellular systems is presented. Using the proposed analytical model, a mathematical relation for the handover margin with

velocity of MS, direction of mobile motion, and propagation environment is derived on the basis of path loss propagation model. Relationship for the ratio between the radius of coverage area and the overlapped region between adjacent cells is also derived, which guarantees to satisfy the required handover margin. Moreover, the impact of velocity and direction of MS's motion on the handover margin is comprehensively analyzed. Finally, the impact of propagation environment on the handover margin is also analyzed and a comprehensive analysis on the basis of theoretical results is presented.

Finally, Chapter 7 provides a brief summary of the thesis, discusses the future research work based on the proposed results in the thesis, and presents the concluding remarks.

Chapter 2

GEOMETRICALLY BASED CHANNEL MODELS

This chapter discusses a detailed overview of the physical nature of wireless channels. In section 2.1, basics of multipath phenomena are presented. In section 2.2, an overview of land mobile radio cellular channels along with a brief introduction of different types of cellular environments is presented. Section 2.4 provides a detailed overview of geometrically based channel models in literature and indicates the problems which are addressed later in this thesis.

2.1 Basics of Multipath Propagation

In wireless communication systems, the signal emitted from the transmitter antenna propagates through the radio environment and its multiple copies are received at the receiver. This is due to various physical phenomena which occur during the interaction of emitted signal with the propagation environment, namely: reflection, refraction, diffraction, and scattering. Fig. 2.1 depicts a typical outdoor multipath propagation environment.

2.1.1 Reflection

Reflection is a physical phenomenon of propagating waves, which means throwing back of incident waves from the surface of an object. It occurs when a propagating wave incidents on a surface with dimensions larger than the signal's wavelength. The signal reflects from a smooth surface with an angle equal to the angle of its incidence [31]. Whereas, when the surface of object is not smooth, surface scattering occurs [32], as shown in Fig. 2.1.

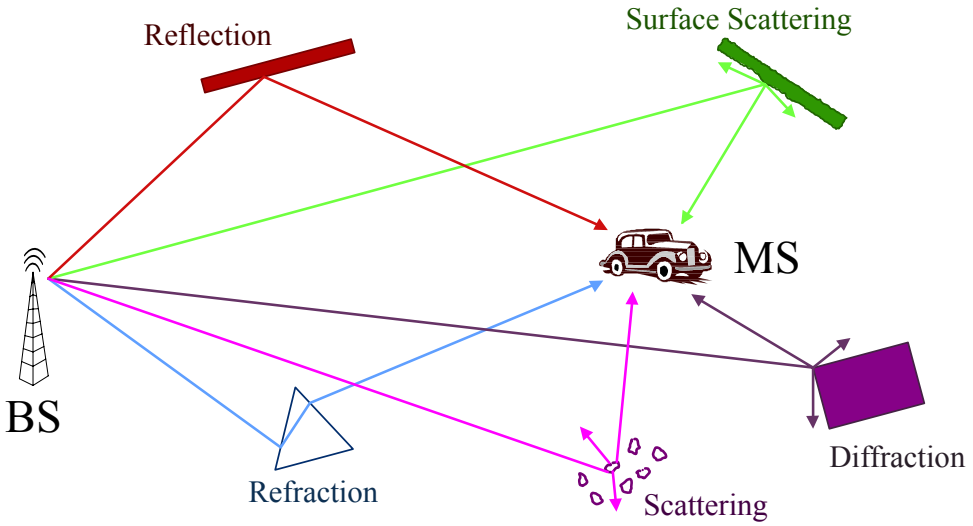

FIGURE 2.1: Multipath phenomenon.

2.1.2 Refraction

Refraction is a physical process which refers to the change in direction of propagating wave caused due to the change in its propagating speed. It usually occurs when a wave enters from a medium to another medium with different medium density.

2.1.3 Diffraction

Diffraction is a physical phenomenon which refers to the bending of waves around the stricken object. It occurs when propagating wave encounters edge of an obstacle. In wireless communications, this phenomenon helps to make the coverage available in the regions shadowed by big obstacles (buildings).

2.1.4 Scattering

Scattering is a physical phenomenon which refers to lossy and deviated reradiation of incident wave in all directions from an obstacle with its facing dimension smaller than the signal's wavelength [33]. The energy of an incident wave is divided and reradiated in directions away from the scattering object.

Cellular Environment	Scattering objects	BS antenna height	Cell radius
Macro-cell	only around MS	>> the height of average rooftop level	kilometers
Micro-cell	both around BS and MS	$\leq$ the height of average rooftop level	few dozen meters
Pico-cell	both around BS and MS	$\cong$ the height of MS antenna	a floor or an entire building

TABLE 2.1: Land mobile radio cellular environments

2.2 Land Mobile Radio Cellular Environments

In order to increase the capacity of wireless communication systems, the available frequency spectrum is spatially reused, which results in the division of geographical area into small independent cells. These cells are designed based upon the propagation mechanism and density of users in the coverage area. Depending upon the propagation mechanism, these cells are categorized into three groups, viz: macro-, micro-, and pico-cellular land mobile radio systems. A brief summary of these cellular environments is given in Table 2.1.

2.2.1 Macro-cell Environment

In a typical macro-cell environment, the distance between MS and BS is usually very large, i.e., in the order of kilometers. The antenna height of BS is more than the average rooftop level of surrounding environment, consequently, the surroundings of BS are free of scattering objects. Hence, the scattering objects are only present around the MS, which causes to the arrival of multipath signals at MS and BS. A typical macro-cell environment is shown in Fig. 2.2. The multipath signals received at MS and BS arrive either from the local scattering objects around MS or from the dominant distant scattering objects located far from both MS and BS. The multipath components arriving from local scatters in the vicinity of MS are

highly influenced by the mobility of MS resulting in fast time variability of the channel.

2.2.2 Micro-cell Environment

A typical micro-cell environment in depicted in Fig. 2.3. The antenna height of BS is usually less than or equal to the average rooftop level of surrounding environment. Therefore, the scattering objects around both MS and BS correspond to the arrival of signals. However, the number of scattering objects around BS are usually fewer than the scattering objects around MS. The radius of cell is usually less than a kilometer.

2.2.3 Pico-cell Environment

The pico-cell environment is usually a floor of a building or an entire building. The pico-cell environment is depicted in Fig. 2.4, where both BS and MS are surrounded by scatterers. The distance between BS and MS is usually only a few meters. The antenna heights of both MS and BS are relatively low and are approximately equal, therefore, the scattering objects are present around both the ends of a link.

2.3 General Channel Modeling Parameters

2.3.1 Shapes and Dimensions of Scattering Region

The following 2-D and 3-D shapes have been considered in the literature to model the scattering region in different types of cellular environments:

2.3.1.1 Circular Scattering Region

In a typical macro-cell environment, where the BS side is scattering-free region, the scattering region around the MS can be modeled as a 2-D circular region. As it is two-dimensional (2-D) in nature, it assumes that the propagation take place

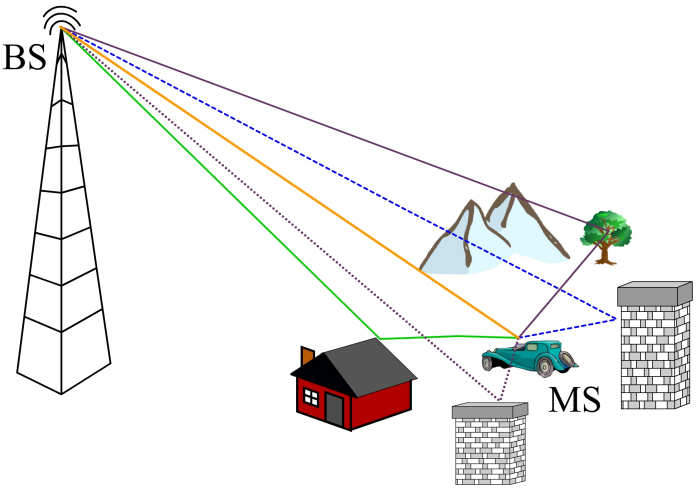

FIGURE 2.2: Macro-cell environment.

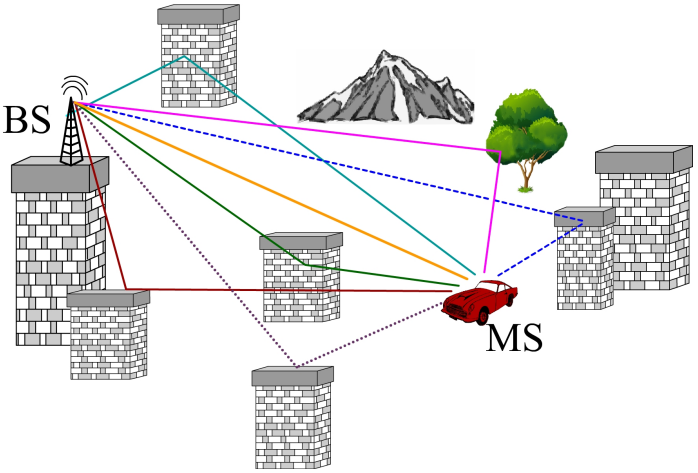

FIGURE 2.3: Micro-cell environment.

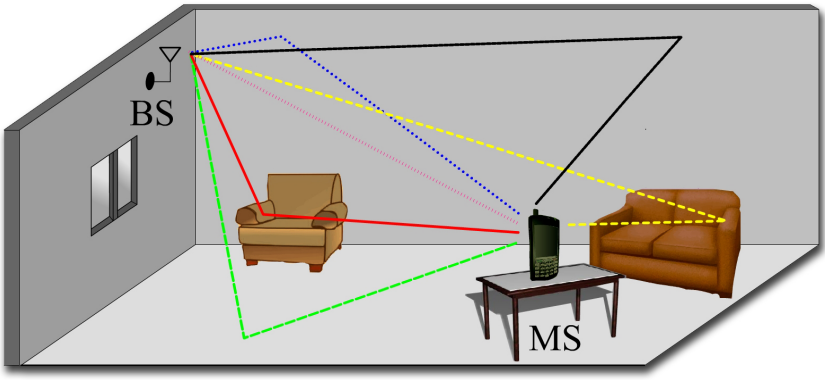

FIGURE 2.4: Pico-cell environment.

only in a horizontal 2-D plane between transmitting and receiving antennas, thus, reduces the complexity. Various models are available in the literature [13, 15, 19, 20, 24, 26–29, 34, 35], which assume the 2-D circular scattering region with a certain scatter density. A circular hollow disc is also considered to model the scattering region around MS in [18].

2.3.1.2 Spherical Scattering Region

A number of authors [22, 23, 36–38] have used spherical region to model the scattering objects around MS in a macro-cellular environment. Apart from the computational simplicity of 2-D model, 3-D models offer more realistic statistics. Spherically shaped scattering region allows the propagation of waves in 3-D planes and provides not only the azimuth but also the elevation plane spatial characteristics.

2.3.1.3 Cylindrical Scattering Region

Cylindrical shape has also been considered to model the scattering region around the MS in [39, 40].

2.3.1.4 Elliptical and Ellipsoidal Scattering Regions

Elliptical and Ellipsoidal regions are used to model the scattering objects in micro- and pico-cell environments, where the scattering objects exists around both the ends of a communication link. The BS and the MS are assumed to be located at the foci points of ellipse/ellipsoidal. Spatial and temporal characteristics of micro- and pico-cell environments have been derived by a number of authors [13, 15, 19, 25, 41, 42] using the elliptical/ellipsoidal shape to model the scattering region with uniform and/or Gaussian scatter densities. The elliptical scattering region considers only the propagation to take place in 2-D plane, hence such modeling of scattering region provide only the azimuthal plane characteristics. Whereas, ellipsoidal scattering regions offer more realistic statistics as it allows the propagation of waves in 3-D environment.

2.3.2 Distribution of Scattering Objects

The following are the notable distribution functions, found in the literature, used to model the distribution of scattering objects:

2.3.2.1 Uniform Scatter Density

Uniform distribution of scatterers offers simplicity in derivation of the spatial models, hence a number of authors have assumed uniform distribution of scatterers to model the scattering region [13, 22, 24, 26, 42, 43]. Uniformly placed and spaced scatterers are kept confined within a scattering region of certain shape and dimensions.

2.3.2.2 Gaussian Scatter Density

Gaussian distribution is used to model the distribution of scatterers by a number of authors [19, 27, 28, 44, 45]. In [19], Gaussian distribution is shown as more realistic consideration to model the scattering objects compared to the uniform distribution of scatterers. In Gaussian scatter density, high number of scatterers are assumed in the regions closer to the MS and the number of scatterers reduce as we observe the regions away from the MS.

2.3.2.3 Hyperbolic Scatter Density

The hyperbolic scatter density is also considered to model the scattering objects located in the vicinity of MS by a number of authors [16, 20, 34, 35, 46]. The angular statistics for hyperbolic scatter density found in [20, 35] are also compared with experimental data, which validated the choice of hyperbolic distribution.

2.4 Literature Review and Problems Statement

Directional antennas along with multiple antenna arrays have been in use in modern wireless communication systems since last decade to achieve better performance in terms of beamforming and diversity gains. Spatio-temporal statistics of

a wireless communication channel are required to produce the finer beams at BS which leads to the reduction of interference caused by undesired multipath signals. Such statistics are also necessary for avoiding antenna correlations to design diversity techniques with improved diversity gain in MIMO systems. To evaluate the capabilities of beam oriented technologies, the angular and temporal representation of the dispersion of multipath waves in 3-D propagation environment is essentially required. Such representation can only be achieved with the use of spatial channel models. Therefore, a number of different types of geometrical models are proposed in the literature for the characterization of the spatial and temporal domain of a radio channel [13–26]. A survey of some notable spatial channel models found in the literature is given in Table 2.2.

A geometrically-based generalized model for spatial statistics of cellular channels is presented in [13], where the uniform distribution is considered to model scattering region. An Eccentric Scattering Model (ESM) is also proposed, along with a thorough comparison with other previous 2-D models for pico-, micro-, and macro-cell environments. The joint and marginal PDFs of AoA and ToA are derived for 2-D elliptical and circular scattering models in [14] and [15], respectively. In [17], the temporal statistics of cellular mobile channel are observed for pico-, micro-, and macro-cell environments with a generic closed-form formula presented for PDF of ToA, which can be used to deduct the previous 2-D models. The derived theoretical results have been used to simulate the temporal dispersion of the multipath signals in a variety of propagation conditions which can help in the design of efficient equalizers to combat Inter Symbol Interference (ISI) over fading channels. The geometrical model proposed in [18] considers a hollow-disc centered at the MS for uplink/downlink PDF of ToA/AoA. The results are shown for varying thickness of hollow disc which lets the spatial density to degenerate to the well-known uniform-circular or uniform-disc density. In [16], a 2-D Geometrically-Based Hyperbolic Distributed Scatterers (GBHDS) model is proposed to investigate the

temporal and spatial behavior of macro-cell mobile environment. In [19], Gaussian Scatter Density Model (GSDM) is proposed. Angular and temporal statistics of the cellular mobile channels considering 2-D circular and elliptical scattering regions with Gaussian distributed scatterers are derived. The obtained theoretical results are verified with experimental measurements. However, under certain conditions the 2-D GSDM is not suitable for micro- and pico-cell environments [13]. The geometrically-based model proposed in [20] considers hyperbolic distribution to model the distribution of random scatterers between BS and MS. Expressions for the hyperbolic AoA PDF, power azimuth spectrum, ToA PDF, and power delay spectrum are derived. Furthermore, the theoretical results are compared with a set of empirical data and with those obtained for GSDM. In [44], the PDFs of ToA and Angle-of-Departure (AoD) of downlink are derived for GSDM. In the literature [13, 19, 27, 28, 44, 47], Gaussian distribution is proven as an effective consideration to model the scattering region. Whereas, such study for the case of 3-D propagation environments with Gaussian distributed scatterers is absent from the literature.

In macro- and micro-cell environments, the signals reflected from rooftop and high rise buildings raises the importance of the inclusion of elevation plane in a model. Therefore, modeling the scatterers around MS in 3-D with elevated BS offers more precise spatial and temporal statistics. In [21], power spectral density and PDF of AoA for non zero elevation plane using a 3-D scattering model are derived and the results are compared with field measurements. In [22], a 3-D geometric model is proposed that considers the angular arrival of multipath waves in both azimuth and elevation planes to derive the closed-form expressions for the PDF of AoA seen at MS and BS and the results are further used to find first and second order angular statistics. In [23], uplink/downlink trivariate distributions of ToA and AoA have been found using a 3-D hemispheroid scattering model similar to that of [22]. However, this model is not suitable to be considered for macro-cell environment, as BS and MS are assumed to be resided at the same height and the scatterers

around MS are assumed to be confined in a spherical region with the same radius in both azimuth and elevation planes. 3-D macro-cell environment can be modeled more appropriately by taking an elevated BS and a scattering semi-spheroid with different lengths of major and minor axes (major axis along horizontal plane and minor axis along elevation plane). A 3-D macro-cell scattering model is presented in [24] and spatial domain parameters of uplink radio channel at BS are derived, where, the obtained theoretical results are also compared with measured data. This model assumes an elevated BS but the scattering objects are kept confined in a 2-D non-elevated circular disk. However, a macro-cell environment can be modeled more precisely by using 3-D distributed scatterers around a MS for spatio-temporal characteristics [22]. Another 3-D ellipsoid model is proposed in [25] to demonstrate the joint distribution of angle and time of arrivals assuming the scatterers are distributed both around the MS and the BS. The model can be applicable to micro- and pico-cell environments. Nevertheless, there is a need of a generalized 3-D geometrical scattering model that can deduce to a 3-D or a 2-D scattering model with an appropriate choice of a few parameters. Therefore, *the first part of this research aims to develop a geometrically based generalized 3-D scattering model, which can be deduced to other 2-D and 3-D scattering models found in the literature with an appropriate choice of a few parameters.*

A 2-D Geometrically Based Single Bounce Macro-cell model (GBSBM) with directional antenna at BS is presented in [26] which provides the power distribution of multipath components along with PDF of angle and ToA. It has been shown in [26] that the level crossing rate of the fading envelope decreases and the envelope correlation increases significantly if a directional antenna is employed at BS. A similar kind of work is done in [27] and [28] by using directional antenna at BS for Gaussian scatter density around MS where PDFs of AoA are found. In [29], directional antennas are applied at both ends of a communication link and the spatial characteristics are thoroughly observed. In this regard, the impact of directional

antennas on the performance of a land mobile radio communication link has properly been investigated and analyzed for the case of uniform and Gaussian scatter density in 2-D scattering environments [26–28, 47, 48]. However, such study and analysis is absent from the literature for the case of 3-D scattering environments. As 3-D scattering models are more realistic and accurate to model the behavior of multipaths in spatial and temporal domains; hence the effects of directional antennas should also be intensively analyzed, so that more reliable wireless links can be designed for the future high-rate communications in time-varying mobility environments. Therefore, *it is considered to be within the first part of this research to analyze the effects of directional antenna at BS on the angular and temporal statistics of land mobile radio cellular systems.*

The second and third parts of the research aims at characterizing the impact of mobility on the performance of cellular communication links. Mobility usually imposes two impacts, viz: the introduction of time-variability in radio fading channel and performance degradation of the handover procedure, in cellular mobile communication systems. The second part of this thesis aims to characterize the 3-D propagation channel for Doppler shift spectrum. The study in [42] proposes the relationship between Doppler spectrum and the distribution of power over angular arrivals of multipath waves in 2-D space. A uniform scatter density for elliptical channel model is considered and general expressions for the distributions of Doppler, power, and AoA are derived, taking the distance-dependent path-loss into consideration. A similar approach is used in [35] for hyperbolic scatter density and general expressions for the PDFs of Doppler, power, and the AoA at MS are derived. Moreover in the literature [26, 30, 34, 35, 42, 47, 50], a comprehensive analysis on the relationship between the PDFs of azimuth AoA and Doppler spectrum for directional and omni-directional antennas have been presented. A brief summary of the channel models found in the literature which provide an analysis of Doppler spectrum is presented in Table 2.3.

Scattering Models.	Targeted Environment.	Distribution of Scatterers.	Modeling of Scattering Region.	Elevated BS	Directional antenna.
Ertel *et al.*, (1999), [15].	Pico−, micro−, and macro-cell	Uniform	2−D, Circular and Elliptical	No	No
Jaafar *et al.*, (2008), [18].	Pico−, micro−, and macro-cell	Uniform	2−D, Hallow disk and Elliptical	No	No
Liberti *et al.*, (1996), [14].	Pico− and micro-cell	Uniform	2−D, Elliptical	No	No
Piechocki *et al.*, (1998), [49].	Macro-cell	Uniform	2−D, Elliptical (with controllable eccentricity),	No	No
Mahmoud *et al.*, (2008), [16].	Macro-cell	Hyperbolic	2−D, unbounded around MS	No	No
Khoa *et al.*, (2009), [20].	Macro-cell	Hyperbolic	2−D, unbounded around MS	No	No
Kong *et al.*, (2009), [44].	Macro-cell	Gaussian	2−D, Circular	No	No
Janaswamy, (2002), [19].	Pico−, Micro−, and macro-cell	Gaussian	2−D, Circular, Elliptical	No	No
Khan *et al.*, (2008), [13].	Pico−, micro−, and macro-cell	Uniform / Gaussian	2−D, Elliptical (with controllable eccentricity)	No	No
Lotter *et al.*, (1999), [27].	Pico−, micro−, and macro-cell	Gaussian	2−D, Circular	No	at BS
Lopez *et al.*, (2005), [28].	Macro−cell	Gaussian	2−D, Circular	No	at BS
Petrus *et al.*, (2002), [26].	Macro−cell	Uniform	2−D, Circular	No	at BS
Bilal *et al.*, (2009), [29].	Micro− and Macro−cell	Uniform	2−D, Circular	No	at MS and BS
Baltzis *et al.*, (2009), [24].	Macro−cell	Uniform	2−D, Circular Disk	Yes	No
Alsehaili *et al.*, (2006), [25].	Pico−cell	Uniform	3−D, Ellipsoidal	No	No
Olenko *et al.*, (2006), [23].	Not specified	Uniform	3−D, Hemispheroid (same major and minor radii)	No	No
Janaswamy, (2002), [22].	Macro−cell	Uniform	3−D, Semi-spheroid (different major and minor radii)	Yes	No

TABLE 2.2: Survey of notable spatial channel models found in the literature.

It is observed that in the case of an omni-directional antenna at the BS, the angular distribution of multipath components arrived at MS in the azimuth plane is uniform [22, 28, 48, 51] (i.e., $1/2\pi$, from $-\pi$ to π) with a U-shaped Doppler spectrum [26, 30, 47, 50], no matter what scatter density (uniform or Gaussian) and dimension of the environment (2-D or 3-D) are assumed. However, the distribution of the azimuth AoA, observed at MS gets non-uniformly distributed, when a directional antenna with narrow beam towards the desired user is used at BS. Consequently, the shift in Doppler spectrum decreases [26, 28]. In [26], a geometrically based 2-D propagation model for macro-cell environment is presented and the AoA statistics of the multipath components along with Doppler spectrum are proposed. It is observed that, as the beam-width of directional antenna reduces, the PDF of the azimuth AoA deforms from the uniform distribution. As a result, there is reduction in the Doppler spread, which further leads to the slow variations in fading envelopes. In [47], Gaussian distribution is used to model the scatterers in 2-D space around MS and general expressions for the distribution of AoA and Doppler spectrum are derived. It is shown in [47] that the distribution of Doppler spectrum has significant dependence on the beam pattern of antennas. The Doppler power spectrum for wireless mobile channels is derived in [30], while considering the directional antennas at both ends of the communication link with 2-D uniform and Gaussian scatter densities. Recently, in [52], the distribution of Doppler spectrum for 3-D scattering environments is presented, where the general expressions for the relationship between PDF of elevation AoA and the distribution of Doppler spectrum are presented. The analysis in [52] is conducted on the basis of angular statistics provided by the propagation models in [22] and [51], which consider the omni-directional antenna at BS. However, *the impact of directional antenna on the characteristics of Doppler shift distributions in 3-D propagation environments is not discussed in the literature so far. Therefore, an analytical model encompassing the effects of directional antennas on the characteristics of Doppler power spectrum for 3-D mobile radio propagation channel is required for on going research in MIMO communication in dynamic downtown urban environment.*

Scattering Models.	Targeted Environment.	Distribution of Scatterers.	Modeling of Scattering Region.	Elevated BS.	Directional antenna.
Lotter *et al.*, (1999), [27].	Pico−, micro−, and macro-cell	Gaussian	2−D, Circular, centered at MS	No	at BS
Lopez *et al.*, (2005), [28].	Macro−cell	Gaussian	2−D, Circular, centered at MS	No	at BS
Castrellon *et al.*, (2007), [47].	Macro-cell	Gaussian	2-D, Circular, centered at MS	No	at BS
Iqbal *et al.*, (2009), [30].	Macro-cell	Uniform / Gaussian	2-D, Circular, centered at MS	No	at MS and BS
Petrus *et al.*, (2002), [26].	Macro−cell	Uniform	2−D, Circular, centered at MS	No	at BS
Ertel *et al.*, (1998), [42].	Micro−cell	Uniform	2−D, Elliptical, BS and MS at foci points	No	No
Shouxing Qu *et al.*, (1999), [21].	Macro-cell	Uniform	3−D	No	No
Shouxing Qu, (2009), [52].	Macro-cell	Uniform	3−D / 2−D, semi-spheroid, centered at MS	Yes	No

TABLE 2.3: Literature survey of land mobile radio cellular systems for Doppler spectrum.

To fulfill the increasing demands of capacity in future land mobile radio cellular networks, the spatial reuse of the available frequencies along with MIMO technologies are suggested to be the promising candidates. Despite the fact of higher deployment cost increasing the spatial reuse factor of the available frequency spectrum will probably force to shrink the coverage area of each radio cell. This further leads to the need of optimized overlapped region of adjacent cells. Moreover, in pico-cellular environment, attenuation may also restrict the cell size to only a few meters [53]. In pico- and micro-cellular environments, user may move with slow (pedestrian) and fast (vehicle) speeds respectively. In next generation networks, the handover of communication sessions among different types of cellular technologies should be transparent, smooth, and uninterrupted. Therefore, a number of researchers [54–62] have proposed various handover algorithms and presented the analysis for the effects of different propagation parameters on the performance

of handover procedures. In [63], analysis for the influence of MS's velocity on the handover delay is presented and path-loss model is used to model both communication channels (i.e., MS to serving and target BSs). The analysis is based on the assumption that MS moves straight towards the target BS, which is not a realistic consideration. However, *there is no study available in the literature which provides such analysis for the impact of propagation environments on the performance parameters of handover. Therefore, there is a scope to conduct such geometrically-based analysis that includes the impact of propagation environment on the handover procedure, so that uninterrupted communication links can be maintained with minimum handover delay. Thus, the third and last part of this research aims to provide a geometrically based analysis of the impact of the propagation environment, velocity of MS, and direction of MS's motion on the performance of handover procedure.*

Chapter 3

GENERALIZED 3-D SCATTERING MODEL

In this chapter, a generalized 3-D scattering model for macro-cell environment is presented, which assumes uniform and Gaussian distribution of scattering objects confined in a semi-spheroid around MS and employees a directional antenna at an elevated BS. Section 3.1 describes the channel modeling assumptions. In Section 3.2, the proposed 3-D scattering model is presented, which will be used throughout this thesis. Section 3.3 describes the proposed generalized channel model for uniform and Gaussian scatter densities. Finally, summary and observations are presented in Section 3.4

3.1 Common Channel Modeling Assumptions

Derivations of channel model in this thesis is based on the assumptions which are commonly used in the literature [13, 19, 22–24, 26, 28, 30, 34, 35, 42, 48, 52, 64]; these assumptions are listed as under:

i. Multipath signals received at MS from an elevated BS are assumed to arrive from both horizontal and vertical planes with an equal strength.

ii. The scattering objects around MS are assumed to be uniformly distributed within a 3-D semi-spheroid centered at MS.

iii. The propagation between MS and BS antennas is assumed to take place via single scattering object (which is an isotropic obstacle).

iv. Each scatterer is assumed to be an omnidirectional lossless reradiating element, which reflects some part of the incident wave directly towards the MS without any influence from the other scattering objects.

v. All scattering objects are assigned equal scattering coefficients with uniform random phases.

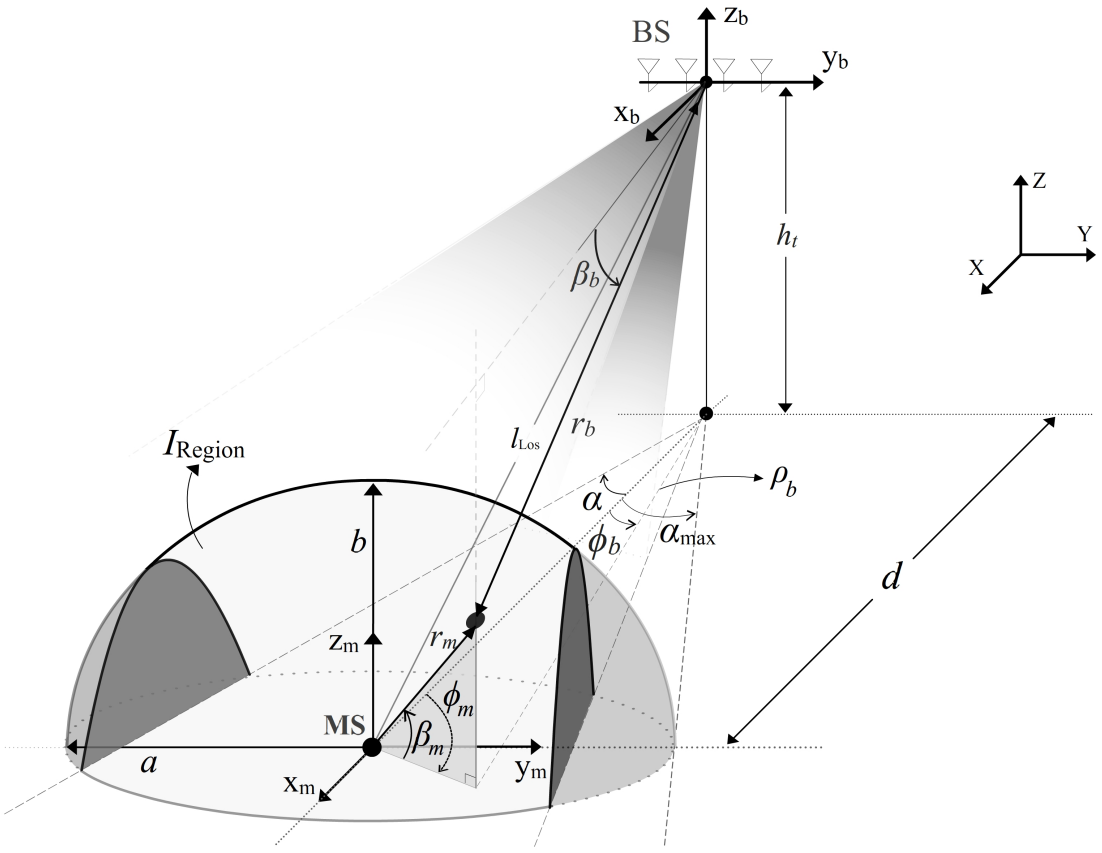

FIGURE 3.1: Proposed 3-D scattering model for macro-cell environment.

3.2 Proposed 3-D Generalized Scattering Model

In this section, we describe the proposed 3-D scattering model for macro-cell environment which assumes uniform distribution of scattering objects around MS that are confined in a semi-spheroid and the BS is equipped with a directional antenna. The proposed 3-D scattering model is depicted in Fig. 3.1, where the major and minor dimensions of the scattering semi-spheroid are taken a and b respectively and the BS is employed with a directional antenna of beam-width α and height h_t. The angles made in azimuth and elevation planes with direction of signal arrivals at BS are symbolized by ϕ_b & β_b and at MS are symbolized by ϕ_m & β_m, respectively. The horizontal distance from BS to MS is d, line-of-sight

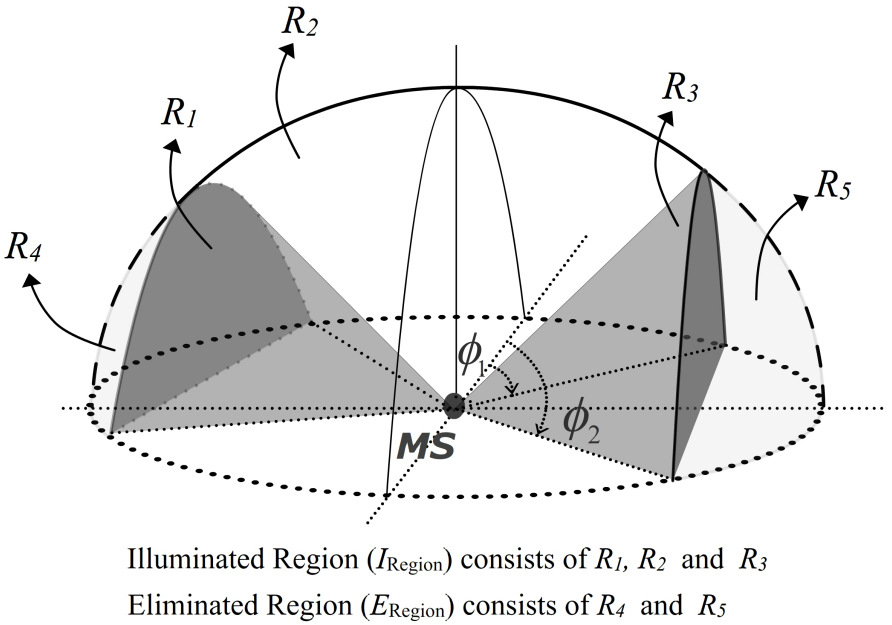

FIGURE 3.2: Geometrical Composition of the eliminated and illuminated scattering regions.

(LoS) distance from BS to MS is l_{Los}, and the distance of scattering objects from MS and BS is r_m and r_b respectively.

The following are the relations for transformations among different coordinates,

$$\mathrm{x_m} = r_m \cos\beta_m \cos\phi_m \qquad \textit{Eq (3.1)}$$

$$\mathrm{y_m} = r_m \cos\beta_m \sin\phi_m \qquad \textit{Eq (3.2)}$$

$$\mathrm{z_m} = r_m \sin\beta_m \qquad \textit{Eq (3.3)}$$

$$\mathrm{x_b} = \mathrm{x_m} + d\ , \qquad \mathrm{x_b} = r_b \cos\beta_b \cos\phi_b \qquad \textit{Eq (3.4)}$$

$$\mathrm{y_b} = \mathrm{y_m}\ , \qquad \mathrm{y_b} = r_b \cos\beta_b \sin\phi_b \qquad \textit{Eq (3.5)}$$

$$\mathrm{z_b} = \mathrm{z_m} + h_t\ , \qquad \mathrm{z_b} = r_b \sin\beta_b \qquad \textit{Eq (3.6)}$$

We mainly exploit reflection, refraction, and scattering phenomena over the microwave frequency band for 2G, 3G, and 4G land mobile radio networks, from $0.9 - 10$ GHz, i.e., 33cm to 3cm wavelength. At this range of wavelength, the radio waves do not have any significant variation in their propagation characteristics except attenuations that increases gradually, and almost all the scattering structures in the propagation environment appear to be big opaque or quasi-opaque ellipsoids, which reflect, refract, and scatter the incident radio waves [13].

The elevated BS, equipped with a flat-top directional antenna with unity gain (which is a common assumption used in the literature [26–28, 30, 48]), is mounted at height h_t. The directional antenna at BS is assumed as capable of computing the precise azimuth angle of MS's location and steer the antenna pattern in the direction of MS with optimum Signal-to-Noise Ratio (SNR), which can be accomplished with a linear antenna array by adaptively applying the phase weights across the elements of array [65, 66]. The beam-width of antenna at BS is controllable in horizontal plane, with its angular beam-width of 2α. Whereas, for a certain horizontal beam-width α, the vertical beam-width is fixed to illuminate all the scattering region in vertical plane.

In Fig. 3.1, $\alpha_{\max}$ is the maximum beam-width of directional antenna which illuminates the whole scattering semi-spheroid and can be expressed as

$$\alpha_{\max} = \arcsin\left(\frac{a}{d}\right) \qquad \textit{Eq (3.7)}$$

The directional antenna at BS results in clipping of scattering region and the illuminated scattering region seen in its beam is shown by I_{Region}. Furthermore the scattering semi-spheroid is composed of sub-regions i.e., R_1, R_2, R_3, R_4 and R_5, as shown in Fig. 3.2. The beam of directional antenna illuminates only the scatterers present in region R_1, R_2 and R_3 (i.e. I_{Region}) and does not illuminate the eliminated scattering region that consists of R_4 and R_5, (i.e. E_{Region}).

The portions R_1, R_2 and R_3 of the illuminated region can further be grouped into two partitions, i.e., R_2 alone and the union of R_1 and R_3. The angles ϕ_1 and ϕ_2 shown in Fig. 3.2 and 3.3 are calculated to separate among the above-mentioned two partitions for zero elevation plane. Therefore, the angles ϕ_1 and ϕ_2 can be expressed as,

$$\phi_1 = \phi_{t1}\Big|_{\beta_m=0^o}, \qquad \phi_2 = \phi_{t2}\Big|_{\beta_m=0^o}$$

which can be obtained as,

$$\left.\begin{matrix}\phi_1 \\ \phi_2\end{matrix}\right\} = \cos^{-1}\left(\frac{d}{a}\sin^2\alpha \pm \left(\frac{\cos\alpha}{a}\sqrt{a^2-(d\sin\alpha)^2}\right)\right) \qquad \textit{Eq (3.8)}$$

The threshold angles ϕ_{t1} and ϕ_{t2} are derived to separate among the said two partitions for a certain elevation angle β_m. These threshold angles are found to be the functions of elevation angle β_m and the beam-width α which can be expressed as,

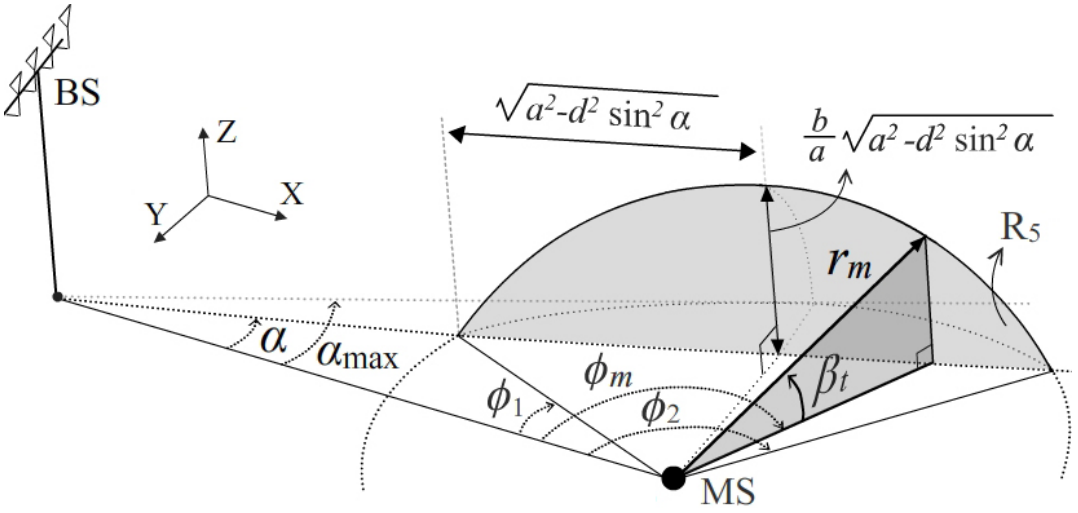

FIGURE 3.3: Threshold angles in azimuth plane

$$\phi_{t1} = \begin{cases} \arccos\left(\dfrac{d\sin^2\alpha}{a\cos\beta_m} + \dfrac{\cos\alpha}{a\cos\beta_m}\sqrt{(a\cos\beta_m)^2 - (d\sin\alpha)^2}\right) \\ \qquad\qquad ; \quad 0 \le \beta_m < \arccos\left(\frac{d\sin\alpha}{a}\right) \\ (\pi/2) - \alpha \qquad ; \quad \arccos\left(\frac{d\sin\alpha}{a}\right) \le \beta_m \le \pi/2 \end{cases} \qquad \textit{Eq (3.9)}$$

$$\phi_{t2} = \begin{cases} \arccos\left(\dfrac{d\sin^2\alpha}{a\cos\beta_m} - \dfrac{\cos\alpha}{a\cos\beta_m}\sqrt{(a\cos\beta_m)^2 - (d\sin\alpha)^2}\right) \\ \qquad\qquad ; \quad 0 \le \beta_m < \arccos\left(\frac{d\sin\alpha}{a}\right) \\ (\pi/2) - \alpha \qquad ; \quad \arccos\left(\frac{d\sin\alpha}{a}\right) \le \beta_m \le \pi/2 \end{cases} \qquad \textit{Eq (3.10)}$$

The angles ϕ_{t1} and ϕ_{t2} for elevation angle β_m are plotted in Fig. 3.4 (a). The angle β_t shown in Fig. 3.3, separates among the said two partitions in elevation plane.

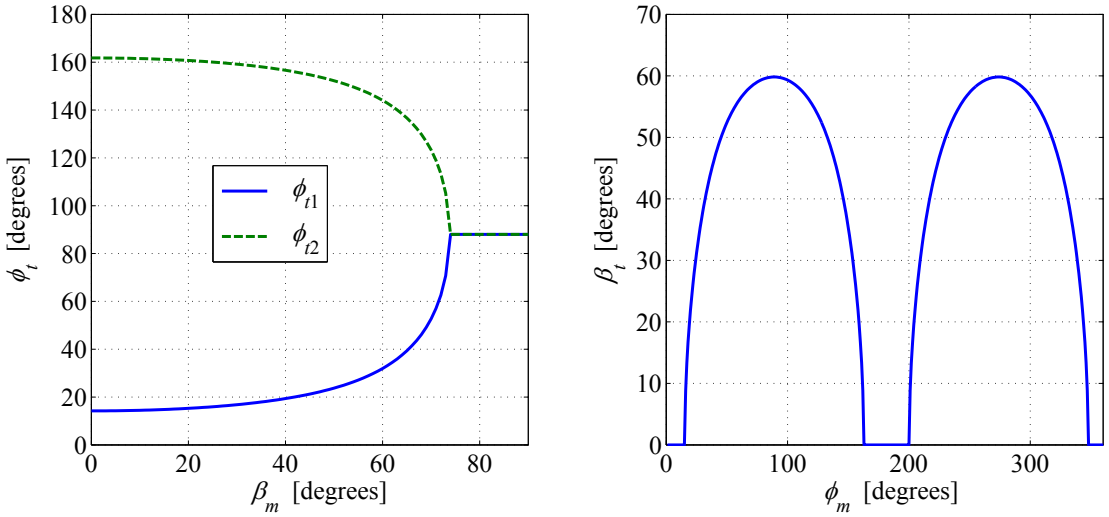

FIGURE 3.4: Threshold angles. (a) Threshold angles ϕ_{t1} and ϕ_{t2} with respect to β_m, (b) The threshold angle β_t with respect to ϕ_m, ($h_t = 100$m, $d = 800$m, $a = 100$m, $b = 50$m and $\alpha = 2^o$)

This angle is found to be the function of azimuth angle ϕ_m and the beam-width α. The angle β_t can be expressed in its simplified form as,

$$\beta_t = \begin{cases} \cot^{-1}\left(\dfrac{ad\csc(\alpha+\phi_m)\sin\alpha}{b\sqrt{a^2 - d^2\csc^2(\alpha+\phi_m)\sin^2\alpha}}\right) \\ \qquad\qquad ; \quad \phi_1 \leq |\phi_m| \leq \phi_2 \\ 0 \qquad\qquad ; \quad \text{otherwise} \end{cases} \qquad \textit{Eq (3.11)}$$

The threshold angle β_t w.r.t. azimuth angle ϕ_m is plotted in Fig. 3.4 (b). The limits for illuminated region (R_1, R_2 and R_3) are defined in correspondence with azimuth and elevation angles. As discussed earlier, the R_1 and R_3 are grouped in partition P_1 as

$$P_1 \rightarrow R_1 \& R_3 \rightarrow \left\{ \begin{array}{c} 0 \leq \beta_m \leq \beta_t \\ \text{or} \\ \phi_{t1} \leq |\phi_m| \leq \phi_{t2} \end{array} \right\} \qquad \textit{Eq (3.12)}$$

Furthermore, the limits for partition P_2 are

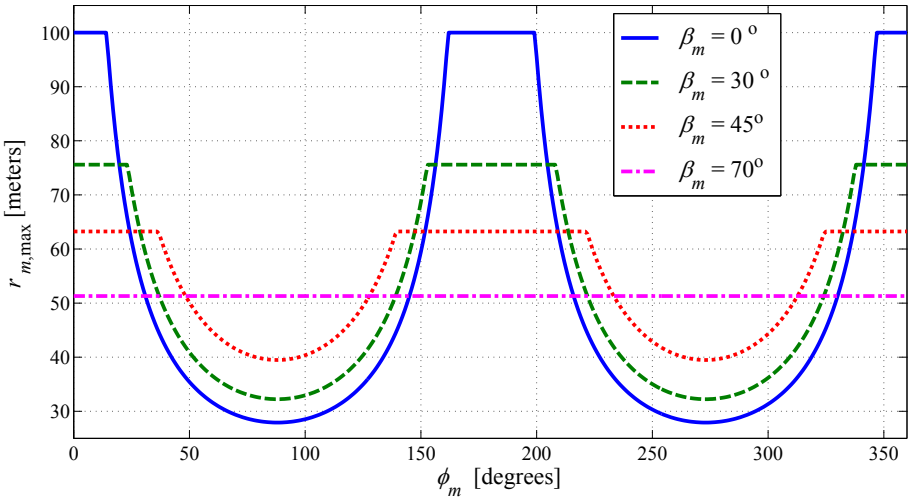

FIGURE 3.5: Radius $r_{m,\max}$ as joint function of ϕ_m and β_m, $(h_t = 100\text{m}, d = 800\text{m}, a = 100\text{m}, b = 50\text{m}$ and $\alpha = 2^o)$

$$P_2 \rightarrow R_2 \rightarrow \left\{ \begin{array}{c} \beta_t < \beta_m \leq \dfrac{\pi}{2} \\ \text{or} \\ -\phi_{t1} \leq \phi_m \leq \phi_{t1} \\ \text{or} \\ \phi_{t2} \leq \phi_m \leq -\phi_{t2} \end{array} \right\} \qquad \textit{Eq (3.13)}$$

The distance of MS from the scattering objects at the boundary of scattering region is $r_{m,\max}$, which is found as function of angles seen at MS (i.e. ϕ_m and β_m), is written below for both the partitions of I_{Region}, as

$$r_{m,\max}(\phi_m, \beta_m, \alpha) = \begin{cases} d \csc(\alpha + \phi_m) \sec \beta_m \sin \alpha & ; P_1 \\ \sqrt{\dfrac{a^2 b^2}{b^2 \cos^2 \beta_m + a^2 \sin^2 \beta_m}} & ; P_2 \end{cases} \qquad \textit{Eq (3.14)}$$

The distance of the scattering object from the MS and the BS is r_m and r_b, respectively. Hence, the propagation path's length that the radio signal has to travel in both uplink and downlink can be expressed as,

$$l = r_b + r_m \qquad \textit{Eq (3.15)}$$

The distance r_b can be written in simplified form as,

$$r_b = \sqrt{r_m^2 + l_{\text{LoS}}^2 - 2r_m(d\cos\beta_m\cos\phi_m + h_t\sin\beta_m)} \qquad \textit{Eq (3.16)}$$

where, l_{LoS} is the length of LoS multipath component (i.e., shortest propagation path between MS and BS), which is different from the horizontal LoS distance d between MS and BS.

$$l_{\text{LoS}} = \sqrt{d^2 + h_t^2} \qquad \textit{Eq (3.17)}$$

The longest propagation path between MS and BS is, $l_{\max} = a + \sqrt{h_t^2 + (d+a)^2}$. By substituting *Eq (3.16)* in *Eq (3.15)*, the simplified solution for r_m can be written as,

$$r_m = \frac{l^2 - l_{\text{LoS}}^2}{2(l - d\cos\beta_m\cos\phi_m - h_t\sin\beta_m)} \qquad \textit{Eq (3.18)}$$

The following limits are very essential in the proposed 3-D model, as they govern the basic simplification operations.

$$0 \le \phi_m < 2\pi, \quad 0 \le \beta_m \le \frac{\pi}{2}, \quad 0 \le \beta_t \le \frac{\pi}{2}$$

$$0 \le |\phi_{t1}| \le \arccos\left(\tfrac{a\cos\beta_m}{d}\right), \ \arccos\left(\tfrac{a\cos\beta_m}{d}\right) \le |\phi_{t2}| \le \pi$$

The proposed 3-D scattering environment containing MS, BS and scatterers is shown in Fig. 3.6. Top view of the same environment is reproduced in Fig. 3.7 to

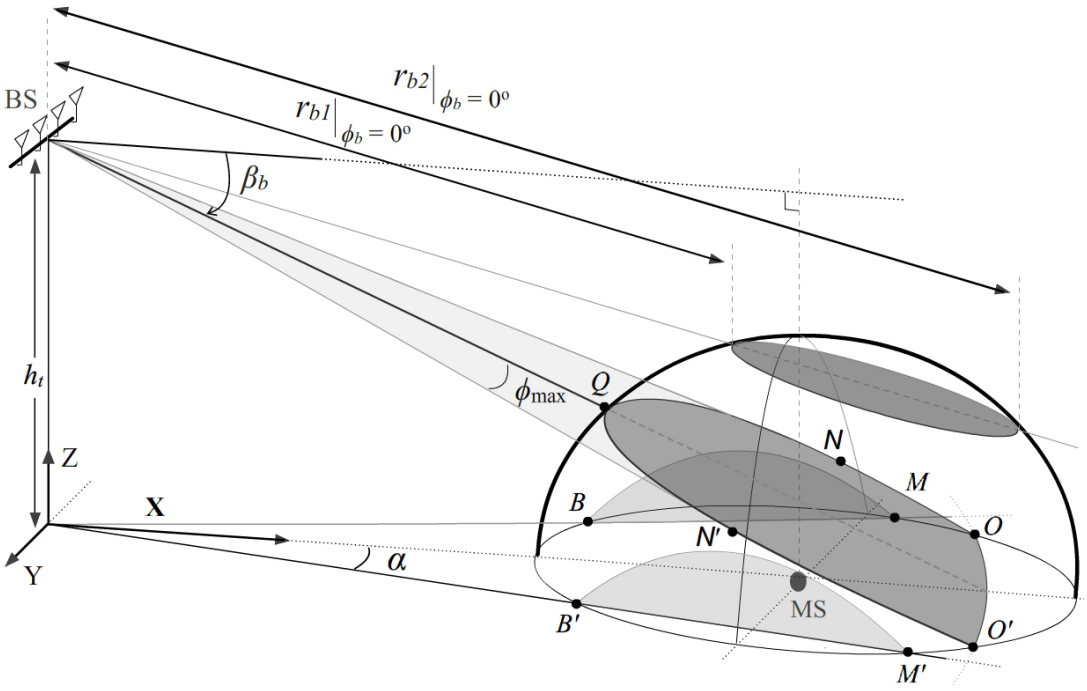

FIGURE 3.6: Geometrical composition of illuminated planes of scatterers for different elevation angles β_b.

elaborate the geometry of the scattering regions. The distance ρ_b is the projection of r_b on azimuth plane which can be defined as, $\rho_b = r_b \cos\beta_b$. For a particular direction defined by ϕ_b and β_b, the distance from the BS to the intersection points of semi-spheroid are taken as r_{b1} and r_{b2}. The plane developed by the longitudinal crossection of conical beam for different values of β_b is varied. If the varying geometry containing the illuminated plane of scatterers is analyzed, we see that before it touches the ground, the geometry forms spherical segments of varying dimensions (see Fig. 3.6). If the process of varying β_b is continued after the illuminated scattering plane touches the ground, the shape of the plane become some area bounded by the arcs $\overline{NQN'}$, $\overline{NO}$, $\overline{OO'}$, and $\overline{O'N'}$, as shown in Fig. 3.7. Arc $\overline{OO'}$ increases from its initial value of zero, to its maximum at the far edge of the scattering semi-spheroid and then reduces gradually to zero at point Q. ϕ_c is the half of the angle subtended by the arc $\overline{OO'}$, which can be written in simplified form [22] as

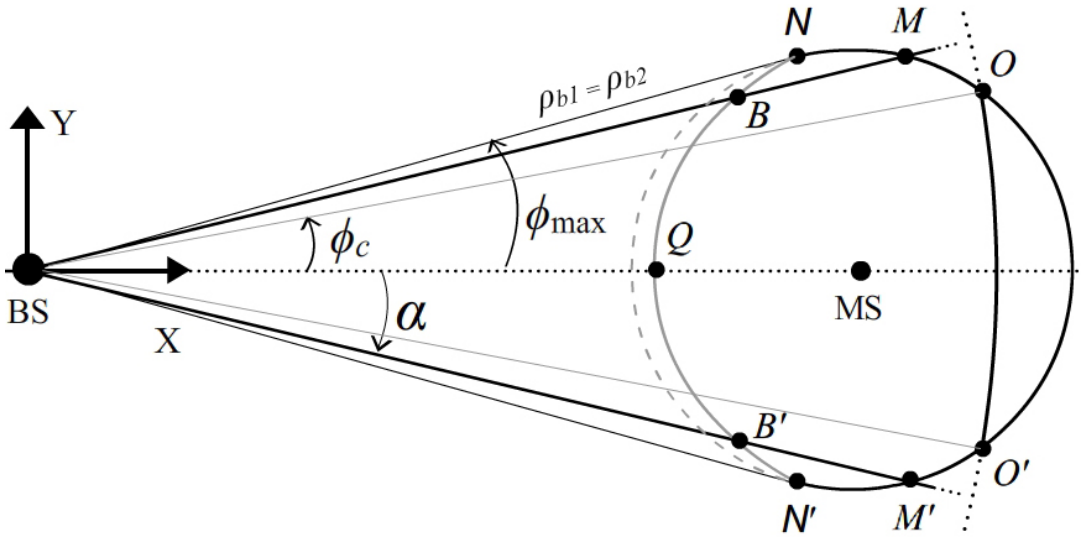

FIGURE 3.7: Top view of the proposed scattering environment.

$$\phi_c = \arccos\left(\frac{h_t^2 + (d^2 - a^2)\tan^2\beta_b}{2dh_t \tan\beta_b}\right) \qquad \textit{Eq (3.19)}$$

The angle ϕ_c takes values from zero to $\phi_{\max}$, where $\phi_{\max}$ is the maximum azimuth angle for some particular elevation angle β_b, [22] as

$$\phi_{\max} = \arccos\left(-\frac{a^2}{db^2}h_t \tan\beta_b + \frac{1}{d}\sqrt{\left(d^2 - a^2 + \frac{a^2}{b^2}h_t^2\right)\left(1 + \frac{a^2}{b^2}\tan^2\beta_b\right)}\right) \qquad \textit{Eq (3.20)}$$

The distances ρ_{b1} and ρ_{b2} are the projections of r_{b1} and r_{b2} on the azimuth plane respectively. The distance ρ_{b1} follows the arc $\overline{NQN'}$ in Fig. 3.7. The distance ρ_{b2} follows three different arcs $\overline{NO}$, $\overline{OO'}$, and $\overline{O'N'}$ depending upon two different limits of ϕ_b. The distances ρ_{b1} and ρ_{b2} can be written in closed-form as in *Eq (3.21)* and *Eq (3.22)*, respectively.

$$\rho_{b1} =$$

$$\frac{1}{b^2 + a^2 \tan^2 \beta_b} \left(a^2 h_t \tan \beta_b + b^2 d \cos \phi_b \right.$$

$$\left. - b \sqrt{(a^2 - d^2)(b^2 + a^2 \tan^2 \beta_b) + a^2 (2 d h_t \cos \phi_b \tan \beta_b - h_t^2) + b^2 d^2 \cos^2 \phi_b} \right)$$

Eq (3.21)

$$\rho_{b2} =$$

$$\begin{cases} \dfrac{1}{b^2 + a^2 \tan^2 \beta_b} \left(a^2 h_t \tan \beta_b + b^2 d \cos \phi_b \right. & \\ \left. + b \sqrt{(a^2 - d^2)(b^2 + a^2 \tan^2 \beta_b) + a^2 (2 d h_t \cos \phi_b \tan \beta_b - h_t^2) + b^2 d^2 \cos^2 \phi_b} \right) & \\ & ; \quad \phi_c \leq \phi_b \leq \phi_{\max} \\ \dfrac{h_t}{\tan \beta_b} & ; \quad 0 < \phi_b < \phi_c \quad \text{or} \quad \beta_b \geq \arctan \left(\dfrac{h_t}{\sqrt{d^2 - a^2}} \right) \end{cases}$$

Eq (3.22)

If the azimuth angle ϕ_b is taken equal to $\phi_{\max}$, the distances ρ_{b1} and ρ_{b2} become equal. The side views of the proposed 3-D scattering model is shown in Fig. 3.8. The angles $\beta_{\min}$ and $\beta_{\max}$ define the limits for the arrival of multipaths in elevation plane, which can be expressed as

$$\beta_{\min} = \arctan \left(\frac{h_t d - \sqrt{h_t^2 a^2 + b^2 (d^2 - a^2)}}{d^2 - a^2} \right) \qquad \textit{Eq (3.23)}$$

$$\beta_{\max} = \arctan \left(\frac{h_t}{d - a} \right) \qquad \textit{Eq (3.24)}$$

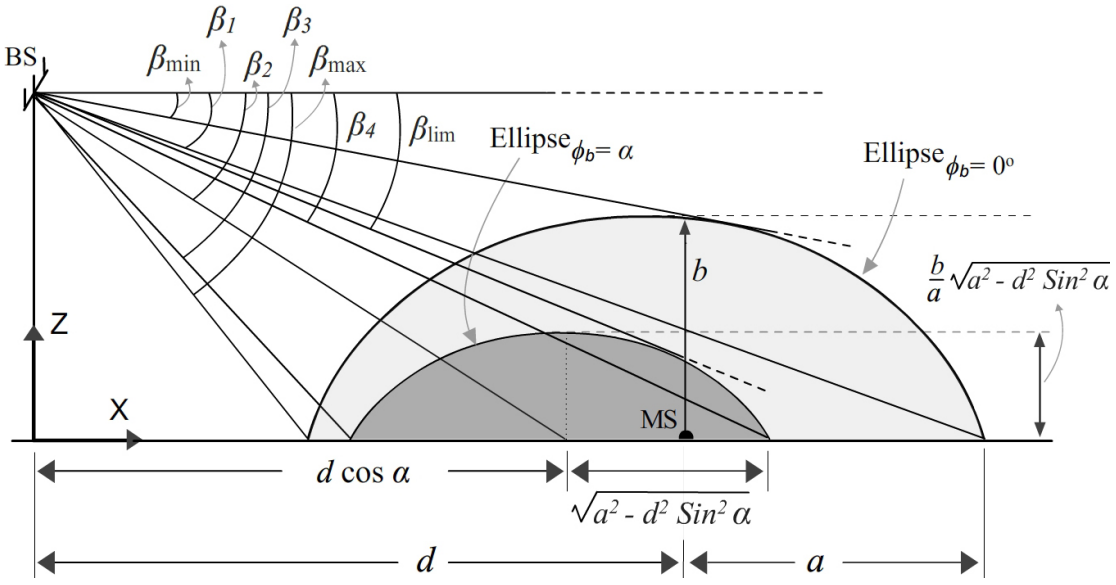

FIGURE 3.8: Side view of the proposed 3-D scattering model for ϕ_b = constant and varying elevation angle β_b.

The angle β_{lim} is the function of azimuthal beam-width α, which operates as a threshold angle to exert the effects of directional antenna on the geometry explained in Fig. 3.7 and Fig. 3.8, β_{lim} can be expressed in simplified form as

$$\beta_{\text{lim}} = \arctan\left(\frac{1}{\sqrt{2}\,a(a^2-d^2)}\left(-a\sqrt{2}\,dh_t\cos\alpha + \sqrt{(b^2d^2+a^2(h_t^2-b^2))(2a^2-d^2+d^2\cos(2\alpha))}\right)\right) \qquad \textit{Eq (3.25)}$$

The elevation angle for LoS path is denoted by β_{Los} and can be expressed as,

$$\beta_{\text{Los}} = \arctan\left(\frac{h_t}{d}\right) \qquad \textit{Eq (3.26)}$$

The angle β_1 corresponds to the elevation angle for the longest propagation path from BS to MS, and can be shown as

$$\beta_1 = \arctan\left(\frac{h_t}{d+a}\right) \qquad \textit{Eq (3.27)}$$

The angles β_2, β_3, and β_4 are seen when ϕ_b is set as α as shown in Fig. 3.8. These angles represent the rotated beam in azimuth plane to touch the boundary of the illuminated scattering region clipped by α, and can be expressed as,

$$\beta_2 = \arctan\left(\frac{h_t}{d\cos\alpha}\right) \qquad \textit{Eq (3.28)}$$

$$\beta_3 = \arctan\left(\frac{h_t}{d\cos\alpha - \sqrt{a^2 - d^2\sin^2\alpha}}\right) \qquad \textit{Eq (3.29)}$$

$$\beta_4 = \arctan\left(\frac{h_t}{d\cos\alpha + \sqrt{a^2 - d^2\sin^2\alpha}}\right) \qquad \textit{Eq (3.30)}$$

The maximum angle seen in azimuth plane for a fixed elevation angle, β_b, when α clips the boundary of illuminated scattering region, is other than $\phi_{\max}$, shown by ϕ_L as

$$\phi_L = \begin{cases} \phi_{\max} \quad ; \quad \beta_{\min} \leq \beta_b < \beta_{\lim} \\ \alpha \quad ; \quad \beta_{\lim} \leq \beta_b \leq \beta_{\max} \end{cases} \qquad \textit{Eq (3.31)}$$

3.3 Distribution of Scatterers

3.3.1 Uniform Scatter Density

The volume of I_{Region} is V which can be expressed as

$$V = V_{\text{semi-spheroid}} - 2V_1 \qquad \textit{Eq (3.32)}$$

Where, $V_{\text{spheroid}} = 4\pi a^2 b/3$ is the volume of full spheroid and $2V_1$ is the volume of E_{Region}. The volume V can be expressed as function of the beam-width, α, as

$$V = \frac{2\pi bd \sin\alpha \left(a^2 + d\sin\alpha(a - d\sin\alpha)\right)}{3a} \qquad \textit{Eq (3.33)}$$

If we substitute $\alpha = \alpha_{\max}$ in *Eq (3.33)*, the volume V of I_{Region} is found to be $V = 2\pi a^2 b/3$, which is the volume of the whole semi-spheroid (i.e. $V_{\text{spheroid}}/2$). When scatterers are uniformly distributed in illuminated region (I_{Region}) with volume V, then the SDF can be written as

$$f_U\left(\mathrm{x_m}, \mathrm{y_m}, \mathrm{z_m}\right) = \begin{cases} \dfrac{1}{V} & ;\ (\mathrm{x_m}, \mathrm{y_m}, \mathrm{z_m}) \in I_{\text{Region}} \\ 0 & ;\ \text{otherwise} \end{cases} \qquad \textit{Eq (3.34)}$$

3.3.2 Gaussian Scatter Density

The proposed 3-D propagation model is shown in Fig. 3.9. The deviation of Gaussian distributed scattering region around MS in horizontal and vertical planes is symbolized by σ_a and σ_b, respectively. Hence the deviation can independently be controlled in horizontal and vertical planes. The deviation of scatterers at every independent elevation angle can be expressed as,

$$\sigma(\phi_m, \beta_m) = \sqrt{\frac{\sigma_a^2 \sigma_b^2}{\sigma_b^2 \cos^2\beta_m + \sigma_a^2 \sin^2\beta_m}} \qquad \textit{Eq (3.35)}$$

As in Gaussian distribution, the region from -4σ to $+4\sigma$ encloses the 99.99% of energy. Therefore, the virtual boundary of scattering region is shown at 4σ distance from MS. The azimuthal beam-width of directional antenna at BS is shown by α. Whereas, the maximum beam-width of directional antenna to illuminate the 99.99% of scattering region should be at least $\alpha_{\max} = \arcsin(4\sigma_a/d)$.

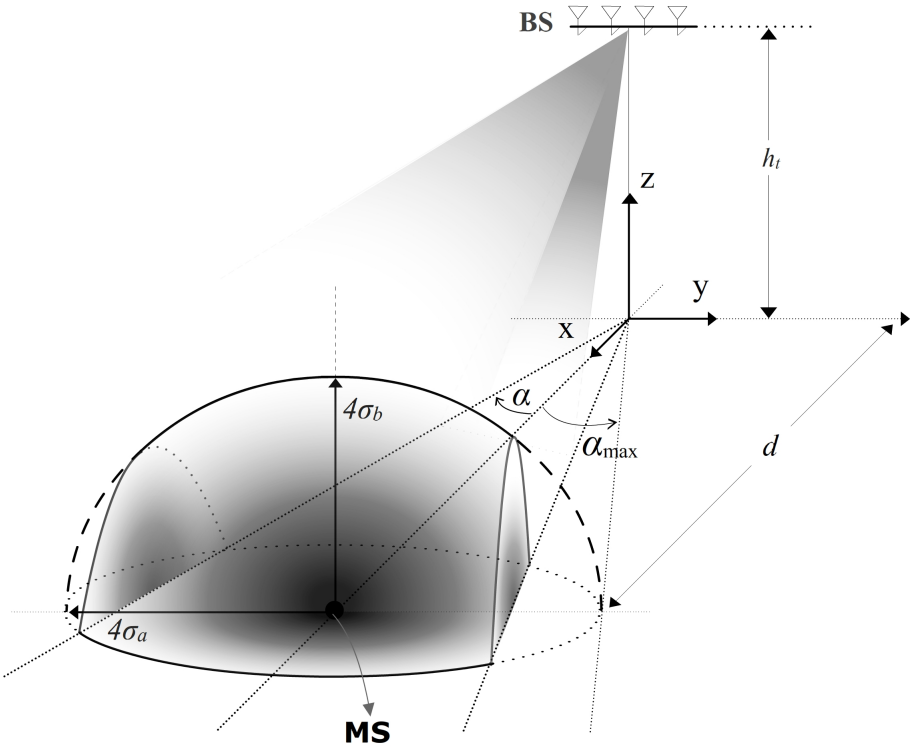

FIGURE 3.9: Proposed 3-D model with Gaussian distributed scatters around MS.

Therefore, any beam-width less than $\alpha_{\max}$ results in clipping of scattering region, which further corresponds to the reduced number of multipath signals arrivals. Hence, the number of Gaussian distributed scatterers corresponding to the arrival of multipath signals can be found as function of beam-width α, as

$$E(\alpha) = \frac{4}{3}\pi\sigma_b\left(\exp\left(-\frac{d^2\sin^2\alpha}{\sigma_a^2}\right)\left(d^2 - 32\sigma_a^2 - d^2\cos(2\alpha)\right)\operatorname{erfc}\left(\frac{d\sin\alpha}{\sigma_a\sqrt{2}}\right) + 32\sigma_a^2\right) \quad \textit{Eq (3.36)}$$

where, erfc(.) is the standard complementary error function. By substituting $\alpha = \alpha_{\max}$ in *Eq (3.36)*, the equation reduces to $E = 128\pi\sigma_a^2\sigma_b/3$, which is the volume of scattering region with virtual semi-spheroid shaped boundary at 4σ. The

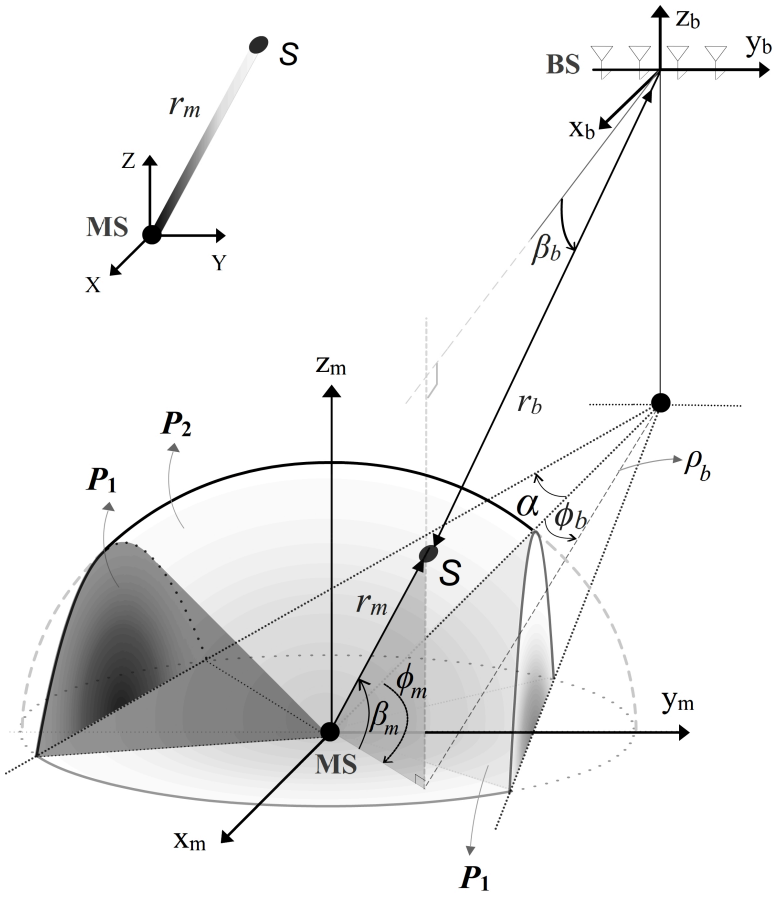

FIGURE 3.10: Proposed 3-D model with Gaussian scatter density.

illuminated scattering region seen in the beam of directional antenna is further divided into two partitions i.e. P_1 and P_2, as shown in Fig. 3.10. To differentiate among these two partitions in azimuth plane, the top view of the proposed model is shown in Fig. 3.11. The azimuth threshold angles ϕ_{t1} and ϕ_{t2} shown in Fig. 3.11 are given in *Eq (3.9)* and *Eq (3.10)*, which can be obtained for the case of Gaussian scatter density by substituting $a = 4\sigma_a$ and $b = 4\sigma_b$ in *Eq (3.9)* and *Eq (3.10)*.

Similarly, to separate among the said two partitions (i.e. P_1 and P_2) in elevation plane, the angle β_t given in *Eq (3.11)* can be used for the case of Gaussian scatter density by substituting $a = 4\sigma_a$ and $b = 4\sigma_b$.

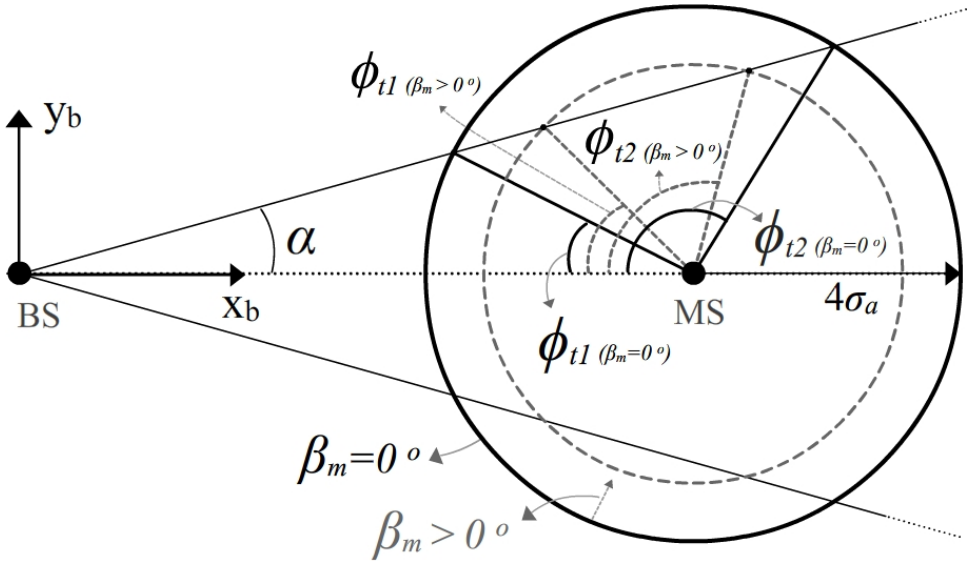

FIGURE 3.11: Top view of proposed 3-D model demonstrating the azimuth threshold angles ϕ_{t1} and ϕ_{t2}

In the case of Gaussian scatter density, the majority of scattering objects are concentrated in the regions near around the MS. The density of scatterers decreases with the increase in distance from MS by following the Gaussian density function. Hence, the scatter density function (SDF) can be expressed as,

$$f_G(\mathrm{x_m}, \mathrm{y_m}, \mathrm{z_m}) = \begin{cases} \dfrac{1}{E} & ; \quad (\mathrm{x_m}, \mathrm{y_m}, \mathrm{z_m}) \in I_{\mathrm{Region}} \\ 0 & ; \quad \text{otherwise} \end{cases} \qquad \textit{Eq (3.37)}$$

where, E is the number of Gaussian distributed scatterers illuminated in the beam of directional antenna at BS.

The distance of MS from the boundary of scattering region is $r_{m,\max}$. The number of scattering objects (effective strength) at a particular direction can be found using Gaussian distribution, as

$$N_{m,\max}(\phi_m, \beta_m) = 8\sigma \int_0^{r_{m,\max}} \frac{1}{\sigma\sqrt{2\pi}} \exp\left(-\frac{x^2}{2\sigma^2}\right) \quad \mathrm{d}x \qquad \textit{Eq (3.38)}$$

The above equation for both the partitions of illuminated scattering region can be expressed in closed-form as,

$$N_{m,\max}(\phi_m, \beta_m) = \begin{cases} 4\sigma \text{ erf}\left(\dfrac{d \csc(\alpha + \phi_m) \sin\alpha}{2\sigma \cos\beta_m}\right) & ; P_1 \\ 4\sigma & ; P_2 \end{cases} \qquad \textit{Eq (3.39)}$$

where, $-\pi \leq \phi_m < \pi$, $0 \leq \beta_m \leq \pi/2$, and erf(.) is the standard error function.

The Gaussian scatterer density function can be found as,

$$f_G(\mathrm{x_m}, \mathrm{y_m}, \mathrm{z_m}) = \frac{1}{(2\pi\sigma^2)^{3/2}} \exp\left(-\frac{\mathrm{x_m}^2}{2\sigma^2} - \frac{\mathrm{y_m}^2}{2\sigma^2} - \frac{\mathrm{z_m}^2}{2\sigma^2}\right) \qquad \textit{Eq (3.40)}$$

where, $\mathrm{x_m}$, $\mathrm{y_m}$, and $\mathrm{z_m}$ are given in *Eq (A.2)*, *Eq (A.3)*, and *Eq (A.4)*, respectively.

3.4 Summary

In this chapter, a 3-D scattering model has been proposed, which assumes a directional antenna with controllable azimuthal beam-width employed at an elevated BS. The scattering objects have been assumed to be confined within a semi-spheroid shaped region with its base centered at MS. The radius of semi-spheroid region is independently controllable along with its major and minor axes. Both uniform and Gaussian distribution functions have been considered to model the scattering objects.

The directional antenna at BS results in the clipping of scattering region and only the illuminated scattering objects correspond to the arrival of waves at receiver. The effects of directional antenna at BS on the geometry of scattering region has thoroughly been investigated and various threshold angular parameters have been established to separate among the partitions of illuminated and eliminated scattering regions.

Chapter 4

SPATIO-TEMPORAL STATISTICS OF RADIO COMMUNICATION LINKS

In this Chapter, spatial and temporal statistics of the radio link for the proposed 3-D propagation model are derived. The effects of directional antenna are thoroughly observed on spatial and temporal characteristics of the proposed model. Closed-form expressions for joint and marginal PDFs of AoA seen at MS and BS in correspondence with azimuth and elevation angles are derived. Furthermore, closed-form expressions for propagation path delays and trivariate joint PDFs of ToA seen at MS and BS in correspondence with azimuth and elevation angles are derived. Moreover, theoretical results along with observations are shown that illustrate the effects of directional antenna on the spatio-temporal statistics of the proposed 3-D model. All the characteristics of the communication channel are derived for both ends of the radio link (i.e. observed at MS and BS). Spatio-temporal statistics of the channel are derived for both uniform and Gaussian scatter densities in Section 4.1 and Section 4.2, respectively.

4.1 Channel Characteristics For Uniform Scatter Density

4.1.1 Spatial Characteristics of Radio Channel

In this section, we derive the joint and marginal PDFs of AoA seen at MS and BS in Section 4.1.1.1 and Section 4.1.1.2 respectively.

4.1.1.1 PDF of AoA at MS

The Joint density function as a function of angles seen at MS and radius r_m can be found as,

$$p\left(r_m, \phi_m, \beta_m\right) = \frac{f_U\left(\mathrm{x_m}, \mathrm{y_m}, \mathrm{z_m}\right)}{\mid J\left(\mathrm{x_m}, \mathrm{y_m}, \mathrm{z_m}\right) \mid} \Bigg|_{\substack{\mathrm{x_m} = r_m \cos\beta_m \cos\phi_m \\ \mathrm{y_m} = r_m \cos\beta_m \sin\phi_m \\ \mathrm{z_m} = r_m \sin\beta_m}} \qquad \textit{Eq (4.1)}$$

The Jacobian transformation $J(\mathrm{x_m}, \mathrm{y_m}, \mathrm{z_m})$ given in *Eq (4.1)* can be expressed (refer to Section A.1) as

$$J\left(\mathrm{x_m}, \mathrm{y_m}, \mathrm{z_m}\right) = \begin{vmatrix} \cos\beta_m \cos\phi_m & -r_m \cos\beta_m \sin\phi_m & -r_m \sin\beta_m \cos\phi_m \\ \cos\beta_m \sin\phi_m & r_m \cos\beta_m \cos\phi_m & -r_m \sin\beta_m \sin\phi_m \\ \sin\beta_m & 0 & r_m \cos\beta_m \end{vmatrix}^{-1} \qquad \textit{Eq (4.2)}$$

$$J\left(\mathrm{x_m}, \mathrm{y_m}, \mathrm{z_m}\right) = \frac{1}{r_m^2 \cos\beta_m} \qquad \textit{Eq (4.3)}$$

Substituting *Eq (A.10)* and *Eq (3.34)* in *Eq (4.1)*, the joint density function can be rewritten as

$$p\left(r_m, \phi_m, \beta_m\right) = \frac{r_m^2 \cos\beta_m}{V} \qquad \textit{Eq (4.4)}$$

The closed-form expression for the joint PDF of AoA for azimuth and elevation angles is then found by integrating *Eq (4.4)* over r_m for appropriate limits

$$p\left(\phi_m, \beta_m\right) = \frac{1}{V} \int_0^{r_{m,\max}} r_m^2 \cos\beta_m \, \mathrm{d}_{r_m} \qquad \textit{Eq (4.5)}$$

$$p\left(\phi_m, \beta_m\right) = \frac{r_m^3 \cos\beta_m}{3V} \Bigg|_0^{r_{m,\max}} \qquad \textit{Eq (4.6)}$$

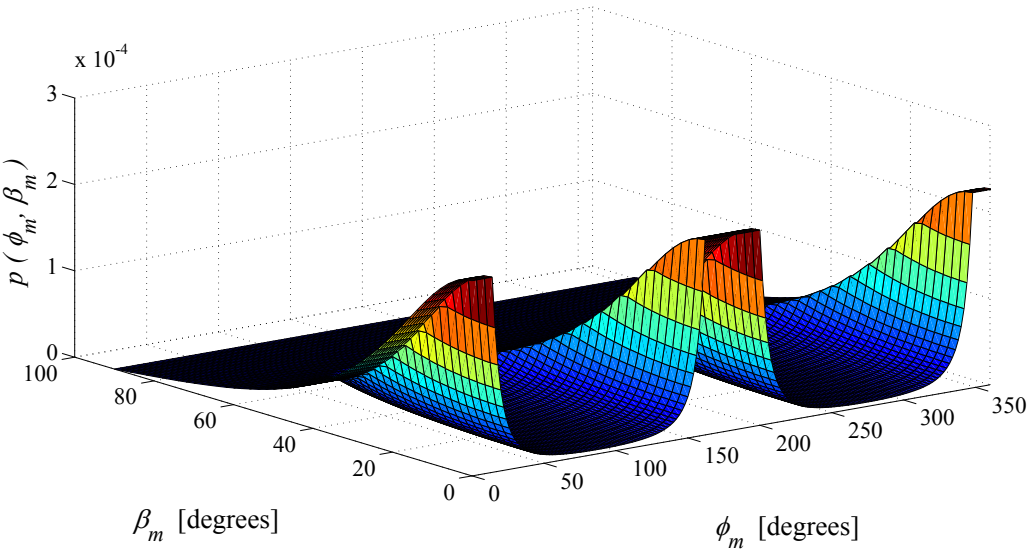

FIGURE 4.1: Joint PDF of AoA observed at MS, ($h_t = 100$m, $d = 800$m, $a = 100$m, $b = 50$m and $\alpha = 2^o$)

The simplified solution can be expressed as,

$$p(\phi_m, \beta_m) = \begin{cases} \dfrac{ad^2 \csc^3(\alpha + \phi_m) \sec^2 \beta_m \sin^2 \alpha}{2\pi b \left(a^2 + d \sin\alpha \left(a - d \sin\alpha\right)\right)} & ; \ P_1 \\ \dfrac{a \cos\beta_m \csc\alpha \left(\frac{a^2 b^2}{b^2 \cos^2\beta_m + a^2 \sin^2\beta_m}\right)^{3/2}}{2\pi b d \left(a^2 + d \sin\alpha \left(a - d \sin\alpha\right)\right)} & ; \ P_2 \end{cases} \qquad Eq\ (4.7)$$

The joint PDF of AoA for both azimuth and elevation planes is plotted in Fig. 4.1. Furthermore, representation of the same joint PDF are shown in Fig. 4.2 and Fig. 4.3, where, only the azimuth and elevation planes are shown respectively, for particular elevation and azimuth angles. When beam-width of directional antenna at BS is set $\alpha \geq \alpha_{\max}$, the angle β_t become zero for the entire azimuth plane; therefore the whole scattering semi-spheroid get illuminated and the PDF of AoA with azimuth angles is seen uniformly distributed which becomes the case of 3-D model by Janaswamy in [22]. In Fig. 4.2, the PDF of AoA in azimuth plane gets uniformly distributed for $\beta_m \geq \beta_t$, where the PDFs are left non-normalized to elaborate the effects of directional antenna. Moreover, when β_m in the elevation

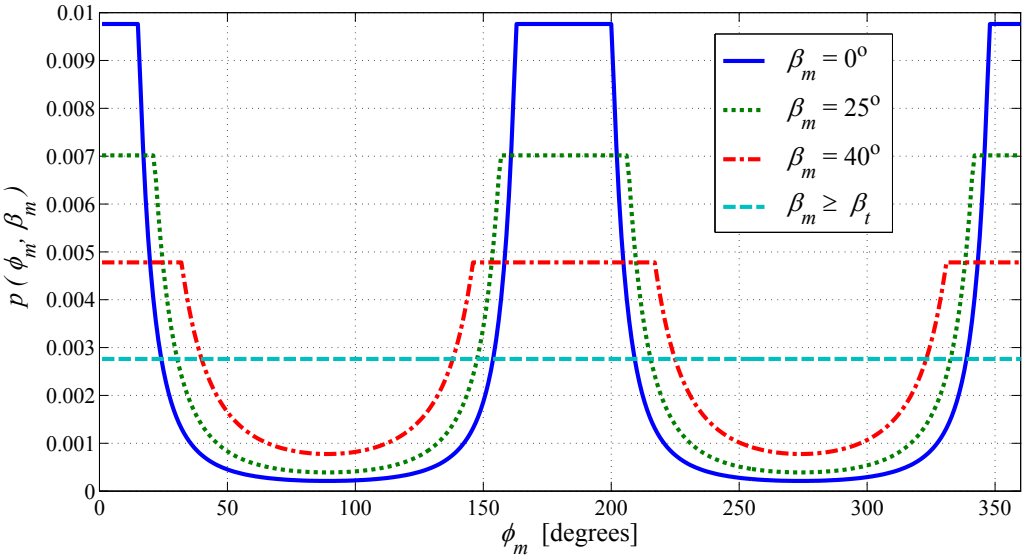

FIGURE 4.2: PDF of AoA in azimuth plane for different elevation angles, (h_t = 100m, d = 800m, a = 100m, b = 50m and $\alpha = 2^o$)

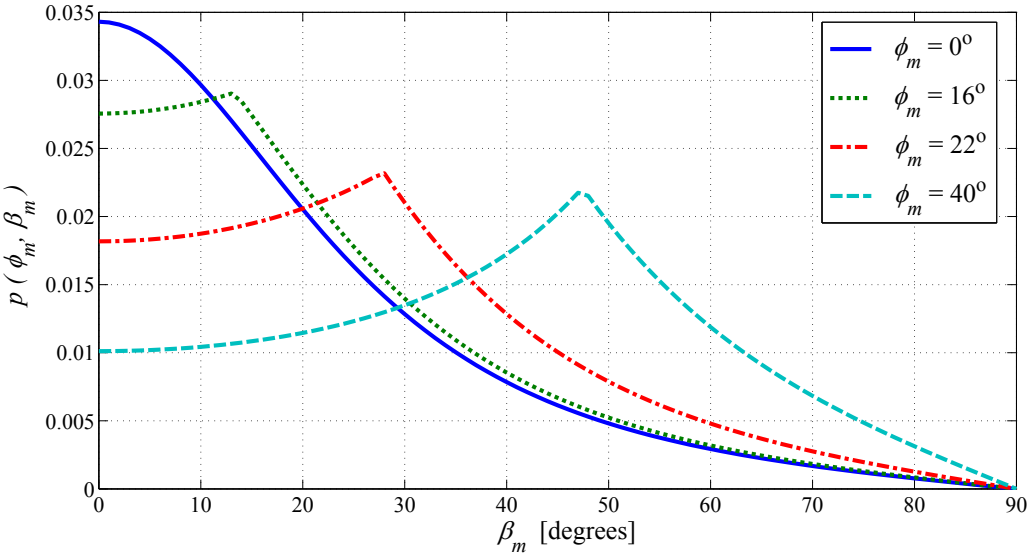

FIGURE 4.3: PDF of AoA in elevation plane for different azimuth angles, (h_t = 100m, d = 800m, a = 100m, b = 50m and $\alpha = 2^o$)

plane is substituted as zero, the PDF of AoA in azimuth plane is seen similar to that proposed by Petrus *et al.* in [26], shown in Fig. 4.2. The marginal PDF of azimuth AoA is found by integrating *Eq (4.7)* over β_m with appropriate limits, which is expressed as

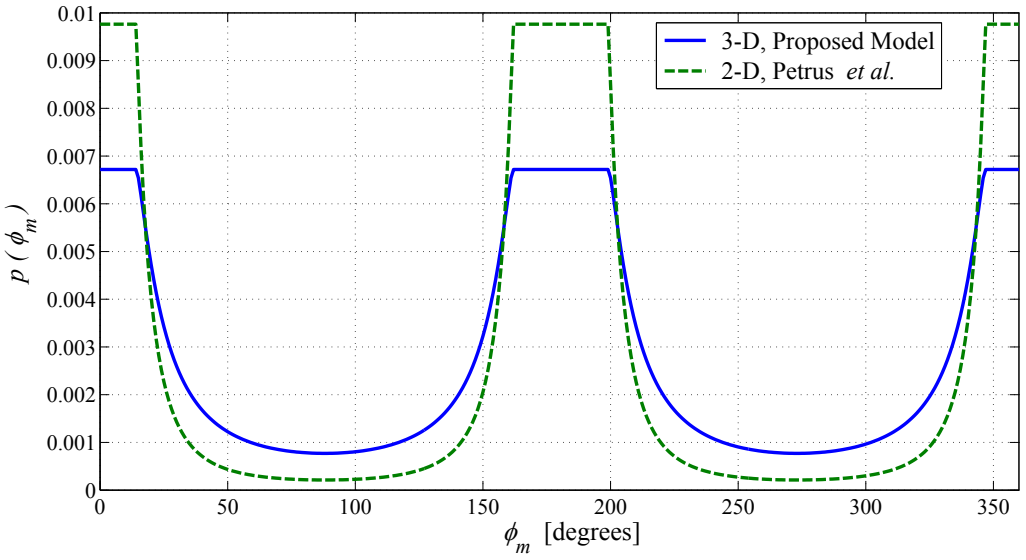

FIGURE 4.4: Marginal PDF of AoA in azimuth plane, (h_t = 100m, d = 800m, a = 100m, b = 50m and $\alpha = 2^o$)

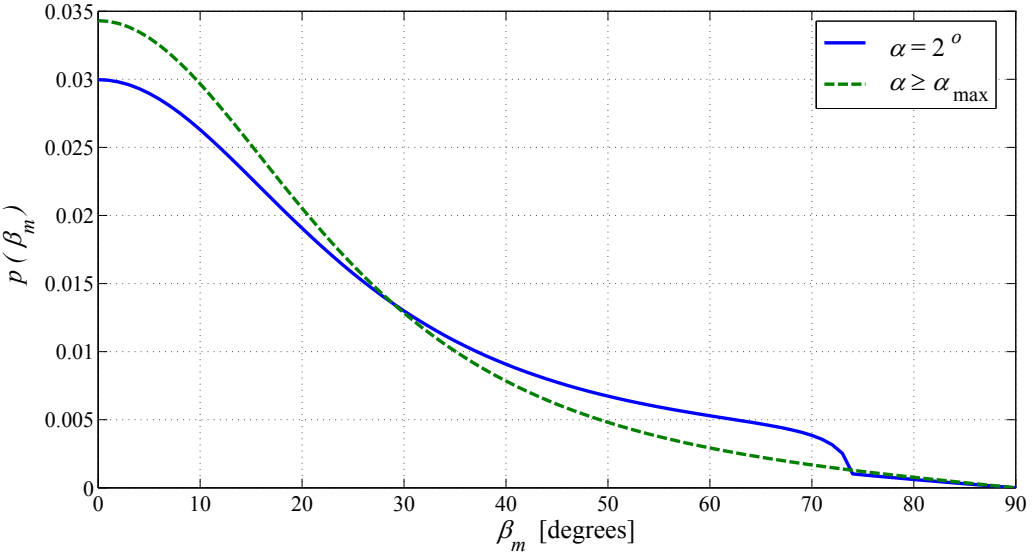

FIGURE 4.5: Marginal PDF of AoA in elevation plane for proposed model, (h_t = 100m, d = 800m, a = 100m and b = 50m)

$$p(\phi_m) = \int_0^{\beta_t} p(\phi_m, \beta_m)\Big|_{P_1} \mathrm{d}\beta_m + \int_{\beta_t}^{\pi/2} p(\phi_m, \beta_m)\Big|_{P_2} \mathrm{d}\beta_m \qquad \textit{Eq (4.8)}$$

The above equation can be rewritten in closed-form as

$$p\left(\phi_m\right) = \frac{1}{2\pi bd\left(a^2 + d\sin\alpha(a - d\sin\alpha)\right)}\Bigg\{ad^3\tan\beta_t\csc^3(\alpha+\phi_m) \times \sin^2\alpha + a^4 b\csc\alpha\left\{\frac{1}{a} - \frac{\sqrt{2}\sin\beta_t}{\sqrt{a^2+b^2+(b^2-a^2)\cos\left(2\beta_t\right)}}\right\}\Bigg\} \quad , \quad 0 \le \phi_m \le 2\pi \qquad \textit{Eq (4.9)}$$

Similarly, the marginal PDF in elevation is obtained by integrating *Eq (4.7)* over ϕ_m with appropriate limits,

$$p\left(\beta_m\right) = 2\int_{\phi_{t1}}^{\phi_{t2}} p\left(\phi_m,\beta_m\right)\Big|_{P_1}\mathrm{d}\phi_m + \int_{-\phi_{t1}}^{\phi_{t1}} p\left(\phi_m,\beta_m\right)\Big|_{P_2}\mathrm{d}\phi_m + \int_{\phi_{t2}}^{-\phi_{t2}} p\left(\phi_m,\beta_m\right)\Big|_{P_2}\mathrm{d}\phi_m \qquad \textit{Eq (4.10)}$$

The above equation can be rewritten in closed-form as,

$$p\left(\beta_m\right) = \frac{1}{bd\pi\left(a^2 + d\sin\alpha\left(a - d\sin\alpha\right)\right)}\Bigg\{\frac{ad^3\sec^2\beta_m\sin^2\alpha}{8} \times \Bigg(\frac{2}{\cos(\alpha+\phi_{t2})-1} - \frac{2}{1+\cos(\alpha+\phi_{t1})} + \csc^2\left(\frac{\alpha+\phi_{t1}}{2}\right) + \sec^2\left(\frac{\alpha+\phi_{t2}}{2}\right) + 4\ln\left(\cot\left(\frac{\alpha+\phi_{t1}}{2}\right)\tan\left(\frac{\alpha+\phi_{t2}}{2}\right)\right) + a\cos\beta_m\csc\alpha\left(\phi_{t1}+\phi_{t2}\right)\left(\frac{a^2b^2}{b^2\cos^2\beta_m + a^2\sin^2\beta_m}\right)^{3/2}\Bigg\} \quad , \; 0 \le \beta_m \le \pi/2 \qquad \textit{Eq (4.11)}$$

If we substitute zero for the elevation angle and h_t, the proposed 3-D model deduces to the 2-D model in [26]. In Fig. 4.4, the theoretical results of PDF of AoA in

azimuth plane for the proposed 3-D model are compared with those obtained for 2-D scattering model in [26]. The marginal PDF of AoA in elevation plane is shown in Fig. 4.5, which illustrates the effects of directional antenna on angular distribution. It is seen that when the beam-width of directional antenna is set as $\alpha_{\max}$, it illuminates the whole scattering semi-spheroid forcing the proposed model (for the case of uniform scatter density) to deduce to [22]. If, we set the azimuthal beam-width $\alpha \geq \alpha_{\max}$ and substitute equal values for major and minor dimensions of the scattering semi-spheroid (i.e. $b = a$) and $h_t = 0$, the proposed model deduces to the 3-D model proposed in [23].

4.1.1.2 PDF of AoA at BS

In this section, PDFs of AoA seen at BS are derived for the proposed 3-D macro-cell environment. The joint density function in correspondence with the angles seen at BS and the distance r_b can be expressed in a similar way as in *Eq (4.1)*, as

$$p\left(r_b, \phi_b, \beta_b\right) = \left. \frac{r_b^2 \cos\beta_b}{V} \right|_{\substack{r_b = \frac{\rho_b}{\cos\beta_b} \\ r_{b1} = \frac{\rho_{b1}}{\cos\beta_b} \\ r_{b2} = \frac{\rho_{b2}}{\cos\beta_b}}} \qquad \textit{Eq (4.12)}$$

The bivariate joint density function in azimuth and elevation angles, can be found by integrating *Eq (4.12)* over r_b from r_{b1} to r_{b2}, which can be expressed as

$$p\left(\phi_b, \beta_b\right) = \frac{\rho_{b2}^3 - \rho_{b1}^3}{3V\cos^2\beta_b} \qquad \textit{Eq (4.13)}$$

Volume of the illuminated scattering region V is derived earlier in *Eq (3.33)*, which when substituted in *Eq (4.13)* gives the simplified solution for the joint PDF of AoA, as

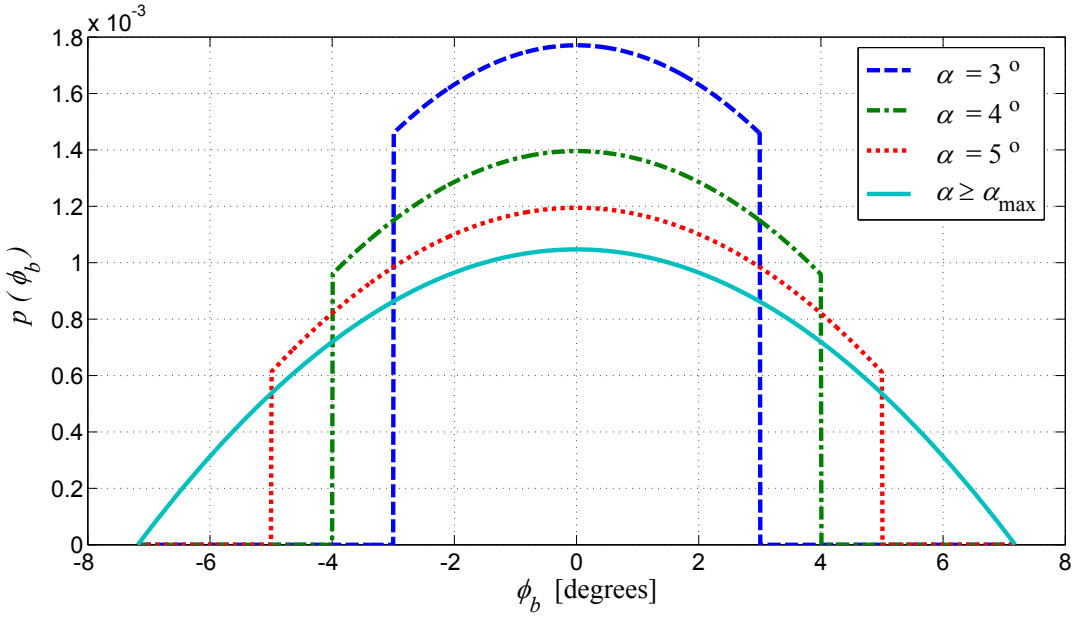

FIGURE 4.6: Marginal PDF of AoA in azimuth plane seen at BS, ($h_t = 100$m, $d = 800$m, $a = 100$m, $b = 50$m, and $\alpha_{\max} = \arcsin(a/d) = 7.18^{\circ}$)

$$p\left(\phi_b, \beta_b\right) = \begin{cases} \dfrac{a \csc\alpha \sec^2\beta_b \left(\rho_{b2}^3 - \rho_{b1}^3\right)}{2\pi b d \left(a^2 + d\sin\alpha\left(a - d\sin\alpha\right)\right)} \\ \qquad ; \quad -\alpha \le \phi_b \le \alpha \quad \text{and} \quad \beta_{\min} \le \beta_b \le \beta_{\max} \\ 0 \qquad ; \quad \text{otherwise} \end{cases} \qquad \textit{Eq (4.14)}$$

Marginal PDF of AoA in azimuth plane seen at BS can be obtained by integrating *Eq (4.14)* over β_b for appropriate limits. However, the closed-form solution can also be obtained in a similar way as in [22], as

$$p(\phi_b) = \int\int_{\text{Ellipse}_{\phi_b}} \frac{1}{V}\, \rho_b \, \mathrm{d}\rho_b \, \mathrm{dz_b} \qquad \textit{Eq (4.15)}$$

$$p(\phi_b) = \frac{d\cos\phi_b}{V}\, A_{e,\phi_b} \qquad \textit{Eq (4.16)}$$

Where, A_{e,ϕ_b} is area of the scattering ellipse seen for a fixed angle ϕ_b. Finally, the closed-form expression for the marginal PDF of azimuth AoA seen at BS can be expressed as

$$p\left(\phi_b\right) = \begin{cases} \dfrac{3\cos\phi_b \csc\alpha(a^2 - d^2\sin^2\phi_b)}{4(a^2 + d\sin\alpha(a - d\sin\alpha))} & ;\ -\alpha \leq \phi_b \leq \alpha \\ 0 & ;\ \text{otherwise} \end{cases} \qquad \textit{Eq (4.17)}$$

The PDF of AoA seen at BS for azimuth plane is shown in Fig. 4.6 for different values of beam-width i.e. $\alpha = 3^o$, $\alpha = 4^o$, $\alpha = 5^o$ and $\alpha \geq \alpha_{\max}$. The marginal PDF for elevation AoA seen at BS can be obtained by integrating *Eq (4.14)* over ϕ_b for appropriate limits, as

$$p(\beta_b) = \frac{1}{3V\cos^2\beta_b}\int_{-\phi_L}^{\phi_L}(\rho_{b2}^3 - \rho_{b1}^3)\mathrm{d}\phi_b \qquad \textit{Eq (4.18)}$$

Substituting the value of V from *Eq (3.33)* in *Eq (4.18)*, the PDF of AoA for elevation plane seen at BS can be written as

$$p(\beta_b) = \frac{a\csc\alpha\sec^2\beta_b}{2\pi bd(a^2 + d\sin\alpha(a - d\sin\alpha))}\int_{-\phi_L}^{\phi_L}(\rho_{b2}^3 - \rho_{b1}^3)\mathrm{d}\phi_b \qquad \textit{Eq (4.19)}$$

In Fig. 4.6, it is observed that when the beam-width is set as $\alpha \geq \alpha_{\max}$, there is no clipping of scattering region and the proposed 3-D model provides the same results for the PDF of azimuth AoA, as those obtained in [22]. In Fig. 4.7, the PDFs of elevation AoA seen at BS are shown for h_t set greater and equal to b, where it can be observed that if the beam-width α is set as $\alpha \geq \alpha_{\max}$, there is no clipping of the scattering region and the proposed model provides the same results as those in [22] by Janaswamy. The PDF of azimuth AoA at BS derived in [24] can be obtained by substituting $\alpha \geq \alpha_{\max}$ and $A_{e,\phi_b} = 2\sqrt{a^2 - d^2\sin^2\phi_b}$ in *Eq (4.16)*.

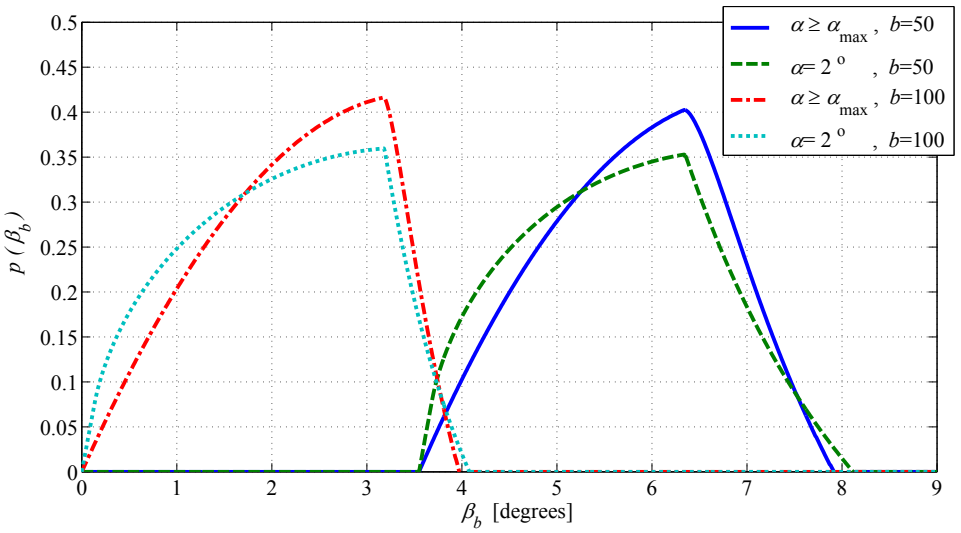

FIGURE 4.7: Marginal PDF of AoA in elevation plane seen at BS (d = 800m, a = 100m, and h_t = 100m)

No closed-form expression for the PDF of elevation AoA is presented. However, the PDF of elevation AoA is plotted using numerical integration techniques, which can easily be obtained by placing $\alpha \geq \alpha_{\max}$, $A_{e,\phi_b} = 2\sqrt{a^2 - d^2 \sin^2 \phi_b}$ and a very small value for the minor axis, b (i.e. b tending towards zero).

4.1.2 Temporal Characteristics of Radio Channel

In this section, the temporal statistics using the proposed model are discussed and the joint and marginal PDF of ToA/AoA are derived. Let τ be the propagation delay of a multipath signal reflected from any scatterer, located in the illuminated 3-D scattering region, which can be expressed in terms of distance of the propagation path and the velocity of radio wave, as

$$\tau = \frac{r_m + r_b}{c} \qquad \textit{Eq (4.20)}$$

The delay for LoS path is τ_o, and the delay of longest propagation path is $\tau_{\max}$, which can be expressed as

$$\tau_o = \frac{l_{\text{Los}}}{c} \qquad \textit{Eq (4.21)}$$

$$\tau_{\max} = \frac{a + \sqrt{h_t^2 + (d+a)^2}}{c} \qquad \textit{Eq (4.22)}$$

Propagation path delay of waves reflected from the scatterers located at the boundary of scattering region for a particular azimuth and elevation angle is symbolized by τ_{lim}, which can be expressed as

$$\tau_{\text{lim}}(\phi_m, \beta_m) = \frac{r_m(\phi_m, \beta_m) + r_b(\phi_m, \beta_m)}{c} \qquad \textit{Eq (4.23)}$$

The distances $r_{m,\max}$ and r_b are found earlier in *Eq (3.14)* and *Eq (3.16)* respectively. r_b is the distance of a scatterer from BS and can be written in simplified form as,

$$r_b(r_m, \phi_m, \beta_m) = \sqrt{r_m^2 + l_{\text{Los}}^2 - 2r_m(d\cos\beta_m\cos\phi_m + h_t\sin\beta_m)} \qquad \textit{Eq (4.24)}$$

Substituting *Eq (4.24)* in *Eq (4.20)* and solving for r_m, the equation can be rearranged as

$$r_m(\tau, \phi_m, \beta_m) = \frac{c^2\tau^2 - l_{\text{Los}}^2}{2(c\tau - d\cos\beta_m\cos\phi_m - h_t\sin\beta_m)} \qquad \textit{Eq (4.25)}$$

Similarly, the distance r_b of the scatterer from BS can be found in correspondence with angles seen at BS, as

$$r_b(\tau, \phi_b, \beta_b) = \frac{c^2\tau^2 - l_{\text{Los}}^2}{2(c\tau - d\cos\beta_b\cos\phi_b - h_t\sin\beta_b)} \qquad \textit{Eq (4.26)}$$

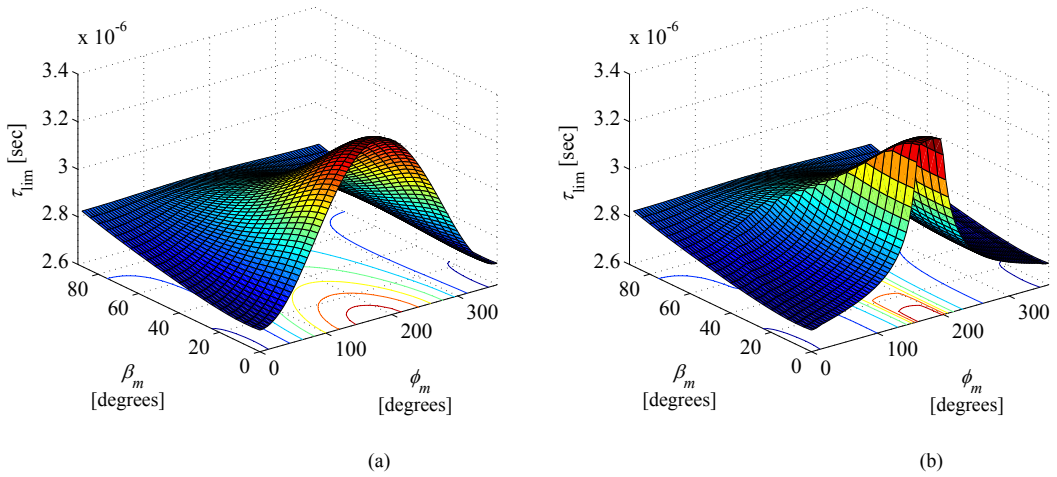

FIGURE 4.8: Propagation paths delay limit in correspondence with azimuth and elevation AoA for beam-width $\alpha = 2^{\text{o}}$ and $\alpha = \alpha_{\max}$, in (a) and (b), respectively, ($h_t = 100$m, $d = 800$m, $a = 100$m and $b = 50$m)

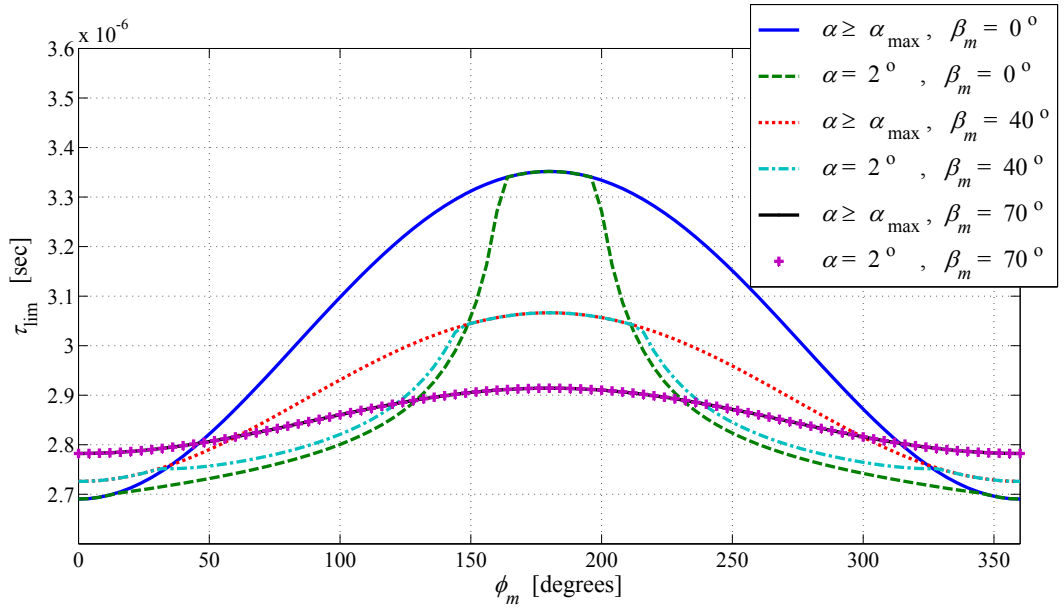

FIGURE 4.9: Propagation paths delay limit in correspondence with azimuth and elevation AoA; with and without the effects of directional antenna at BS, ($h_t = 100$m, $d = 800$m, $a = 100$m and $b = 50$m)

The scattering objects present at the boundary of the scattering region cause the maximum propagation path delay for a particular azimuth and elevation angle. Maximum propagation path delay in azimuth plane is plotted in Fig. 4.9 for different values of β_m (i.e. $\beta_m = 0^o, 40^o, 70^o$) and α (i.e. $\alpha \geq \alpha_{max}$ and $\alpha = 2^o$),

where the effects of directional antenna on propagation path delays can be observed clearly.

4.1.2.1 PDF of ToA

The joint density function for ToA / AoA can be found [23] as,

$$p(\tau, \phi_m, \beta_m) = \frac{p(r_m, \phi_m, \beta_m)}{\mid J(r_m, \phi_m, \beta_m) \mid} \qquad Eq\ (4.27)$$

Where r_m is given in *Eq (4.25)*, the Jacobian transformation $J(r_m, \phi_m, \beta_m)$ shown in *Eq (4.27)*, can be found as

$$J(r_m, \phi_m, \beta_m) = \left| \frac{\partial r_m}{\partial \tau} \right|^{-1} \qquad Eq\ (4.28)$$

$$J(r_m, \phi_m, \beta_m) = \frac{2(d\cos\beta_m\cos\phi_m - c\tau + h_t\sin\beta_m)^2}{c(l_{\text{Los}}^2 + c^2\tau^2 - 2c\tau(d\cos\beta_m\cos\phi_m + h_t\sin\beta_m))} \qquad Eq\ (4.29)$$

Substituting *Eq (4.29)* and *Eq (4.4)* in *Eq (4.27)*, the joint density function for ToA / AoA can be re-written in simplified form as,

$$\begin{aligned} p(\tau, \phi_m, \beta_m) = & \\ & \frac{1}{8V(d\cos\beta_m\cos\phi_m - c\tau + h_t\sin\beta_m)^4}\Big\{c\,(l_{\text{Los}}^2 - c^2\tau^2)^2 \\ & \times\big(c^2\tau^2 + l_{\text{Los}}^2 - 2c\tau(d\cos\beta_m\cos\phi_m + h_t\sin\beta_m)\big)\cos\beta_m\Big\} \end{aligned} \qquad Eq\ (4.30)$$

Similarly, the joint density function in correspondence with the angles seen at BS can be found as,

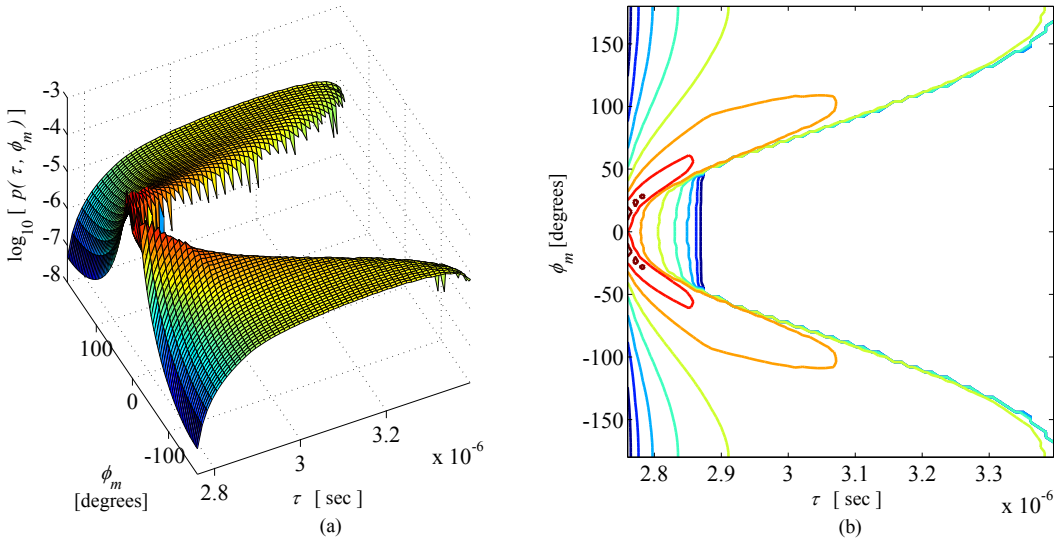

FIGURE 4.10: Joint PDF of ToA / AoA in correspondence with azimuth angles, (a) 3-D plot (b) contour plot, ($\alpha \geq \alpha_{max}$, $h_t = 100$m, $d = 800$m, $a = 100$m and $b = 50$m)

$$p(\tau, \phi_b, \beta_b) =$$

$$\frac{1}{8V(d\cos\beta_b\cos\phi_b - c\tau + h_t\sin\beta_b)^4}\Big\{c\,(l_{\text{Los}}^2 - c^2\tau^2)^2 \qquad \textit{Eq (4.31)}$$

$$\times\big(c^2\tau^2 + l_{\text{Los}}^2 - 2c\tau(d\cos\beta_b\cos\phi_b + h_t\sin\beta_b)\big)\cos\beta_b\Big\}$$

The joint PDF of ToA in azimuth and elevation planes seen at MS can be then found by integrating *Eq (4.30)* over elevation and azimuth angles respectively.

$$p(\tau, \phi_m) = \int_0^{\frac{\pi}{2}} p(\tau, \phi_m, \beta_m)\mathrm{d}\beta_m \qquad \textit{Eq (4.32)}$$

$$p(\tau, \beta_m) = \int_{-\pi}^{\pi} p(\tau, \phi_m, \beta_m)\mathrm{d}\phi_m \qquad \textit{Eq (4.33)}$$

The joint PDF of ToA in azimuth and elevation planes seen at BS can be then found by integrating *Eq (4.31)* over elevation and azimuth angles respectively.

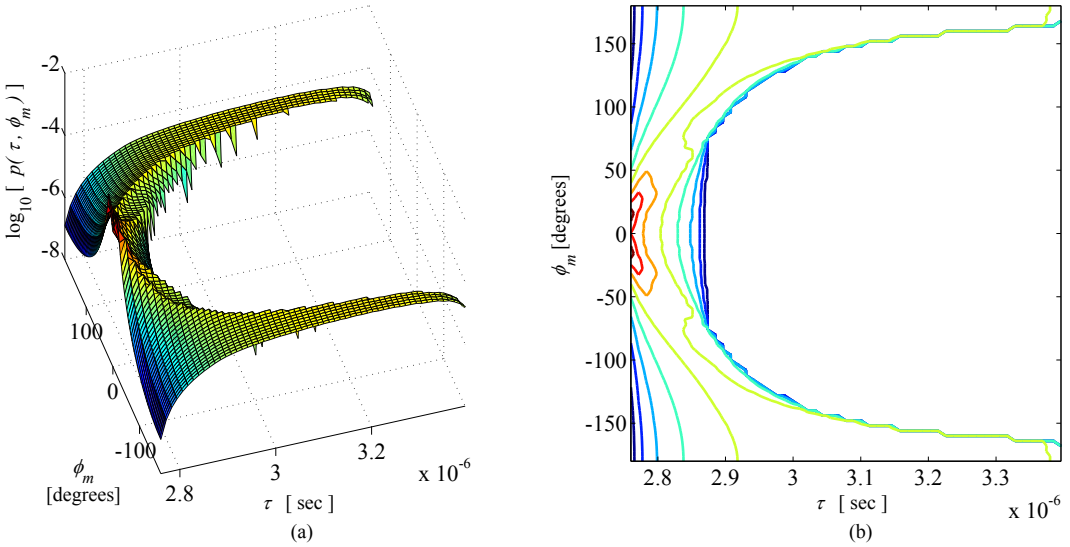

FIGURE 4.11: Joint PDF of ToA / AoA in correspondence with azimuth angles along with the effects of directional antenna at BS, (a) 3-D plot (b) contour plot, ($\alpha = 2^{\text{o}}$, $h_t = 100$m, $d = 800$m, $a = 100$m and $b = 50$m)

$$p(\tau, \phi_b) = \int_{\beta_{\min}}^{\beta_{\max}} p(\tau, \phi_b, \beta_b) \mathrm{d}\beta_b \qquad \textit{Eq (4.34)}$$

$$p(\tau, \beta_b) = \int_{-\phi_{\max}}^{\phi_{\max}} p(\tau, \phi_b, \beta_b) \mathrm{d}\phi_b \beta_{\max} \qquad \textit{Eq (4.35)}$$

where, $\tau_o \leq \tau \leq \tau_{\lim}(\phi_m, \beta_m)$, $-\pi \leq \phi_m < \pi$, $0 \leq \beta_m \leq \pi/2$, $-\phi_{\max} \leq \phi_b \leq \phi_{\max}$, and $\beta_{\min} \leq \beta_b \leq \beta_{\max}$.

Thus, the marginal PDF of ToA can be found by integrating any of the equations *Eq (4.32)*-*Eq (4.35)* over corresponding angles, as

$$p(\tau) = \int_{-\pi}^{\pi} \int_{0}^{\frac{\pi}{2}} p(\tau, \phi_m, \beta_m) \, \mathrm{d}\beta_m \, \mathrm{d}\phi_m \qquad \textit{Eq (4.36)}$$

The joint statistics of ToA with azimuth angles are shown in Fig. 4.10 and Fig. 4.11 for $\alpha \geq \alpha_{\max}$ and $\alpha = 2^o$ respectively by solving the integration in *Eq (4.32)* numerically. Similarly, the joint PDF of ToA in correspondence with elevation

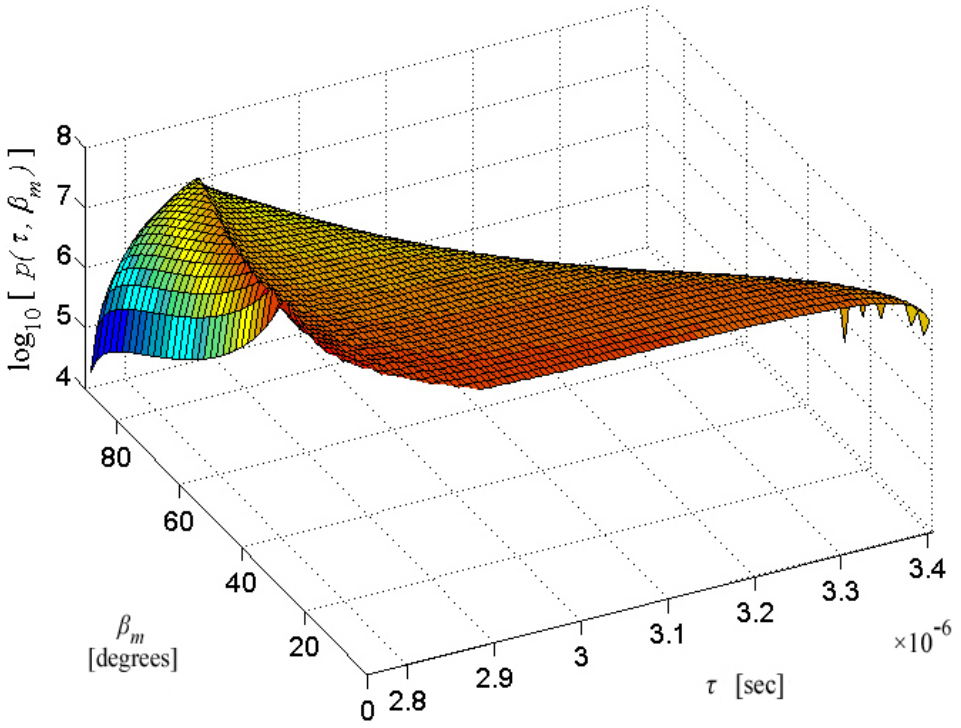

FIGURE 4.12: Joint PDF of ToA / AoA in elevation plane, ($\alpha \geq \alpha_{\max}$, h_t = 100m, d = 800m, a = 100m and b = 50m)

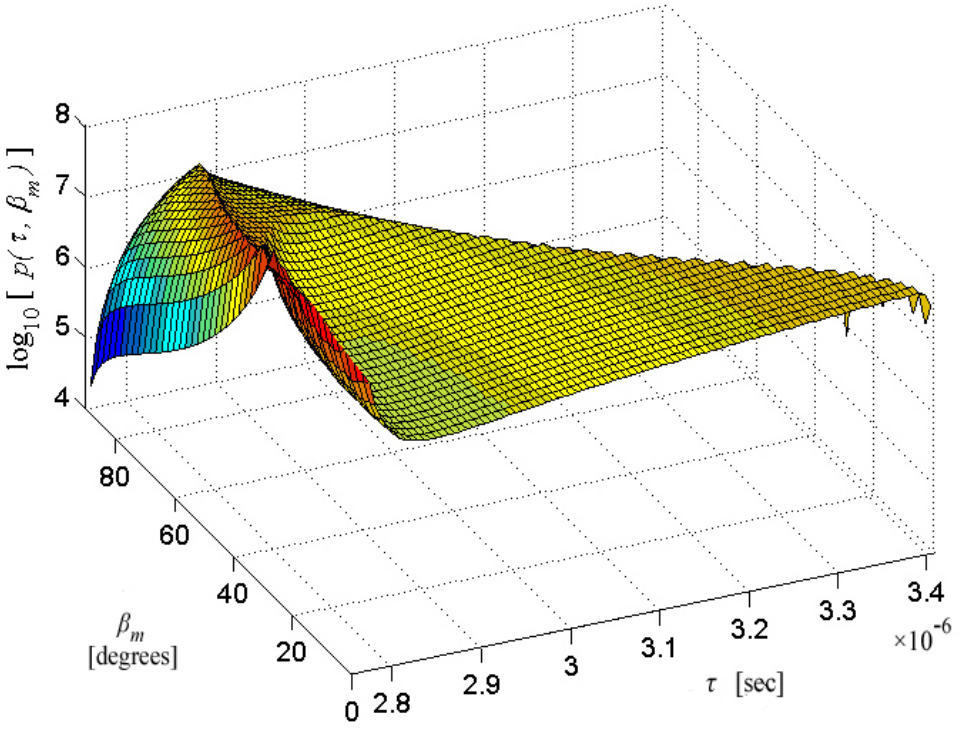

FIGURE 4.13: Joint PDF of ToA / AoA in elevation plane with effects of directional antenna at BS, ($\alpha = 2^o$, h_t = 100m, d = 800m, a = 100m and b = 50m)

Scattering Models.	Targeted Environment.	Elevated BS.	Directional Antenna at BS.	Modeling of Scattering Region.	Substitutions to obtain the statistics of other models from proposed model.
Proposed.	Macro-cell.	Yes.	Yes.	3-D semi-spheroid (i.e. different major and minor axes), Centered at MS.	–
Janaswamy, 2002, [22].	Macro-cell.	Yes.	No.	3-D semi-spheroid (i.e. different major and minor axes), Centered at MS.	$\alpha = \alpha_{\max}$.
Olenko *et al.*, 2006, [23].	Not specified.	No.	No.	3-D hemispheroid (i.e. same major and minor axes), Centered at MS.	$\alpha = \alpha_{\max}$, $h_t = 0$, and $b = a$.
Baltzis *et al.*, 2009, [24].	Macro-cell.	Yes.	No.	2D circular disc, Centered at MS.	$\alpha = \alpha_{\max}$, $V = A_c$, and $b \to 0$.
Petrus *et al.*, 2002, [26].	Macro-cell.	No.	Yes.	2D circular disc, Centered at MS.	$h_t = 0$, $\beta_{m,b} = 0$, and $V = A_c$.
Ertel *et al.*, 1999, [15].	Macro-cell/ Micro-cell.	No.	No.	2D circular disc, Centered at MS / 2D elliptical disc with foci at MS and BS.	$\alpha = \alpha_{\max}$, $h_t = 0$, $\beta_{m,b} = 0$, and $V = A_c$.
Khan *et al.*, 2008, [13]	Macro-cell/ Micro-cell/ pico-cell.	No.	No.	2D circular/ elliptical disc (for macro-cell $a = b$, i.e. circular disc centered at MS).	$\alpha = \alpha_{\max}$, $h_t = 0$, $\beta_{m,b} = 0$, and $V = A_c$.

TABLE 4.1: Comparison of the proposed model with notable models found in the literature (for uniform scatter density)

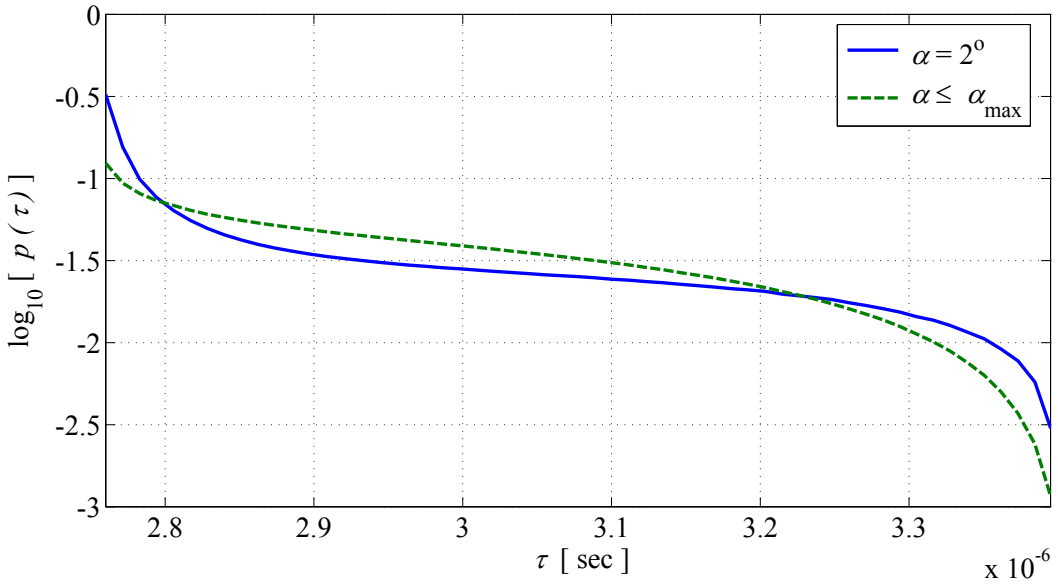

FIGURE 4.14: Marginal PDF of ToA for uniform SDF, (h_t = 100m, d = 800m, a = 100m and b = 50m)

plane is shown in Fig. 4.12 and Fig. 4.13 for $\alpha \geq \alpha_{\max}$ and $\alpha = 2^o$ respectively. The marginal PDFs of ToA for proposed 3-D scattering environments are shown in Fig. 4.14 for $\alpha \geq \alpha_{\max}$ and $\alpha = 2^o$ respectively. If we substitute $h_t = 0$ and $a = b$ in *Eq (4.30)*, the proposed model deduces to the model presented in [23] and similar temporal statistics can be found. Moreover, if we substitute zero for both β_m and h_t in *Eq (4.30)*, the proposed model deduces to the 2-D model given in [15] and the joint function for ToA/AoA is found to be the same, as

$$p\,(\tau, \phi_m) = \frac{c(d^2 - c^2\tau^2)^2(d^2 + c^2\tau^2 - 2c\tau d\cos\phi_m)}{8\ A_c\ (d\cos\phi_m - c\tau)^4} \qquad \textit{Eq (4.37)}$$

Where, A_c is the area of illuminated scattering plane centered at MS in the base of the scattering semi-spheroid, which can be expressed as a function of azimuthal beam-width α, as

$$A_c(\alpha) = a^2(\pi + \phi_1 - \phi_2) + 2d\sin\alpha\sqrt{a^2 - d^2\sin^2\alpha} \qquad \textit{Eq (4.38)}$$

If we substitute $\alpha \geq \alpha_{\max}$, the angles ϕ_1 and ϕ_2 become equal and the equation reduces to $A_c = \pi a^2$ (i.e. the area of circle with radius a). If we integrate *Eq (4.37)* over azimuth angle for appropriate limits, an expression for the marginal PDF of ToA can be obtained in closed-form as derived in [15] for the case of 2-D scattering model.

In order to establish the validity and to demonstrate the generalization of the proposed model, comparison of the proposed model with some notable models found in the literature [13, 15, 22–24, 26] is presented in Table 4.1. The theoretical results for a 3-D macro-cell model in [24], have been validated by comparing with those obtained in [22] and an empirical set of data in [67–69]. Whereas, these models [22,24] can be deduced from the proposed model with an appropriate choice of a few parameters. Furthermore, the statistics for the case of 2-D scattering model in [13] (case of macro-cell) can also be obtained from the proposed model, whereas, these statistics have been validated with experimental data provided in [70].

The proposed theoretical results are useful in designing antenna beam-widths for a practical 3-D scattering environment. Performance analysis of the advanced MIMO techniques using planar antenna arrays can be made more and more precise based upon the azimuthal and vertical angular spreads of the scattering region in correspondence with the spacing among antenna elements, horizontally and vertically. Such performance analysis can be further utilized either in enhancing the data rate of MIMO streams or in sharpening the beam-width of the phased array by manipulating the correlations among antenna elements.

4.2 Channel Characteristics For Gaussian Scatter Density

In this section, we derive the angular and temporal characteristics of radio link for the case of Gaussian scatter density. The spatial and temporal characteristics of radio communication link are derived in Section 4.2.1 and Section 4.2.2, respectively.

4.2.1 Spatial Characteristics of Radio Channel

In this section, the spatial statistics observed at both the ends of a communication link are derived for the case of Gaussian scatter density.

For the case of Gaussian scatter density, the majority of scattering objects are concentrated in the region near to MS. The density of scatterers decreases with the increase in distance from MS by following the Gaussian density function. Substituting the scatter density SDF $f_G(\mathrm{x_m}, \mathrm{y_m}, \mathrm{z_m})$ as given in *Eq (3.37)*, the joint density function given in *Eq (4.1)* can be rewritten as

$$p\left(r_m, \phi_m, \beta_m\right) = \frac{r_m^2 \cos\beta_m}{E} \qquad \textit{Eq (4.39)}$$

where, E adopts the strength of scattering region normalized with Gaussian scatter density. The closed-form expression for the joint PDF of AoA for azimuth and elevation angles is then found by integrating *Eq (4.39)* over r_m for appropriate limits, as

$$p\left(\phi_m, \beta_m\right) = \frac{1}{E}\int_0^{N_{m,\max}} r_m^2 \cos\beta_m \, \mathrm{d}_{r_m} \qquad \textit{Eq (4.40)}$$

$$p\left(\phi_m, \beta_m\right) = \frac{r_m^3 \cos\beta_m}{3E}\Bigg|_0^{N_{m,\max}} \qquad \textit{Eq (4.41)}$$

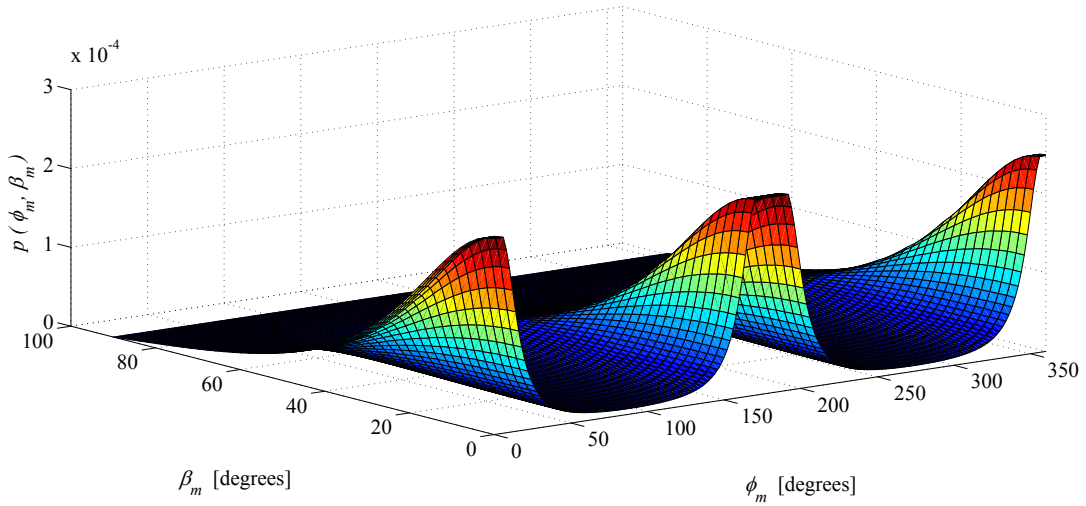

FIGURE 4.15: Joint PDF of AoA in correspondence with azimuth and elevation angles seen at MS for Gaussian scatter density, ($\sigma_a = 50, \sigma_b = 15, \alpha = 2^o, d = 800m,$ and $h_t = 100m$)

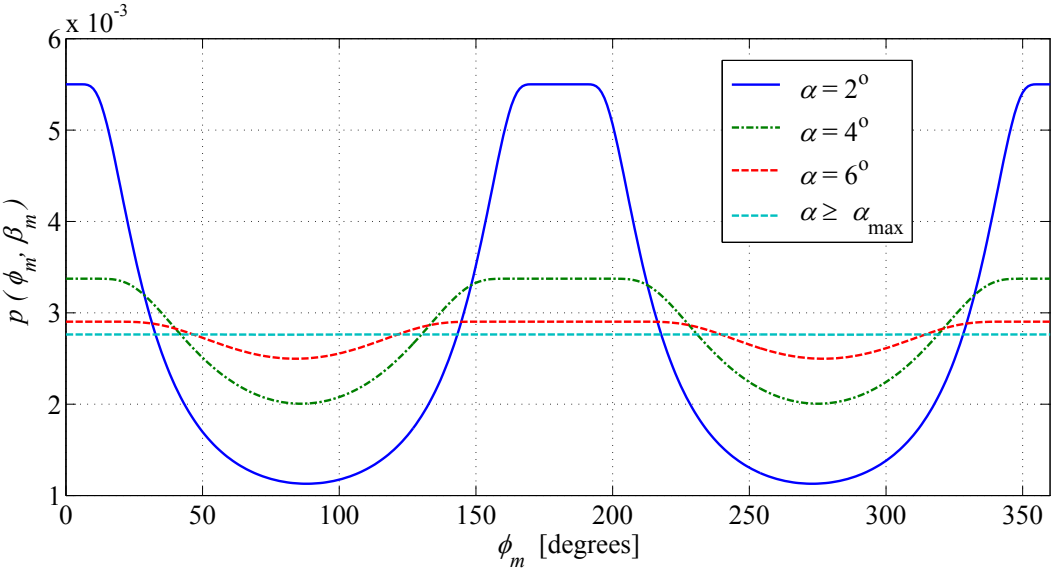

FIGURE 4.16: Marginal PDF of azimuth AoA, seen at MS, ($\sigma_a = 50, \sigma_b = 15, d = 800m,$ and $h_t = 100m$)

The closed-form solution can be written as,

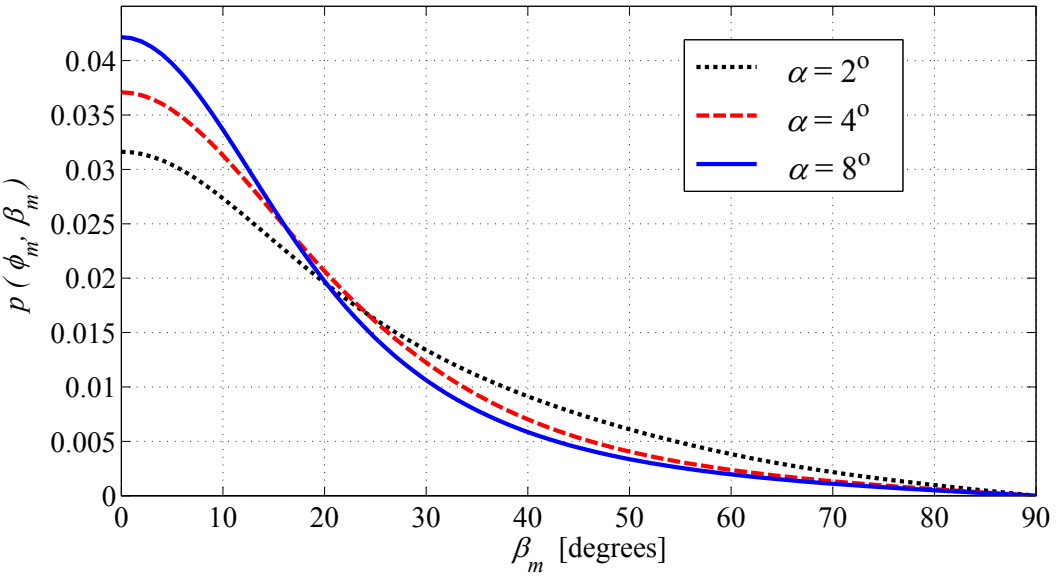

FIGURE 4.17: Marginal PDF of elevation AoA, seen at MS for Gaussian SDF, ($\sigma_a = 50, \sigma_b = 15, \alpha = 2^o, d = 800m,$ and $h_t = 100m$)

$$p(\phi_m, \beta_m) = \begin{cases} \dfrac{64\sigma_a^3\sigma_b^3 \cos\beta_m \operatorname{erf}\left(\dfrac{d\sin\alpha\sqrt{\sigma_b^2\cos^2\beta_m + \sigma_a^2\sin^2\beta_m}}{\sqrt{2}\sigma_a\sigma_b\sin(\alpha+\phi_m)\cos\beta_m}\right)^3}{3\ E\ \left(\sigma_b^2\cos^2\beta_m + \sigma_a^2\sin^2\beta_m\right)^{3/2}} & ;\ P_1 \\ \dfrac{64}{3\ E}\cos\beta_m \left(\dfrac{\sigma_a^2\sigma_b^2}{\sigma_b^2\cos^2\beta_m + \sigma_a^2\sin^2\beta_m}\right)^{3/2} & ;\ P_2 \end{cases} \qquad \textit{Eq (4.42)}$$

The marginal PDF of AoA in azimuth plane can be obtained by integrating *Eq (4.42)* over β_m for appropriate limits, as

$$p(\phi_m) = \int_0^{\beta_t} p(\phi_m, \beta_m)\Big|_{P_1} \mathrm{d}\beta_m + \int_{\beta_t}^{\pi/2} p(\phi_m, \beta_m)\Big|_{P_2} \mathrm{d}\beta_m \qquad \textit{Eq (4.43)}$$

Similarly, the marginal elevation PDF of AoA can be obtained by integrating *Eq (4.42)* over ϕ_m for appropriate limits, as

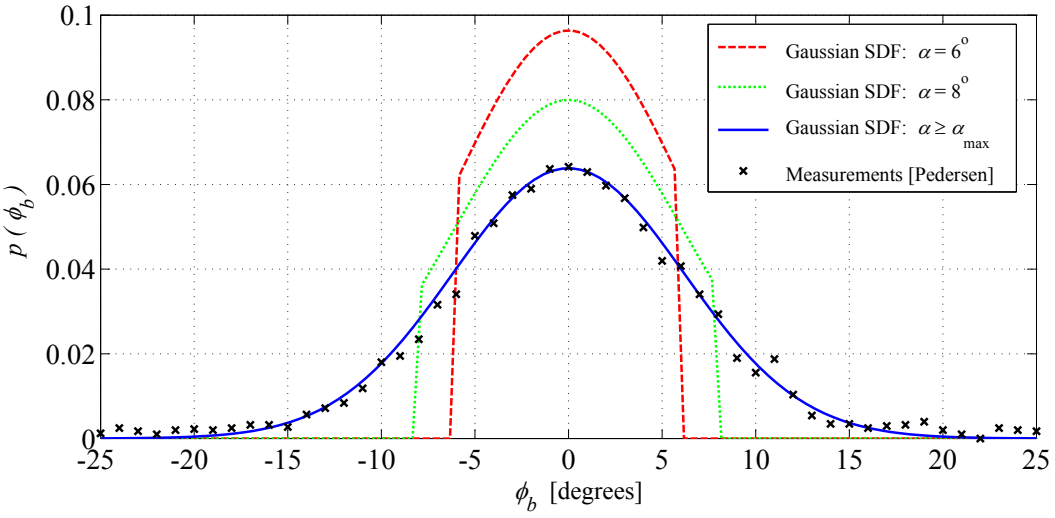

FIGURE 4.18: Marginal PDF of azimuth AoA seen at BS for Gaussian SDF produced for different values of beam-width α along with measurement values provided in [70], ($\sigma_a = 230, \sigma_b = 15, d = 1.5km,$ and $h_t = 100m$)

$$p(\beta_m) = 2\int_{\phi_{t1}}^{\phi_{t2}} p(\phi_m, \beta_m)\Big|_{P_1} \mathrm{d}\phi_m + \int_{-\phi_{t1}}^{\phi_{t1}} p(\phi_m, \beta_m)\Big|_{P_2} \mathrm{d}\phi_m + \int_{\phi_{t2}}^{-\phi_{t2}} p(\phi_m, \beta_m)\Big|_{P_2} \mathrm{d}\phi_m \qquad \textit{Eq (4.44)}$$

Fig. 4.15 depicts the joint PDF of AoA seen at MS in correspondence with azimuth and elevation angles for beam-width $\alpha = 2^o$. These statistics for the spreading of multipath waves in vertical and horizontal axes are useful for designing more reliable communications links, specially when employing the antenna arrays (either vertical or planner). The marginal PDFs of AoA for different beam-widths of directional antenna are plotted in Fig. 4.16 and Fig. 4.17 for azimuth and elevation planes, respectively. These plots are obtained by using the techniques of numerical integration. In Fig. 4.16, it can be seen that with an increase in beam-width, the PDF changes to uniform distribution, which is the case of omnidirectional antenna as in [19, 27].

At BS, the Marginal PDF of azimuth AoA can be obtained in closed-form in a similar way as in [48], as

$$p(\phi_b) = \int \int_{\text{Ellipse}_{\phi_b}} \frac{1}{E}\, \rho_b \, \mathrm{d}\rho_b \, \mathrm{dz_b} \qquad \textit{Eq (4.45)}$$

$$p(\phi_b) = \frac{d \cos \phi_b}{E}\, A_{e,\phi_b} \qquad \textit{Eq (4.46)}$$

Where, A_{e,ϕ_b} is the area of the scattering ellipse seen for a fixed angle ϕ_b and normalized by its Gaussian strength. Finally, the closed-form expression for the marginal PDF of azimuth AoA seen at BS can be expressed as,

$$p(\phi_b) = \frac{\sigma_b \pi d \left(32\sigma_a^2 - d^2 + d^2 \cos(2\phi_b) \right) \exp\left(-\dfrac{d^2 \sin^2 \phi_b}{\sigma_a^2} \right)}{2\, E\, \sigma_a \sec \phi_b} \qquad \textit{Eq (4.47)}$$

The marginal PDF of azimuth AoA at BS for different values of beam-width α is plotted in Fig. 4.18, which clearly demonstrates the effects of directional antenna. Moreover, the obtained theoretical results are compared with the measurements data provided in [70], where the values of parameters for theoretical results are chosen to match with those in [70]. This comparison also demonstrates the validity of the proposed propagation model.

Comparison between the angular statistics obtained for uniform and Gaussian SDFs observed at MS and BS are shown in Fig. 4.19 and Fig. 4.20, respectively. The PDF of AoA seen at MS for Unform SDF has sharp edges as compared to those obtained for Gaussian SDF. Practically measured data found in [70] is also plotted in Fig. 4.20; where, it can be observed that results obtained for Gaussian SDF match well with the measurement data. Hence, it can be established that Gaussian distribution is more realistic choice to model the scatterers around the MS as compared to the uniform distribution.

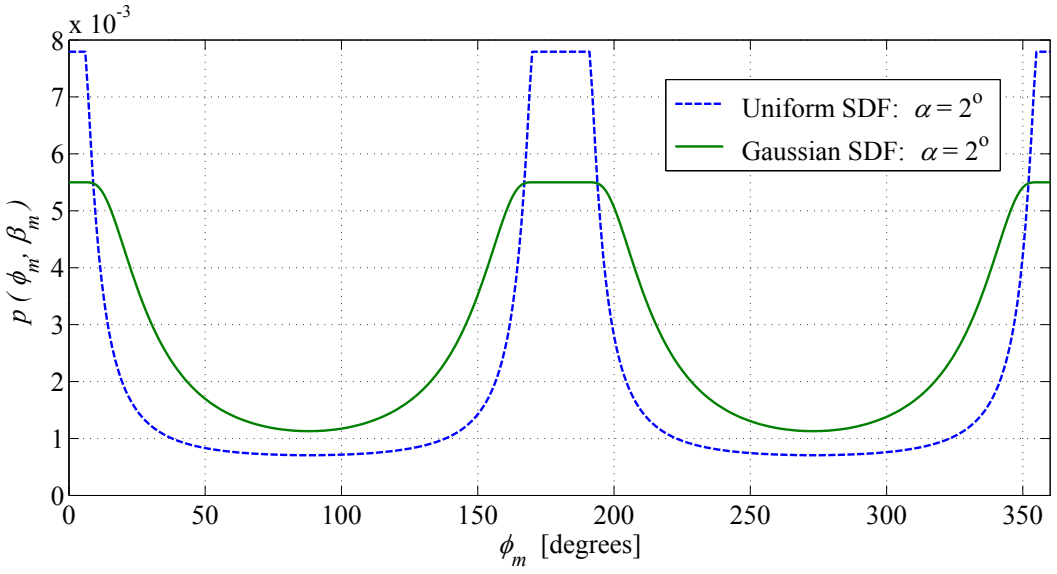

FIGURE 4.19: Comparison between marginal PDF of azimuth AoA seen at MS for both Gaussian and uniform SDFs, produced for beam-width of directional antenna $\alpha = 2^o$, $(\sigma_a = 230, \sigma_b = 15, d = 1.5km, \text{ and } h_t = 100m)$

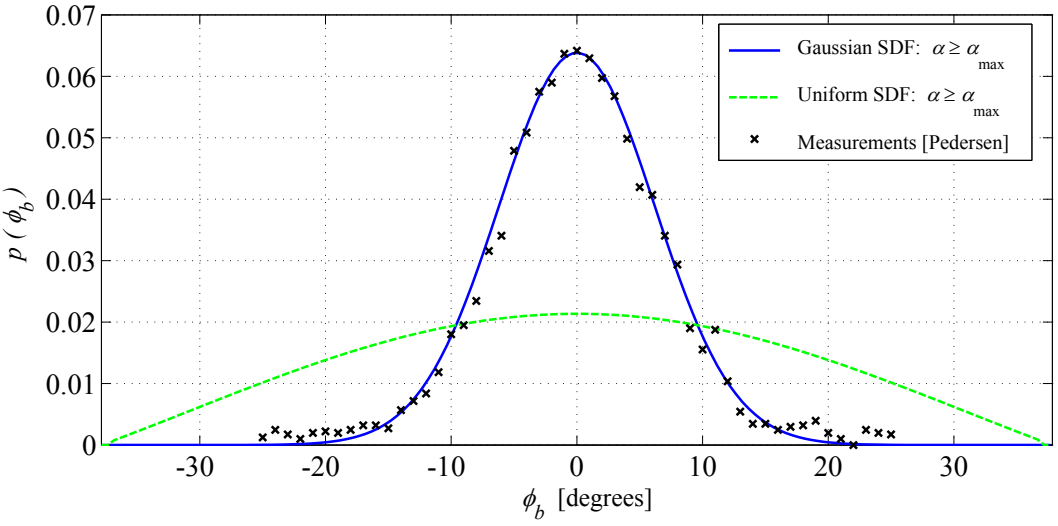

FIGURE 4.20: Comparison between marginal PDFs of azimuth AoA seen at BS for both Gaussian and uniform SDFs, produced for beam-width of directional antenna $\alpha = \alpha_{\max}$, along with measurement values provided in [70], $(\sigma_a = 230, \sigma_b = 15, d = 1.5km, \text{ and } h_t = 100m)$

4.2.2 Temporal Characteristics of Radio Channel

This section describes the temporal statistics for the proposed propagation model for the case of Gaussian scatter density. The joint and marginal PDFs of ToA/AoA

in correspondence with azimuth and elevation angles are derived. The joint density function for ToA / AoA can be found in the same way as for the case of uniform scatter density in *Eq (4.27)*, which is

$$p(\tau, \phi_m, \beta_m) = \frac{p(r_m, \phi_m, \beta_m)}{\mid J(r_{m,\max}, \phi_m, \beta_m) \mid} \qquad \textit{Eq (4.48)}$$

The Jacobian transformation $J(r_m, \phi_m, \beta_m)$ in *Eq (4.48)* is given in *Eq (4.29)*. By substituting *Eq (4.4)* and *Eq (4.29)* in *Eq (4.48)*, the joint density function for ToA / AoA can be expressed in simplified form as,

$$p(\tau, \phi_m, \beta_m) = \frac{c\left(l_{\mathrm{Los}}^2 - c^2\tau^2\right)^2 \cos\beta_m \; f_G(\mathrm{x_m}, \mathrm{y_m}, \mathrm{z_m})}{8\left(d\cos\beta_m\cos\phi_m - c\tau + h_t\sin\beta_m\right)^4}\Big\{l_{\mathrm{Los}}^2 + c^2\tau^2 - 2c\tau(d\cos\beta_m\cos\phi_m + h_t\sin\beta_m)\Big\} \qquad \textit{Eq (4.49)}$$

The joint PDF of ToA in correspondence with azimuth and elevation planes can be found by integrating *Eq (4.52)* over elevation and azimuth angles, respectively.

$$p(\tau, \phi_m) = \int_0^{\frac{\pi}{2}} p(\tau, \phi_m, \beta_m)\mathrm{d}\beta_m \qquad \textit{Eq (4.50)}$$

$$p(\tau, \beta_m) = \int_{-\pi}^{\pi} p(\tau, \phi_m, \beta_m)\mathrm{d}\phi_m \qquad \textit{Eq (4.51)}$$

The limits on propagation path delays, azimuth angles, and elevation angles are $\tau_o \leq \tau \leq \tau_{\mathrm{lim}}(\phi_m, \beta_m)$, $-\pi \leq \phi_m < \pi$, and $0 \leq \beta_m \leq \pi/2$, respectively. Whereas, τ_{lim} is the propagation path delay of waves reflected from the scatterers located at the boundary of illuminated scattering region (both partitions).

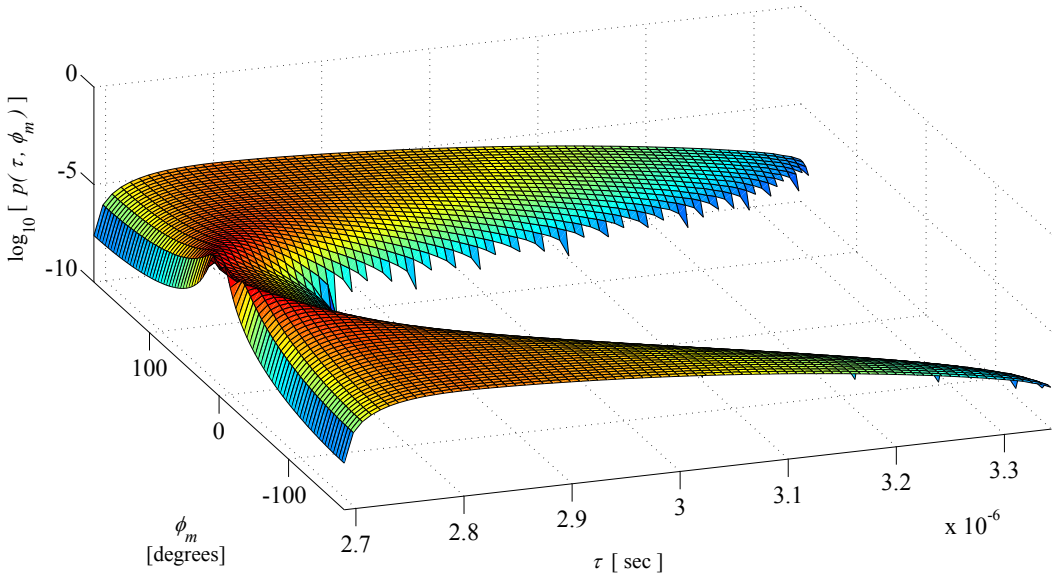

FIGURE 4.21: Joint PDF of ToA / AoA in correspondence with azimuth angles seen at MS for Gaussian SDF, ($\alpha \geq \alpha_{\max}, \sigma_a = 25, \sigma_b = 12, d = 800m,$ and $h_t = 150$)

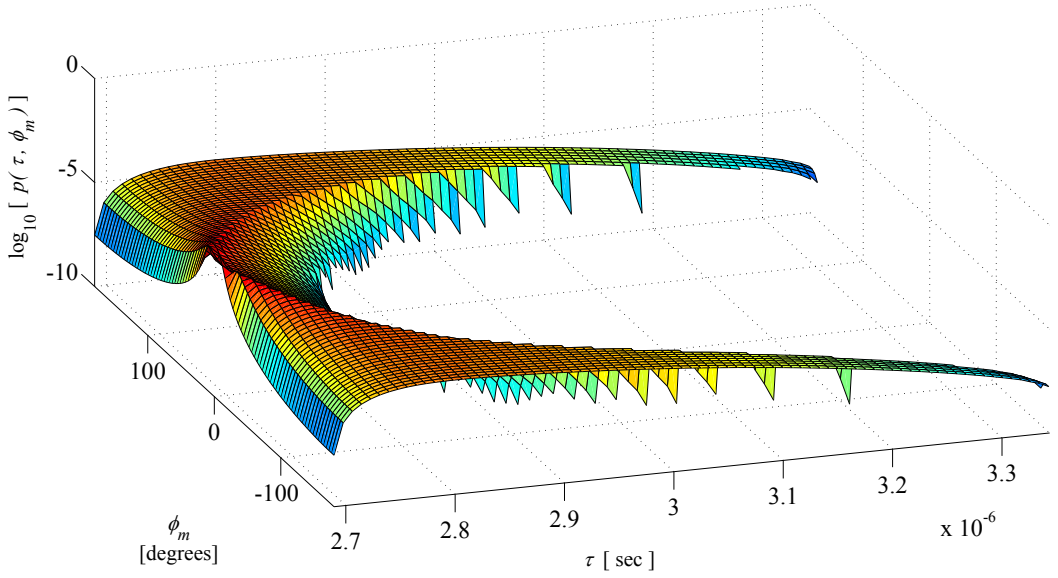

FIGURE 4.22: Joint PDF of ToA / AoA in correspondence with azimuth angles seen at MS for Gaussian SDF, ($\alpha = 2^o, \sigma_a = 25, \sigma_b = 12, d = 800m,$ and $h_t = 150$)

The joint PDF of ToA / AoA in correspondence with azimuth angles is shown in Fig. 4.21 and Fig. 4.22 for beam-width $\alpha \geq \alpha_{\max}$ and $\alpha = 2^o$, respectively, where the effects of directional antenna are observable. Moreover, the PDF of ToA for

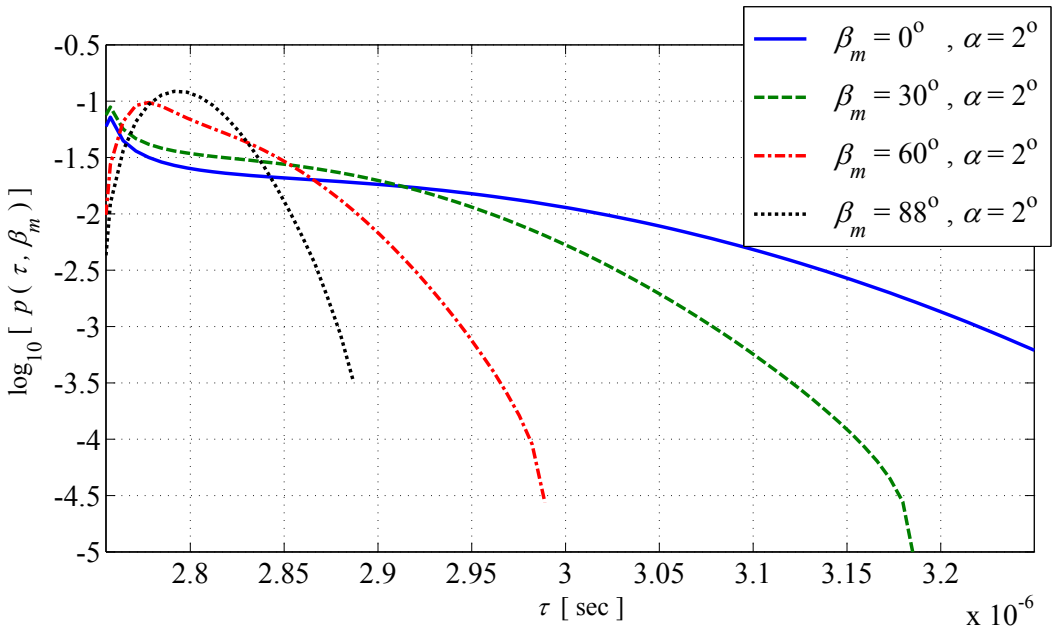

FIGURE 4.23: Joint PDF of ToA / AoA in correspondence with elevation angles seen at MS for Gaussian SDF, ($\alpha = 2^o, \sigma_a = 25, \sigma_b = 12, d = 800m,$ and $h_t = 150$)

different values of elevation angle β_m is shown in Fig. 4.23 for $\alpha = 2^o$. These graphs are obtained by numerically integrating the trivariate density function in *Eq (4.52)* over appropriate parameters and limits. Due to the symmetry in the geometry, the joint trivariate ToA / AoA density function at the BS is similar as found at the MS. However, the scatterers density function and the range of parameters would be different.

$$p(\tau, \phi_b, \beta_b) = \frac{c\left(l_{\text{Los}}^2 - c^2\tau^2\right)^2 \cos\beta_b \; f_G(\mathrm{x_m}, \mathrm{y_m}, \mathrm{z_m})}{8\left(d\cos\beta_b\cos\phi_b - c\tau + h_t\sin\beta_b\right)^4}\Big\{l_{\text{Los}}^2 + c^2\tau^2 - 2c\tau(d\cos\beta_b\cos\phi_b + h_t\sin\beta_b)\Big\} \qquad \textit{Eq (4.52)}$$

The Gaussian scatter density function, $f_G(\mathrm{x_m}, \mathrm{y_m}, \mathrm{z_m})$, given in *Eq (3.40)*, can be expressed in simplified form as,

$$f_G(\mathrm{x_m}, \mathrm{y_m}, \mathrm{z_m}) = \frac{1}{(2\pi\sigma^2)^{3/2}} \exp\left(-\frac{(d_{\mathrm{los}}^2 - c^2\tau^2)^2}{8\sigma^2\left(d\cos\beta_m\cos\phi_m + h_t\sin\beta_m - c\tau\right)^2}\right) \qquad \textit{Eq (4.53)}$$

The provided 3-D spatial statistics are useful for designing vertical and planner antenna arrays. These theoretical results are useful for designing more precise antenna beam-widths and the analysis of the advanced MIMO techniques using antenna arrays. Furthermore, this propagation model analysis can be used as reference for practical measurement based results.

4.3 Summary

In this chapter, the spatial and temporal statistics of up and down radio communication links have been derived for the proposed 3-D propagation model with both uniform and Gaussian scatter densities. The effects of directional antenna has thoroughly been observed on the spatial and temporal statistics in correspondence with the azimuth and elevation angles. Closed-form expressions for the joint and the marginal PDFs of AoA both in azimuth and elevation planes have been derived by assuming the uniform as well as Gaussian distribution of scattering objects. Moreover, to demonstrate the validity of the proposed model, the obtained theoretical results for spatial statistics at BS assuming Gaussian scatter density have been compared with a set of practically measured data provided in [70].

Chapter 5

DOPPLER SPECTRUM IN 3-D MOBILE RADIO PROPAGATION ENVIRONMENTS

Relative motion either between transmitter and receiver or between scatterers and receiver causes small scale fading. In this chapter, an analytical model is proposed for land mobile radio cellular communication systems with directional antennas at an elevated BS to quantify the effects of directivity on the Doppler spectrum in a 3-D radio propagation environment. The impacts of antenna beam-width and motion of MS are thoroughly investigated by considering statistical distribution of the power Doppler spectrum.

5.1 Statistical Characteristics of Doppler Spectrum

In this section, an analytical model along with the derivations of general expressions for joint and marginal distribution functions of power, Doppler spectrum, propagation path-loss, and AoA in relation with the beam-width of directional antenna are presented.

5.1.1 Propagation Model

A model with 3-D radio propagation environment is illustrated in Fig. 5.1. In a typical macro-cell environment (suited for suburban and rural environment), the antenna height of the BS is more than the average roof-top level of surrounding environment, therefore it is viable to assume the surroundings of BS as a scattering free region. The MS is usually located far from the BS and the antenna height of MS is very low, consequently it is surrounded by scattering objects. Therefore, the scattering objects are assumed only around the MS, which are kept confined in a semi-spheroid with its bottom centered at the MS (see Fig. 5.1). This is thus

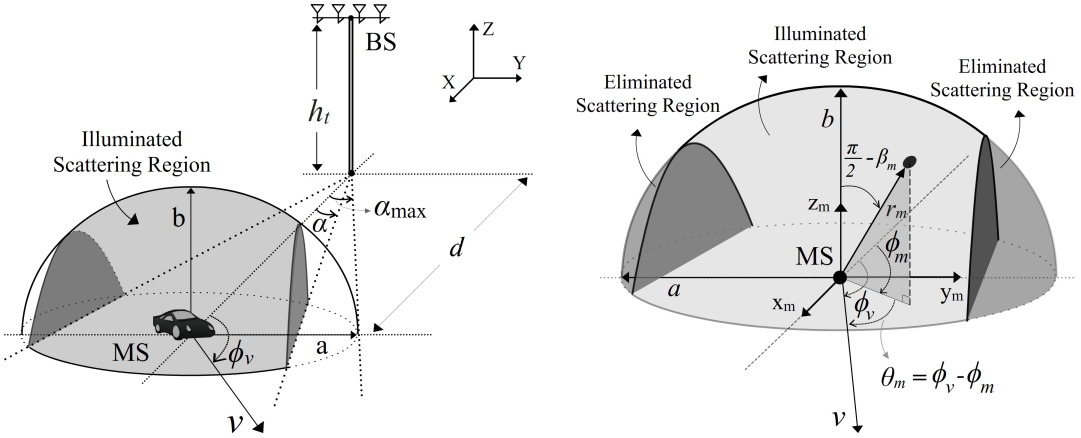

FIGURE 5.1: 3-D propagation environment for land mobile cellular systems, where the elevated BS is equipped with a directional antenna, and the MS is moving with an angle ϕ_v with respect to the LoS component.

due to the large height of the BS compared to the rooftops of suburban buildings, that the street canyons along with their surroundings can also be modeled as semi-spheroid. Whereas, considering micro-cell propagation environment, the buildings aligned parallel along both the sides of the road cause shadowing and hence can be best modeled with elliptical or ellipsoidal scattering regions [13].

The received signal at MS experiences spread in frequency spectrum due to the motion of MS. The velocity and direction of motion of the MS with respect to the LoS component are denoted as v and ϕ_v, respectively. The angle of the motion of MS with the arriving multipath signal is denoted by θ_m, which can be obtained as, $\theta_m = \phi_v - \phi_m$. The relation between the Doppler shift and multipath arrivals of sinusoidal signal, can be expressed as

$$f_{\text{DS}} = f_m \cos\theta_m \cos\beta_m \qquad \textit{Eq (5.1)}$$

whereas, the maximum shift in Doppler spectrum can be expressed as, $f_m = \frac{v}{c} f_c$, where f_c is the carrier frequency and c is the velocity of light. The normalized Doppler spread $\gamma = f_{\text{DS}}/f_m$, can be expressed as

$$\gamma = \cos\theta_m \cos\beta_m \qquad \textit{Eq (5.2)}$$

The AoA observed at MS in azimuth plane (i.e., ϕ_m) can be found as function of Doppler shift, elevation AoA, and direction of movement, which is

$$\phi_m = \phi_v - \cos^{-1}\left(\frac{\gamma}{\cos\beta_m}\right) \qquad \textit{Eq (5.3)}$$

The horizontal beam-width $\alpha_{\max}$ is such that the beam of the directional antenna at BS illuminates all the scattering region (i.e. $\alpha_{\max} = \sin^{-1}(a/d)$). In situations when the beam-width α is less than $\alpha_{\max}$, directional antenna clips the scattering region such that only the illuminated scattering region seen within the beam of directional antenna corresponds to the arrival of multipath waves at the receiver. Furthermore, the illuminated scattering region is divided into two partitions, as shown in Fig. 3.2. The threshold angle β_t shown in Fig. 3.2, is computed to separate among the said two partitions of illuminated scattering region [48, 71], which is given in *Eq (3.11)*. The angles ϕ_{t1} and ϕ_{t2} (see Fig. 3.2) are computed in *Eq (3.9)* and *Eq (3.10)* to separate among the partitions of illuminated scattering region in azimuth plane. For a particular azimuth and elevation angle, the scattering objects located at the boundary of illuminated scattering region corresponds to the longest propagation path. Therefore, the upper bound for propagation path distance is obtained as a function of α, ϕ_m, and β_m, i.e.,

$$\begin{aligned} l_{\lim}(\alpha, \phi_m, \beta_m) &= r_{m,\max} \\ &+ \sqrt{r_{m,\max}^2 + l_{\text{LoS}}^2 - 2r_{m,\max}(d\cos\beta_m\cos\phi_m + h_t\sin\beta_m)} \end{aligned} \qquad \textit{Eq (5.4)}$$

where, $r_{m,\max}$ is the distance of MS from the scattering objects located at boundary of the scattering region, which is obtained as function of α, ϕ_m, and β_m as given in *Eq (3.14)*.

5.1.2 Derivation of PDF Expressions

The joint density function as function of angles observed at MS and propagation path distance, can be derived as

$$p(l, \phi_m, \beta_m) = \frac{p(r_m, \phi_m, \beta_m)}{\mid J(l, \phi_m, \beta_m) \mid} \qquad Eq\ (5.5)$$

The joint density function for ϕ_m, β_m, and r_m can be obtained as for GPM in [48, 71], i.e.,

$$p\left(r_m, \phi_m, \beta_m\right) = f\left(\mathrm{x_m}, \mathrm{y_m}, \mathrm{z_m}\right) r_m^2 \cos\beta_m \qquad Eq\ (5.6)$$

where, $f\left(\mathrm{x_m}, \mathrm{y_m}, \mathrm{z_m}\right)$ is the scatter density function. The Jacobian transformation $J(l, \phi_m, \beta_m)$ in *Eq (5.5)*, is derived as

$$J(l, \phi_m, \beta_m) = \left|\frac{\partial r_m}{\partial l}\right|^{-1} = \frac{2(d\cos\beta_m\cos\phi_m - l + h_t\sin\beta_m)^2}{l_{\mathrm{LoS}}^2 + l^2 - 2l(d\cos\beta_m\cos\phi_m + h_t\sin\beta_m)} \qquad Eq\ (5.7)$$

Hence, substituting $J(l, \phi_m, \beta_m)$, *Eq (5.5)* can be rewritten as

$$p(l, \phi_m, \beta_m) = \{f\left(\mathrm{x_m}, \mathrm{y_m}, \mathrm{z_m}\right)\ (l_{\mathrm{LoS}}^2 - l^2)^2\} \times \frac{(l_{\mathrm{LoS}}^2 + l^2 - 2l(d\cos\beta_m\cos\phi_m + h_t\sin\beta_m))}{8\sec\beta_m(d\cos\beta_m\cos\phi_m - l + h_t\sin\beta_m)^4} \qquad Eq\ (5.8)$$

The power level p_r can be related to multipath propagation path length l_p [35, 42, 64, 71] as,

$$p_r = p_o \left(\frac{l_p}{l_{\text{LoS}}} \right)^{-n} \qquad \textit{Eq (5.9)}$$

where, l_{LoS} is the length of the LoS propagation path from BS to MS, p_o is the received power corresponding to the LoS component, n is the path-loss exponent, and l_p is the length of propagation path (from BS to MS) corresponding to a specific multipath component. By rearranging *Eq (5.9)* for l_p, we get

$$l_p = l_{\text{LoS}} \left(\frac{p_r}{p_o} \right)^{-\frac{1}{n}} \qquad \textit{Eq (5.10)}$$

The joint density function for p_r, ϕ_m, and β_m is derived as

$$p(p_r, \phi_m, \beta_m) = \frac{p(l_p, \phi_m, \beta_m)}{\mid J(l_p, \phi_m, \beta_m) \mid} \Bigg|_{l_p = l_{\text{LoS}}(p_r/p_o)^{-\frac{1}{n}}} \qquad \textit{Eq (5.11)}$$

The Jacobian transformation $J(l_p, \phi_m, \beta_m)$ shown in *Eq (5.11)*, can be derived as

$$J(l_p, \phi_m, \beta_m) = \left| \frac{\partial l_p}{\partial p_r} \right|^{-1} = \frac{n\, p_o}{l_{\text{LoS}}} \left(\frac{p_r}{p_o} \right)^{\frac{n+1}{n}} \qquad \textit{Eq (5.12)}$$

By substituting *Eq (5.12)* in *Eq (5.11)*, the joint function to relate the power level of multipath components with 3-D AoA of multipath components, can be expressed in simplified form as

$$p(p_r, \phi_m, \beta_m) =$$

$$\left\{ \frac{l_{\mathrm{LoS}}^6 \left(\left(\frac{p_r}{p_o} \right)^{-2/n} - 1 \right)^2 f\left(\mathrm{x_m}, \mathrm{y_m}, \mathrm{z_m}\right)}{8np_o \sec\beta_m \left(\frac{p_r}{p_o} \right)^{\frac{n+1}{n}}} \right\}$$

$$\times \left\{ \frac{\left(l_{\mathrm{LoS}} + l_{\mathrm{LoS}} \left(\frac{p_r}{p_o} \right)^{-2/n} - 2 \left(\frac{p_r}{p_o} \right)^{-1/n} \left(d\cos\beta_m \cos\phi_m + h_t \sin\beta_m \right) \right)}{\left(d\cos\beta_m \cos\phi_m - l_{\mathrm{LoS}} \left(\frac{p_r}{p_o} \right)^{-1/n} + h_t \sin\beta_m \right)^4} \right\}$$

Eq (5.13)

The joint density function for p_r, γ, and β_m is obtained as

$$p(p_r, \gamma, \beta_m) = \frac{p(p_r, \phi_m, \beta_m)}{\mid J(p_r, \phi_m, \beta_m) \mid} \Bigg|_{\phi_m = \phi_v - \cos^{-1}(\gamma/\cos\beta_m)} \qquad \textit{Eq (5.14)}$$

The Jacobian transformation $J(p_r, \phi_m, \beta_m)$ shown in *Eq (5.14)*, is derived as

$$J(p_r, \phi_m, \beta_m) = \left| \frac{\partial \phi_m}{\partial \gamma} \right|^{-1} = \sqrt{\cos^2\beta_m - \gamma^2} \qquad \textit{Eq (5.15)}$$

Let $\xi = \left(\frac{p_r}{p_o} \right)^{-1/n}$, the joint density function in *Eq (5.14)* for power level of multipath component, elevation AoA, and Doppler spread can be rearranged as

$$p(p_r, \gamma, \beta_m) =$$

$$\sum_{i=1}^{2} \left\{ \left(\frac{l_{\mathrm{LoS}}^6 \left(\xi^2 - 1\right)^2 \xi^{n+1} f\left(\mathrm{x_m}, \mathrm{y_m}, \mathrm{z_m}\right)}{8np_o \sqrt{1 - \gamma^2 \sec^2\beta_m}} \right) \right.$$

$$\left. \times \left(\frac{\left(l_{\mathrm{LoS}} + l_{\mathrm{LoS}}\xi^2 - 2\xi(d\cos\beta_m \cos\phi_i + h_t \sin\beta_m) \right)}{\left(d\cos\beta_m \cos\phi_i - \xi l_{\mathrm{LoS}} + h_t \sin\beta_m \right)^4} \right) \right\}$$

Eq (5.16)

where,

$$\phi_i = \begin{cases} \phi_v + \cos^{-1}\left(\gamma \sec \beta_m\right) & ; \quad i = 1 \\ \phi_v - \cos^{-1}\left(\gamma \sec \beta_m\right) & ; \quad i = 2 \end{cases} \qquad \textit{Eq (5.17)}$$

Since, $|\cos\theta_m| \leq 1$, the upper bound for elevation AoA can be obtained from *Eq (5.2)*, as $\beta_m \leq \cos^{-1}(|\gamma|)$. The joint PDF for power and Doppler spectrum can be derived by integrating *Eq (5.16)* over β_m for its appropriate range, which is expressed as:

$$p(p_r, \gamma) = \int_0^{\cos^{-1}(|\gamma|)} p(p_r, \gamma, \beta_m)\, \mathrm{d}\beta_m \qquad \textit{Eq (5.18)}$$

The integral for β_m in *Eq (5.18)* cannot be derived analytically, however, it can be obtained by using the techniques of numerical integration. The marginal PDF of Doppler shift is obtained as,

$$p(\gamma) = \int_{p_l}^{p_u} p(p_r, \gamma)\, \mathrm{d}p_r \qquad \textit{Eq (5.19)}$$

The power spectral density (PSD) is obtained as in [35, 42], i.e.,

$$S(\gamma) = \int_{p_l}^{p_u} p_r \;\; p(p_r, \gamma)\, \mathrm{d}p_r \qquad \textit{Eq (5.20)}$$

where, p_u is the power corresponding to the shortest propagation path l_{LoS} (i.e., $p_u = p_o$), and p_l is the power corresponding to the longest propagation path. For a particular azimuth and elevation angle, the waves reflected from the scatterers located at the boundary of scattering region would correspond to the longest propagation path. Furthermore, among all the multipath waves from a certain azimuth

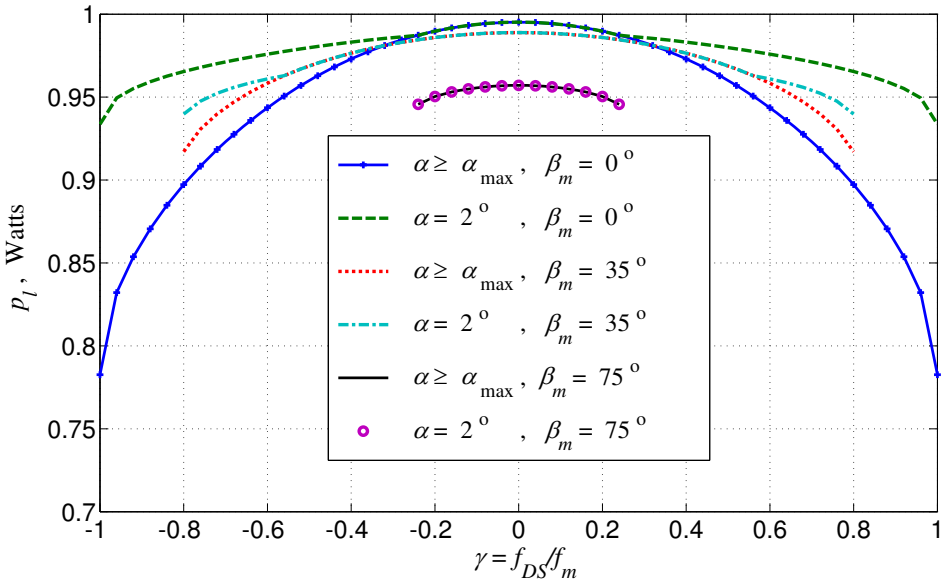

FIGURE 5.2: The lower bound for power as a function of elevation AoA (β_m) and Doppler (γ) for different beam-widths (α) of directional antenna, (d = 800m, a = 100m, b = 30m, h_t = 150m, $\phi_v = 90^o$, $n = 2$, and $p_o = 1$ W)

and elevation angle, the wave with longest path distance would correspond in the lowest power level. The expression for the longest propagation path's distance l_{lim} as a function of azimuth and elevation AoA is shown in *Eq (5.4)*. The lower bound on the power level of multipath waves from a particular direction is shown by p_l, which can be expressed as,

$$p_l = p_o \left(\frac{l_{\text{lim}}}{l_{\text{LoS}}} \right)^{-n} \qquad \textit{Eq (5.21)}$$

The integral for p_r in *Eq (5.20)* can be obtained in closed form if an integer value is set for path-loss exponent n. The longest propagation path's distance l_{lim} can be computed as a function of Doppler shift γ and elevation AoA β_m by substituting *Eq (5.3)* in *Eq (5.4)*. Furthermore, the lower bound of power p_l can also be obtained as a function of Doppler shift γ and elevation AoA β_m by setting the value of ϕ_m as in *Eq (5.3)*. The lower bound of power p_l is plotted in Fig. 5.2 for different values of elevation AoA (i.e., $\beta_m = 0^o$, 35^o, and 75^o) and beam-width of

directional antenna (i.e., $\alpha = 2^o$ and $\alpha_{\max}$). The distance of MS from the boundary of scattering region reduces in those directions where the sharp-beam directional antenna eliminates the distant scattering objects (i.e., Partition 1 of illuminated scattering region, for $\beta_m < \beta_t$). Consequently, for those regions the lower bound of power p_l is higher for the case of sharp-beam directional antenna (i.e., arbitrary small value taken as $\alpha = 2^o$) as compared with the case of omnidirectional antenna (i.e., $\alpha = \alpha_{\max}$), which can be observed in Fig. 5.2. The joint PDF of normalized Doppler shift γ and elevation AoA β_m is obtained as,

$$p(\gamma, \beta_m) = \int_{p_l}^{p_u} p(p_r, \gamma, \beta_m) \mathrm{d}p_r \qquad \textit{Eq (5.22)}$$

The relation for the distribution of elevation AoA and Doppler shift without the consideration of distance-dependent path-loss, can be achieved by adapting the approach used in [52]. Let $\Gamma = \cos\theta_m \cos\beta_m$, the cumulative distribution function (CDF) of the normalized Doppler shift can be expressed as,

$$F_\Gamma(\gamma) = p\left(\Gamma \leq \gamma\right) = \int_0^{\cos^{-1}(|\gamma|)} \left[2 \int_{\cos^{-1}(\gamma/\cos\beta_m)}^{\pi} p(\theta_m, \beta_m) \quad \mathrm{d}\theta_m \right] \mathrm{d}\beta_m \qquad \textit{Eq (5.23)}$$

where $p(\theta_m, \beta_m)$ is the joint PDF of AoA observed at MS, which can be obtained in closed-form by integrating the expression in *Eq (5.6)* over r_m for its appropriate range, which can be expressed for both the partitions of illuminated scattering region as follow:

$$p\left(\theta_m, \beta_m\right) =$$

$$\begin{cases} \frac{1}{3} d^3 \sec^2 \beta_m \ \sin^3 \alpha \ \csc^3\left(\alpha - \theta_m + \phi_v\right) f\left(\mathrm{x_m}, \mathrm{y_m}, \mathrm{z_m}\right) \\ \qquad\qquad\qquad\qquad\qquad\qquad ; \quad 0 \leq \beta_m \leq \beta_t \\ \frac{1}{3} \cos \beta_m \left(\dfrac{a^2 b^2}{b^2 \cos^2 \beta_m + a^2 \sin^2 \beta_m} \right)^{3/2} f\left(\mathrm{x_m}, \mathrm{y_m}, \mathrm{z_m}\right) \\ \qquad\qquad\qquad\qquad\qquad\qquad ; \quad \text{otherwise} \end{cases} \qquad \textit{Eq (5.24)}$$

by substituting *Eq (5.24)* in *Eq (5.23)* and integrating over θ_m for its appropriate range, it can be expressed as

$$F_\Gamma(\gamma) = \int_0^{\cos^{-1}(|\gamma|)} p(\beta_m, \gamma) \quad \mathrm{d}\beta_m \qquad \textit{Eq (5.25)}$$

The marginal PDF of normalized Doppler shift γ and elevation AoA β_m, can be derived as

$$p(\gamma) = \frac{\partial F_\Gamma(\gamma)}{\partial \gamma} \qquad \textit{Eq (5.26)}$$

The direct relation between PDF of Doppler shift and PDF of elevation AoA can be obtained by substituting *Eq (5.25)* in *Eq (5.26)*, which is as follows

$$p(\gamma) = \frac{\partial}{\partial \gamma} \left[\int_0^{\cos^{-1}(|\gamma|)} p(\beta_m, \gamma) \quad \mathrm{d}\beta_m \right] \qquad \textit{Eq (5.27)}$$

These PDFs are general and any distribution of scatterers can be used to define the scatter density function $f\left(\mathrm{x_m}, \mathrm{y_m}, \mathrm{z_m}\right)$. When the scatterers are uniformly distributed in illuminated region (I_{Region}) with volume V, the SDF can be expressed as in *Eq (3.34)*. The directional antenna employed at the BS results in the clipping

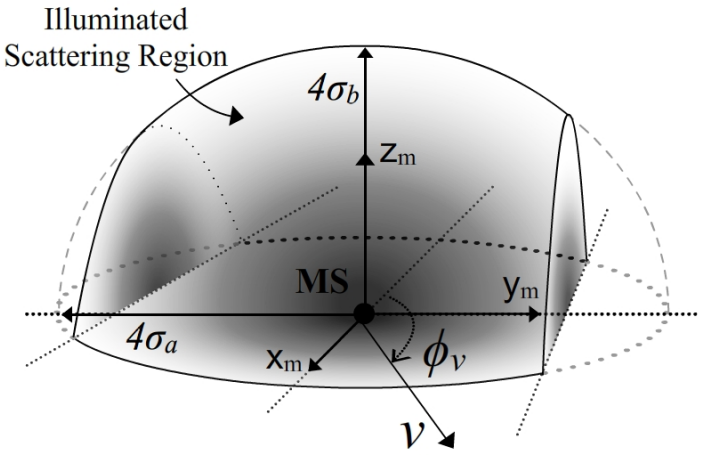

FIGURE 5.3: 3-D Gaussian scatter density around MS, illustrating the clipping caused by directional antenna's beam-width.

of scattering region. Therefore, the volume of the illuminated scattering region as a function of beam-width α is obtained in *Eq (3.33)* [48], which is

$$V = \frac{2\pi bd \sin\alpha \,(a^2 + d\sin\alpha(a - d\sin\alpha))}{3a} \qquad \textit{Eq (5.28)}$$

However, when Gaussian density is assumed for the semi-spheroid shaped scattering region, as shown in Fig. 5.3 with its mean at MS and the virtual boundary at 4σ (as, -4σ to $+4\sigma$ encloses the 99.99% of energy, where, σ is the deviation of scatterers), the scatterer density function is given in *Eq (3.40)*, which is

$$f_G(\mathrm{x_m}, \mathrm{y_m}, \mathrm{z_m}) = \left\{\frac{1}{(2\pi)^{3/2}\sigma_a^2\sigma_b}\right\} \exp\left(-\frac{\mathrm{x_m}^2}{2\sigma_a^2} - \frac{\mathrm{y_m}^2}{2\sigma_a^2} - \frac{\mathrm{z_m}^2}{2\sigma_b^2}\right) \Bigg| \begin{array}{l} \mathrm{x_m} = r_m \cos\beta_m \cos\phi_m \\ \mathrm{y_m} = r_m \cos\beta_m \sin\phi_m \\ \mathrm{z_m} = r_m \sin\beta_m \end{array} \qquad \textit{Eq (5.29)}$$

Where, σ_a and σ_b are the deviations of Gaussian distributed scattering objects in horizontal and vertical planes.

The derived expressions can be exploited to obtain the Doppler distribution characteristics for the most commonly used propagation models in [13, 22–24, 26] with an appropriate choice of a few predefined parameters. The distribution function of Doppler shift for a 3-D propagation model in [22] is derived in [52], where an omnidirectional antenna is considered at the elevated BS. These statistics can be obtained as a special case from the proposed expressions by substituting $\alpha = \alpha_{\max}$, as shown in Fig. 5.7. The plot for the PDF of normalized Doppler shift, for the case of omnidirectional antenna (i.e., $\alpha = \alpha_{\max}$) in Fig. 5.7 is the same as obtained in [52], which validates the theoretical results of proposed analytical model. The power Doppler statistics for the propagation environment in [23] can also be obtained by substituting $a = b$, $h_t = 0$, and $\alpha = \alpha_{\max}$. The proposed analytical model can provide the power Doppler characteristics for the model in [24] by substituting $\alpha = \alpha_{\max}$ and $b \to 0$ (i.e., very small value for b). The expressions for the distribution characteristics of Doppler power spectrum provided in [42] can also be obtained as a special case from the proposed analytical model by substituting $\alpha = \alpha_{\max}$, $h_t = 0$, and $\beta_m = 0^o$. Similarly, the proposed analytical model can also be deduced to obtain the statistics provided by the 2-D scattering model in [26] by substituting zero for BS's antenna height (i.e., $h_t = 0$) and for the elevation AoA (i.e., $\beta_m = 0^o$). Moreover, the statistic distribution of Doppler power spectrum can be obtained for the 2-D scattering (macro-cell) model in [13] by substituting $\alpha = \alpha_{\max}$, $h_t = 0$, and $\beta_m = 0^o$. The above discussion validates the generalization of the proposed analytical model for two- and three-dimensional environments.

5.2 Theoretical Results

In this section, theoretical results obtained for the distributions of Doppler spectrum from the proposed generalized analytical model in relation with direction of mobility, elevation AoA, and the beam-width of directional antenna are presented. The uniform distribution of scatterers is considered to obtain these results. The theoretical results to demonstrate the effects of elevation AoA β_m, azimuthal

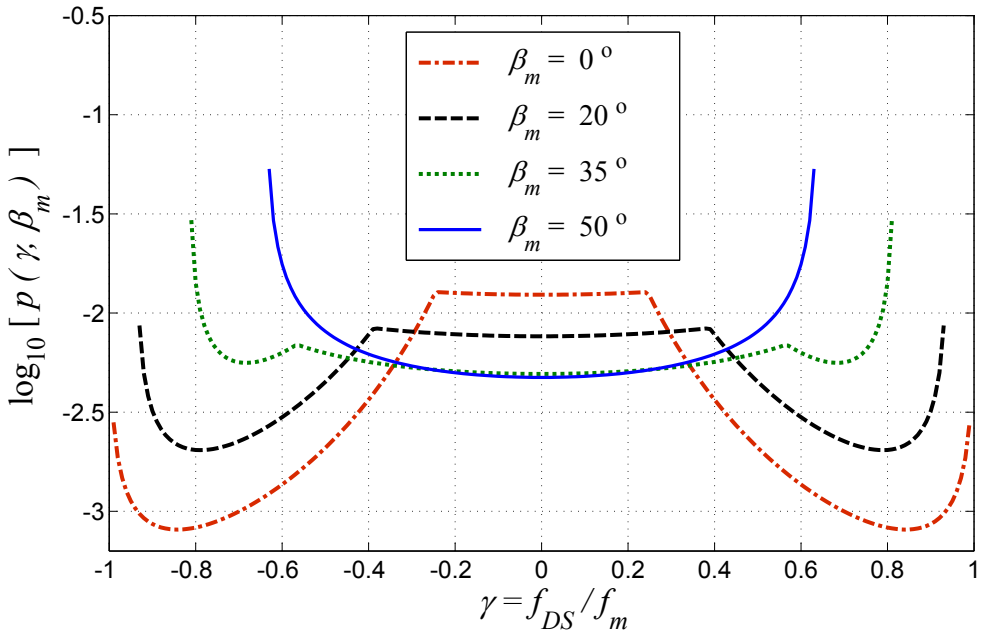

FIGURE 5.4: The distribution of normalized Doppler spread in correspondence with the elevation AoA, ($d = 800$m, $a = 100$m, $b = 30$m, $h_t = 150$m, $\phi_v = 90^o$, $\alpha = 2^o$, $n = 2$, and $p_o = 1$ W)

beam-width of directional antenna α, direction of MS's motion ϕ_v, and scattering region's major-minor ratio a/b on the distribution characteristics of Doppler spectrum are shown in Fig. 5.4, Fig. 5.5, Fig. 5.6, and 5.7, respectively. The following is the detailed discussion on the obtained theoretical results shown in each figure:

5.2.1 Effects of Elevation AoA on Doppler Spectrum

The joint PDF of normalized Doppler shift and elevation AoA is shown in Fig. 5.4 for beam-width $\alpha = 2^o$ and direction of MS's mobility $\phi_v = 90^o$ with respect to LoS component. In Fig. 5.4, it can be observed that by increasing the elevation AoA β_m, the larger values of the PDF of normalized Doppler shift tend to decrease from their maximum when $|\gamma| = 1$ towards the central frequency on the axis of the normalized Doppler shift. This is, because, there is higher probability for the existence of less scatterers in horizontal plane for the higher values of elevation angle β_m. Fig. 5.4 also depicts another important effect of the elevation angle on the Doppler spectrum. It is the gradual absence of clipping for the higher values

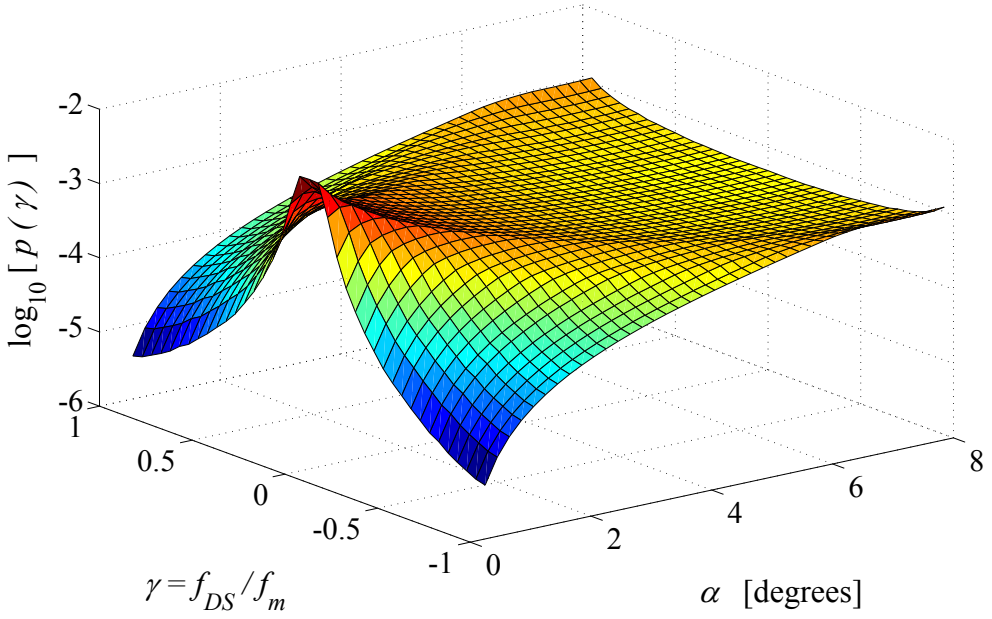

FIGURE 5.5: The PDF of Doppler spread (γ) for different beam-widths (α) of directional antenna, (d = 800m, a = 100m, b = 30m, h_t = 150m, $\phi_v = 90^o$, n = 2, and p_o = 1 W)

of the elevation angles. This is due to the fact that, there is no effect of reducing the azimuthal beam-width on the PDF of AoA for higher values of elevation angle, $\beta_m \geq \beta_t$. Therefore, such geometrical orientation of scatterers forces the PDF of azimuth AoA to uniform and subsequently the PDF of normalized Doppler shift to U-shaped.

5.2.2 Effects of Azimuthal Beam-width of Directional Antenna at BS on Doppler Spectrum

Effects of decreasing beam-width of the directional antenna on the PDF of the normalized Doppler shift, obtained for the direction of motion, $\phi_v = 90^o$, is shown in Fig. 5.5. It is observed that the spread in the PDF of the normalized Doppler shift reduces significantly with a decrease in beam-width of the directional antenna. The reduction in beam-width of the directional antenna from its maximum, $\alpha = \alpha_{\max}$ to an arbitrary small value (taken as 0.5^o in this case) exhibits a converse behavior in the distribution of the Doppler shift. It means that, with a reduction

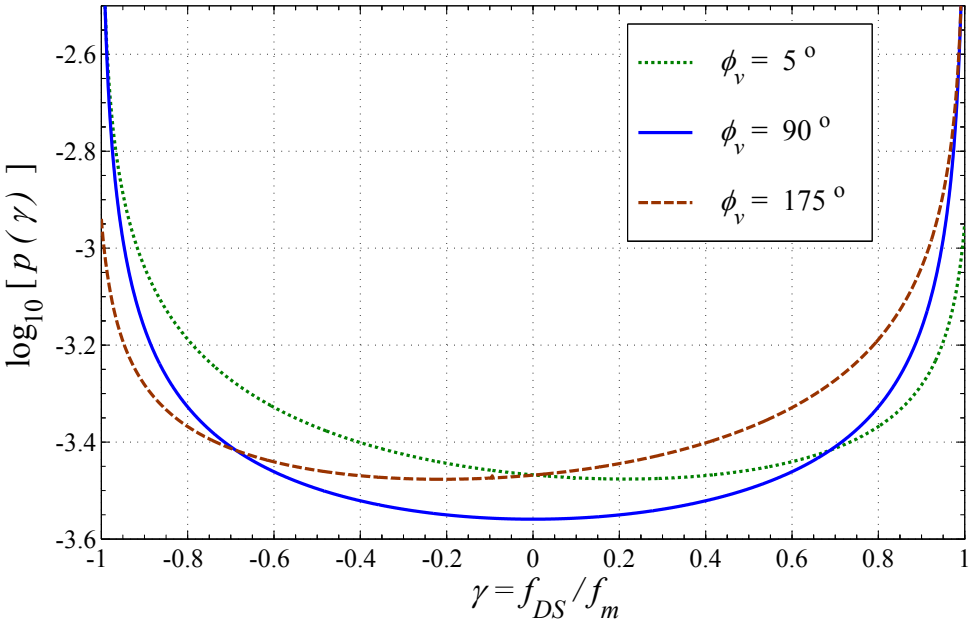

FIGURE 5.6: The distribution of normalized Doppler spread in correspondence with direction of MS's motion, (d = 800m, a = 100m, b = 30m, h_t = 150m, α = $\alpha_{\max}$, n = 2, and p_o = 1 W)

in the beam-width of the directional antenna, the value of the PDF decreases at $|\gamma| = 1$, and increases at $\gamma = 0$.

5.2.3 Effects of Direction of MS's Motion on Doppler Spectrum

Effects of the direction of motion on the distribution of normalized Doppler shift for the case of omnidirectional antenna (i.e., $\alpha = \alpha_{\max}$) is shown in Fig. 5.6, taking $\phi_v = 5^o$, 90^o, and 175^o. It is observed that for $\phi_v = 90^o$, the PDF is seen U-shaped and symmetrical about $\gamma = 0$. This is because when the MS moves in perpendicular to the LoS component, the clipped scattering region is geometrically symmetric and the number of multipath components corresponding to positive and negative Doppler frequencies are equal. Whereas, for $\phi_v = 5^o$ and 175^o the PDF is observed as skewed towards the lower and higher frequencies, respectively, resulted

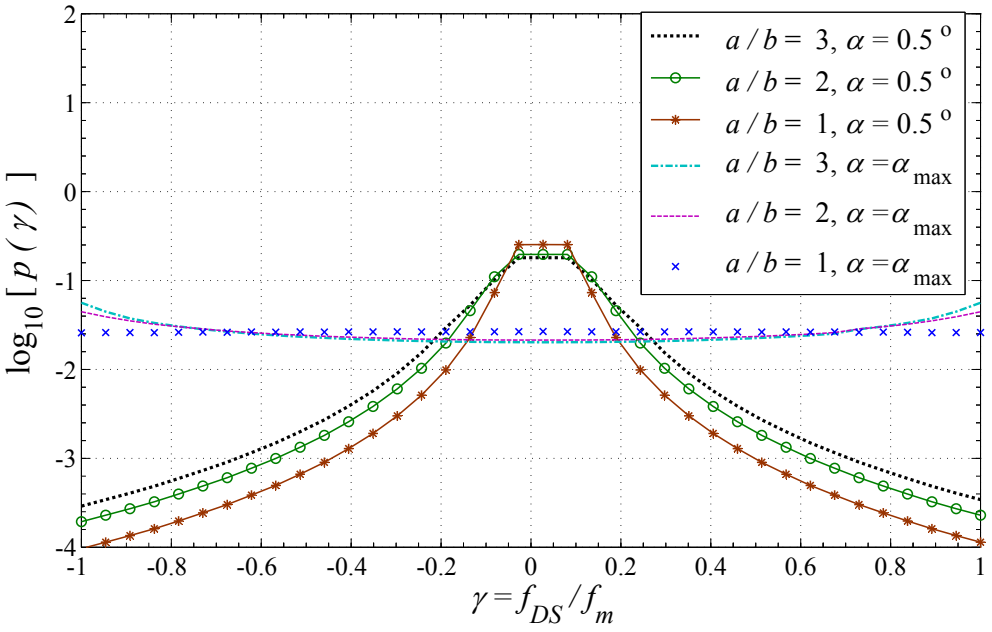

FIGURE 5.7: The PDF of normalized Doppler spread in correspondence with the ratio between radii of scattering-region's major and minor axes (i.e., a/b) and for the cases of directional and omnidirectional antennas, ($d = 800$m, $a = 100$m, $b = 30$m, $h_t = 150$m, $n = 2$, $p_o = 1$ W, $\phi_v = 90^o$)

from the unbalanced number of illuminated scattering objects, with respect to mobile's axis of motion.

5.2.4 Effects of Scattering Region's Geometry on Doppler Spectrum

Effects of changing the geometry of the scattering region is very important, as the high-rise and low height buildings contribute to the Doppler shift differently. Such effects has been studied in Fig. 5.7, considering the case of omnidirectional (i.e., $\alpha = \alpha_{\max}$) and horizontally sharp-beam (i.e., taking arbitrary small value, $\alpha = 0.5^o$) directional antennas. The plots for the case of omnidirectional antenna (i.e., $\alpha = \alpha_{\max}$) are the same as those obtained in [52], which validates the generalization of the proposed analytical model. It is observed that for sharp-beam antenna (sharp in horizontal plane), by increasing the minor axis b of 3-D scattering region, the values of PDF of normalized Doppler shift increases around $|\gamma| = 0$. Which

means that, for a particular scattering environment, taking all the beam-widths of directional antenna, the scatterers located vertically high correspond to significant reduction in Doppler shift. Therefore, it is important to keep the vertical beam-width of directional antenna such that it illuminates those scattering objects which are located vertically high.

5.3 Summary

The impact of directional antenna and motion of MS has thoroughly been investigated on the statistic distribution of power and Doppler shift. A relationship for the distribution of Doppler spectrum and power over multipath waves with the beam-width of directional antenna has been derived for a 3-D mobile radio propagation environment. Closed-form expressions for trivariate PDFs of propagation path distance, power, and Doppler shift in correspondence with the beam-width of the directional antenna have been derived. Moreover, generalized expressions for the relation of elevation AoA with the power and Doppler shift have been presented. Further, to demonstrate the effects of directional antenna on the statistic distribution of Doppler spread, a comprehensive analysis on the basis of obtained theoretical results have been presented.

It has been observed that for the mobility of MS at all the directions, when a directional antenna with sharp beam is used at the BS, the spread in Doppler shift reduces significantly and the higher values of PDF of normalized Doppler shift lie close around the central frequency. It has been observed that, by increasing the elevation AoA β_m, the larger values of the PDF of normalized Doppler shift tend to decrease from their maximum when $|\gamma| = 1$ towards the central frequency on the axis of the normalized Doppler shift. This is, because, there is higher probability for the existence of less scatterers in horizontal plane for the higher values of elevation angle. Furthermore, it has been established that for all the beam-widths of directional antenna, the scatterers located vertically high correspond to significant reduction in Doppler shift.

Chapter 6

GEOMETRICALLY BASED PERFORMANCE ANALYSIS OF HANDOVERS

In this chapter, a performance analysis of handover schemes for the land mobile radio cellular system is carried out by exploiting geometrically based modeling. Impact of various parameters on handover performance is studied. Section 6.1 provides an introduction to some notable types of handover schemes where classification of handover schemes based on control as well as channel assignment is also discussed. In Section 6.2, a performance analysis of handover schemes based on geometrical modeling is presented. Impact of various land mobile radio cellular parameters on the performance of handover process is investigated by exploiting the path loss model.

6.1 Overview of Handover Schemes

The continuous and rapid growth in the telecommunications sector has lead to the increasing development of wireless technologies which has evolved in heterogenous access networks. To provide high-speed access to multiple types of devices, the future generation heterogenous networks are thought to be composed of multiple technologies like, UMTS, WiFi, WiMAX, and LTE. Among many challenges of such heterogenous environments, one major challenge is to provide seamless connectivity to mobile terminals. For maintaining an active connection of moving MS in future generation networks, optimized overlapped wirelessly-connected regions are highly required. Therefore, a number of researchers have recently proposed various handover algorithms along with analytical models in the literature [10, 53–61, 72, 73].

6.1.1 Classification of Handover Schemes w.r.t. Assistance and Control

The control of handover process may be centralized and decentralized in various handover schemes. The handover schemes from decision point of view are broadly classified into three categories (MS assisted, MS controlled, and Network controlled).

6.1.1.1 Mobile Assisted Handover

The selection of the best offering BS among the candidate BSs is very crucial. In mobile assisted handover algorithms, MS maintains the profile of received power and quality of signal from serving and candidate BSs. The transfer of call from a serving BS to a certain BS among the candidates is decided by the network with assistance of MS. This type of handover scheme is used by second generation of mobile cellular systems (e.g, circuit-switched GSM). The time to accomplish the handover process after the decision in a circuit-switched GSM is approximately 1 second [72].

6.1.1.2 MS Controlled Handover

In mobile controlled handover algorithms, the MS solely controls the decision of handover. The MS tracks the power level from all surrounding BSs and measures the interference level of all communication channels. The transfer of call from a serving BS to a certain BS among the candidates is decided and triggered by the MS. This type of handover schemes is used by Digital European Cordless Telephone (DECT) cellular system [74]. The reaction time of mobile controlled handover schemes is very short (on the order of 0.1 second [72]).

6.1.1.3 Network Controlled Handover

In network controlled handover schemes, the network decides and triggers the transfer of mobile user's call by coordination with the serving and candidate BSs.

Network controlled handover is used in first generation of mobile networks (e.g., AMPS).

6.1.2 Types of Handover Schemes w.r.t. Channel Assignment

As far as channel assignment after handover is concerned, handover schemes are broadly classified in to the following two types,

6.1.2.1 Hard Handover

In a hard handover, the communication channel occupied by the MS in a serving cell is released before occupying a channel from the target cell. Therefore, such handover schemes are also known as "break-before-make". The serving BS handovers the mobile user's call to another cell under the control of the network and the MS is linked with only one BS at a time. Hard handover schemes are often used with OFDM and TDMA, where different ranges of frequency spectrum are used in adjacent cells.

6.1.2.2 Soft Handover

In a soft handover scheme, after making the decision of handover, the communication channel in serving cell is maintained for an interval of time in parallel with the channel in target cell. This interval can be short or long till the end of communication session depending upon the feasibility of the channel utilization. If the use of serving channel is not feasible in the target cell, it is released only after the connection with target cell is established. Therefore, such handover schemes are also called "make-before-break". In soft handover schemes, connections with more than one BS may be maintained in order to combine the signals and produce a stronger signal. When such scheme is utilized in both up- and down-link, the handover is termed as softer handover. It is possible only when the involved BSs are operating in same frequency spectrum.

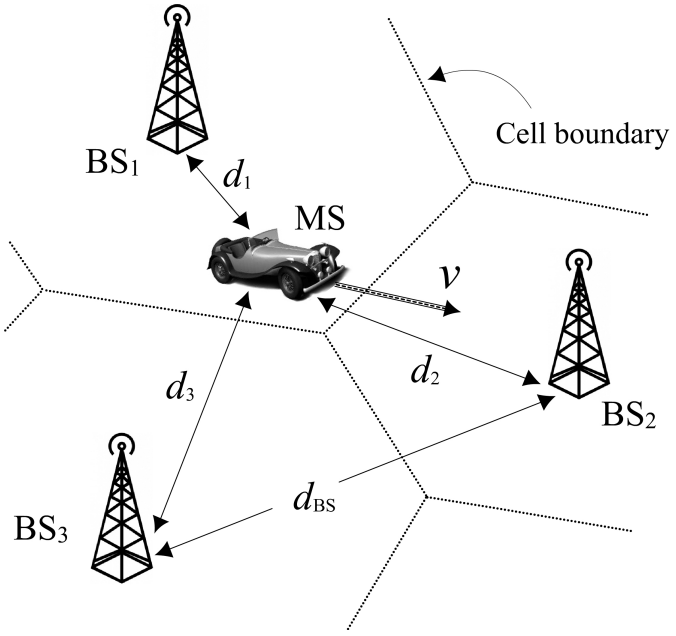

FIGURE 6.1: The land mobile radio cellular network with a MS at boundary of a cell.

6.1.3 Types of Handover Schemes w.r.t. the Technological Composition of Communication Systems

One of the major targets of future heterogenous networks is to provide seamless connectivity to mobile users. Vertical handover refers to the transfer of communication link from serving cell with a certain technology to another cell with some different technology, by maintaining uninterrupted communication session. This is different from the horizontal handover of communication call between different BSs, where the technology of serving and candidate cells is the same.

6.2 Performance Analysis of Handovers

In this section an impact of the velocity of MS, direction of MS's motion, and the propagation environment on the handover margin is intensively analyzed.

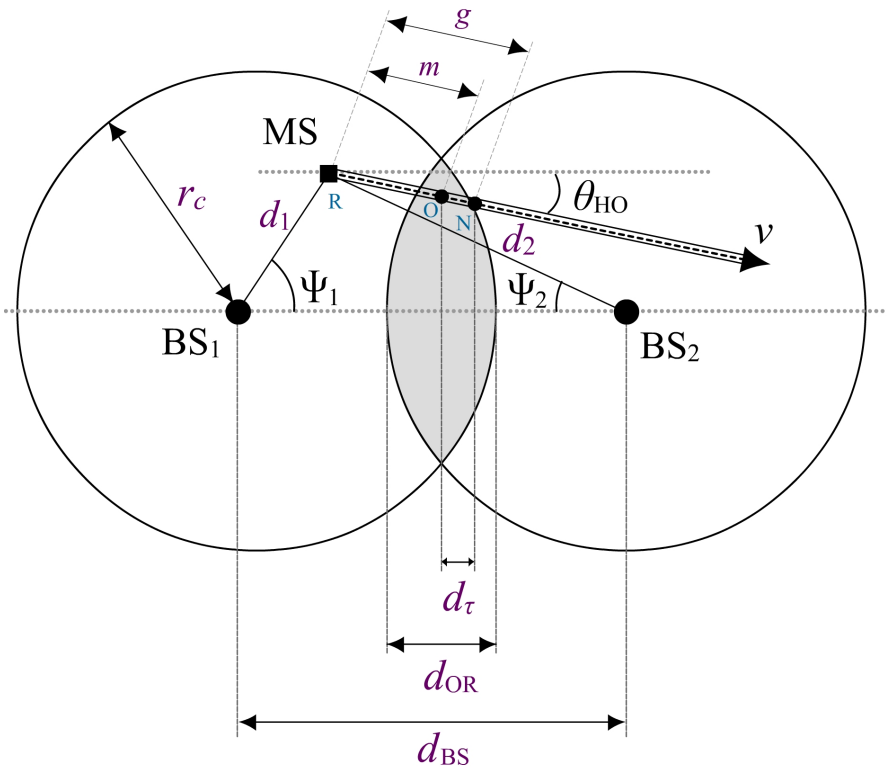

FIGURE 6.2: Top view of the land mobile Radio cellular Network.

6.2.1 Analytical Handover Model

The handover scenario, when an MS moves from a serving cell to an adjacent cell is depicted in Fig. 6.1. The MS moving with velocity v is shown at distance d_1, d_2, and d_3 from BS_1, BS_2, and BS_3, respectively. The distance among the BS's of adjacent cells is d_{BS}. The top view of the land mobile radio cellular network with serving and target BSs is shown in Fig. 6.2. Radius of each cell is shown by r_c. The direction of MS's motion with respect to the line joining BS_1 to BS_2 is θ_{HO}. The AoAs of LoS components from mobile received at BS_1 and BS_2 are shown by Ψ_1 and Ψ_2, respectively. d_{OR} is the maximum horizontal distance of the overlapped region between two adjacent cells. The distance d_τ is the horizontal distance which MS has to travel between the points of initiating and completing handover.

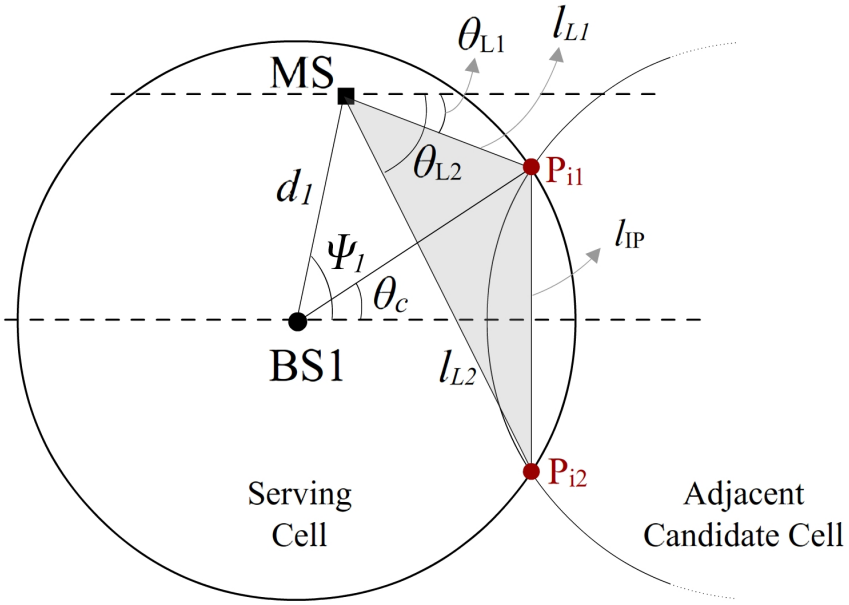

FIGURE 6.3: Handover scope of MS w.r.t. its direction of motion.

We assume that the starting position of the MS is known at the serving BS, BS_1, in form of the distance d_1 and angle Ψ_1 as shown in Fig. 6.2. The distance of MS from the BS of adjacent cell (i.e., BS_2) is shown by d_2, which can be found as

$$d_2 = \sqrt{d_{\text{BS}}^2 + d_1^2 - 2d_{\text{BS}}d_1\cos(\Psi_1)} \qquad \textit{Eq (6.1)}$$

Also the azimuthal AoA of LoS component observed at the BS_2 can be found as,

$$\Psi_2 = \arcsin\left(\frac{d_1}{d_2}\sin\Psi_1\right) \qquad \textit{Eq (6.2)}$$

The MS handovers the communication session to a certain BS which is within the scope of MS with respect to its initial position and direction of motion, i.e., the handover from a serving BS (i.e., BS1) to a candidate BS (i.e., BS2) occurs only when the angle of MS's motion w.r.t. the line joining the serving and candidate BSs is within the the angular limits of θ_{L1} and θ_{L2}, as shown in Fig. 6.3. The length

of the line joining the two intersection points of overlapping cells (i.e., serving and candidate cells), can be found as,

$$l_{\mathrm{IP}} = 2\sqrt{r_c^2 - \left(\frac{d_{\mathrm{BS}}}{2}\right)^2} \qquad \textit{Eq (6.3)}$$

The angular limits of θ_{L1} and θ_{L2} can be easily derived and simplified as following;

$$\theta_{\mathrm{L1}} = \arccos\left(\frac{d_{\mathrm{BS}} - 2d_1\cos(\Psi_1)}{2\ l_{\mathrm{L1}}}\right) \qquad \textit{Eq (6.4)}$$

$$\theta_{\mathrm{L2}} = \arccos\left(\frac{d_{\mathrm{BS}} - 2d_1\cos(\Psi_1)}{2\ l_{\mathrm{L2}}}\right) \qquad \textit{Eq (6.5)}$$

where, the distances l_{L1} and l_{L2} (Fig. 6.3) can be found as,

$$l_{\mathrm{L1}} = \sqrt{d_1^2 + r_c^2 - 2d_1 r_c\cos(\theta_c - \Psi_1)} \qquad \textit{Eq (6.6)}$$

$$l_{\mathrm{L2}} = \sqrt{d_1^2 + r_c^2 - 2d_1 r_c\cos(\theta_c + \Psi_1)} \qquad \textit{Eq (6.7)}$$

where, the angle, θ_c, shown in Fig. 6.3 can be found as, $\theta_c = \arccos(d_{\mathrm{BS}}/2r_c)$. The position of MS changes due to the mobility of MS; therefore, the new position of MS can be found as a function of velocity v, direction θ_{HO}, and the duration τ of MS's motion, as

$$d_{1,n} = \sqrt{d_1^2 + (v\ \tau)^2 - 2d_1 v\ \tau\cos(\pi - \Psi_1 - \theta_{\mathrm{HO}})} \qquad \textit{Eq (6.8)}$$

$$d_{2,n} = \sqrt{d_2^2 + (v\ \tau)^2 - 2d_2 v\ \tau\cos(\Psi_2 - \theta_{\mathrm{HO}})} \qquad \textit{Eq (6.9)}$$

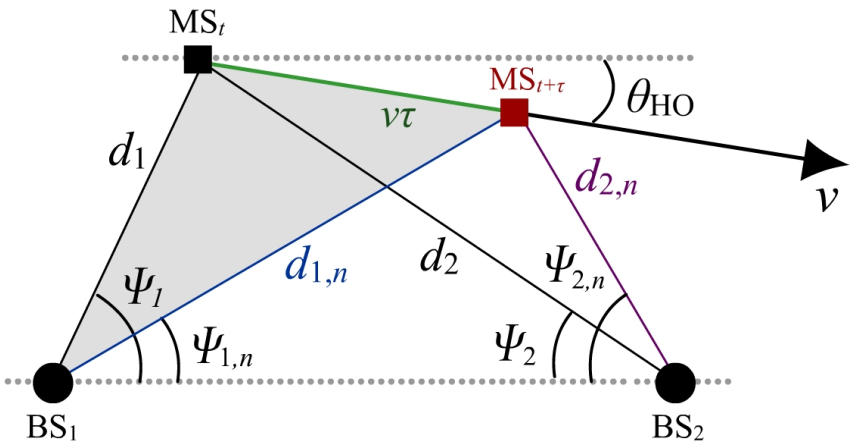

FIGURE 6.4: Mobility of MS from the serving BS towards the adjacent cell.

$$\Psi_{1,n} = \Psi_1 - \arcsin\left(\frac{v\ \tau}{d_{1,n}}\sin(\pi - \theta_{\mathrm{HO}} - \Psi_1)\right) \qquad \textit{Eq (6.10)}$$

$$\Psi_{1,n} = \Psi_2 + \arcsin\left(\frac{v\ \tau}{d_{2,n}}\sin(\pi - \theta_{\mathrm{HO}} - \Psi_2)\right) \qquad \textit{Eq (6.11)}$$

Assuming, the MS starts to move with a certain velocity, v, and angle, θ_{HO} within limits of θ_{L1} and θ_{L1}, from its initial position R at time instant t (see Fig. 6.2) and reaches the point O (point where handover is triggered) after a time delay of m/v, and further research point N (point where handover completes) after a total time delay of, $\tau = g/v$. Thus, the time margin available to perform handover can be found as,

$$\tau_{\mathrm{marg}} = \frac{1}{v}\Big(g - m\Big) \qquad \textit{Eq (6.12)}$$

where, the distances m and g can be found as,

$$m = \sec\theta_{\mathrm{HO}}\ \ \Big(\frac{d}{2} - d_1\cos\Psi_1\Big) \qquad \textit{Eq (6.13)}$$

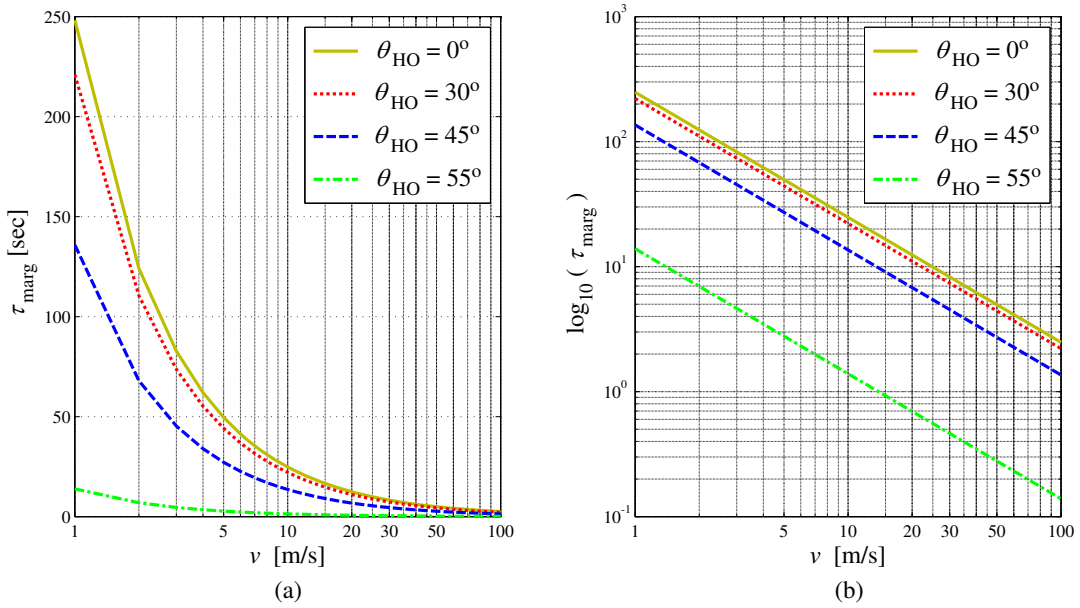

FIGURE 6.5: The handover margin, τ_{marg}, in correspondence with velocity, v, of MS for different angles of MS's motion by using the geometrically based model, θ_{HO},($d_{\text{BS}} = 1000\text{m}, d_1 = 100\text{m}, K_2 = 40dB, \Psi_1 = 40^o$, and $r_c = 700\text{m}$). (a) Shown on linear scale (along y-axis), (b) shown on logarithmic scale (along y-axis).

$$g = -d_1 \cos(\theta_{\text{HO}} + \Psi_1) + \sqrt{-d_1^2 + r_c^2 + d_1^2 \cos^2(\theta_{\text{HO}} + \Psi_1)} \qquad \textit{Eq (6.14)}$$

The handover margin, τ_{marg}, for different values of velocity v and direction of mobile motion, θ_{HO}, is shown in Fig. 6.5, where the effects of direction of MS motion can easily be observed.

6.2.2 Performance Analysis of Handover Schemes Using Pathloss Model

The received power of the mobile at any distance d_i from the i^{th} BS can be expressed in terms of the measured power, p_o, at some known distance, d_o (usually termed as the close-in reference distance) from the same BS, and path-loss exponent, n, as

$$p_{r,i}(d_i) = p_o \left(\frac{d_o}{d_i}\right)^n \qquad \textit{Eq (6.15)}$$

Eq (6.15) can also be expressed in logarithmic scale as,

$$p_{r,i}(d_i) = K_1 - K_{2,i}\ \log_{10}(d_i) \qquad \textit{Eq (6.16)}$$

where, $K_1 = 10\ \log_{10}(p_o d_o^n)$, is constant for each of these BSs with in the network, assuming all the BSs are transmitting the same power and exploits similar kind of antennas at transmitter and receiver. $K_{2,i} = 10n$, is the environment specific attenuation characteristics [75–77] of the region around i^{th} BS.

The MS continuously measures the strength of signals from the serving cell's BS and from the BSs of adjacent cells. When the MS moves into the overlapped region between serving cell and candidate adjacent cell, the process of handover starts. In this case, ideally, the signal strength from the serving BS starts to decrease and the signal strength from the neighboring cell (in which MS is entering) starts to increase, hence the process of handover gets triggered. In certain scenarios, certain problems due to cell dragging may arise. The signals of the previously serving cell may cause interference with those of new cell and this may lead to pingpong handovers. Pingpong is the continuously happening handover process among the currently connected BS and the previous serving cell's BS. Pingpong is highly undesired, as it causes wastage of resources and also reduces overall network GoS.

It is challenging to provide a reliable and seamless handover of radio link between two neighboring cells. However, as the handover of our interest is network-initiated and MS-assisted [73, 75], it is easy to implement any intermediate processing algorithm at the central network controller (like an MSC in many cases). The process of handover can be simplified in three main steps, i.e., initialization, preparation and execution [78]. The MS after certain time period provides the measurements

to the BS. This is done on the basis of measuring power of the pilot channel (in GSM also known as broadcast channel) which is transmitted known reference symbols (RS). Based on the received power (usually known as Received Signal Strength Indicator (RSSI)) there can be certain predefined handover conditions or thresholds within the network to trigger a handover procedure. For this purpose, the MS should track the instantaneous received signal (i.e., the RSSI) and compare it with the predefined threshold.

Let's assume the received power at MS from the serving BS is denoted as $p_{r,1}$, the distance between the MS and serving BS is d_1 and the predefined handover threshold in terms of expected minimum usable received power is p_{th}. The received power profile matrix is defined as the matrix containing the received power vectors of the serving and candidate BSs, i.e.,

$$\mathbf{P}_r = [\mathbf{p}_{r,1}(d_2), \mathbf{p}_{r,2}(d_2), \ldots, \mathbf{p}_{r,M}(d_M)] \qquad \textit{Eq (6.17)}$$

where, subscript $i = 1, 2, ..., M$ shows the M base-stations that take part in the handover procedure. Out of these M base-stations, BS1 (denoted with subscript 1) is the serving BS and other $M - 1$ base-stations (refereed with subscript $i = 2, 3, ..., M$) are the candidate BSs.

The handover procedure is required to be triggered if the following condition is satisfied, i.e.,

$$p_{r,1}(d_1) \leq p_{th} \leq \max(\mathbf{P}_r) \qquad \textit{Eq (6.18)}$$

However, merging towards this condition is not unique in every cell, as it is dependent upon the structure of terrain within a certain cell. Most of the time, variability of terrain as well as dense urban structure causes unavailability of LoS for a very short interval of time. This creates fluctuations in the received

power profile, which are subsequently used by the MS to initiate a false trigger for handover. This occurrence is widely known as Pingpong handover between the serving and the candidate cells. To avoid such scenario, two major solutions are available, either to use an avoidance timer [79] or to use the hysteresis margin algorithms [73]. Both methods still have certain failure rates; especially at cell boundaries and dense urban areas. This problem can be solved by taking sliding averages of the previous power measurements denoted as $\mathbf{P}_a$, whose elements can be expressed as

$$p_{a,i}(d,w) = \frac{1}{d_w}\int_{d-d_w}^{d} p_{r,i}(x)dx \qquad \textit{Eq (6.19)}$$

where, $i \in \{1,2,...M\}$ and d_w is the averaging interval's distance. The averaging window's time interval thus can be found as $w = d_w/v$. The derivations in the rest of this chapter are, thus, based on the above mentioned time-averaged received power. The average received power matrix $\mathbf{P_a}$ can be written as

$$\mathbf{P_a} = [\mathbf{p}_{a,1}, \mathbf{p}_{a,2}, ..., \mathbf{p}_{a,M}] \qquad \textit{Eq (6.20)}$$

In Fig. 6.6, the averaged received power from the serving BS and two candidate BSs is plotted. The residual power ratio vector $\mathbf{q}$ can be expressed as

$$\mathbf{q} = [q_2, q_3..., q_{M-1}] \qquad \textit{Eq (6.21)}$$

where, the residual power ratio of the i^{th} candidate BS is $q_i = (P_{a,1} - P_{a,i})$, at any time instant. Handover decision is required to be made to the BS, which provides $max(\mathbf{q})$. Lets assume the survived BS with the maximum residual power ratio denoted as $q_1 = \max(\mathbf{q})$. The points O and N in Fig. 6.2 show the positions of MS when the process of handover is triggered and when it is completed, respectively. The distance traveled by the MS from its initial position R to points O and N

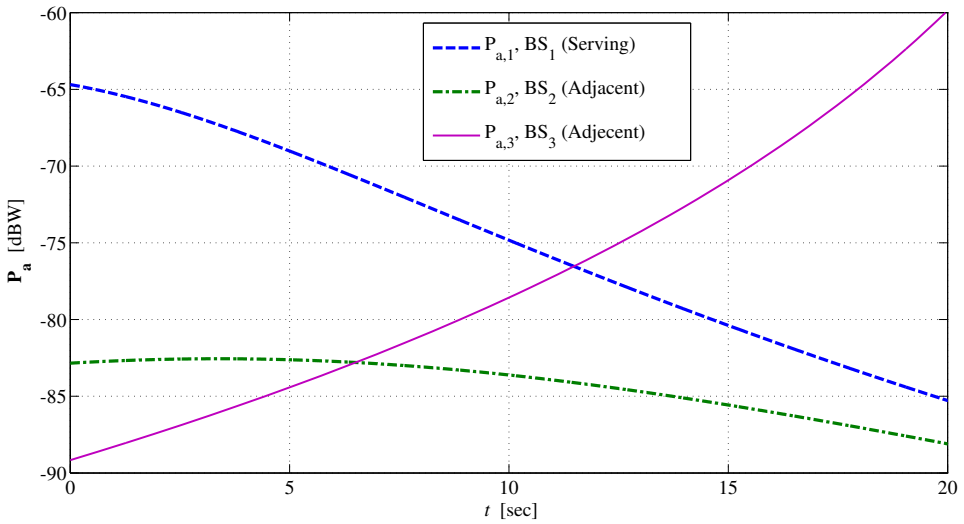

FIGURE 6.6: The averaged received power at MS from serving and adjacent candidate BSs, ($K_1 = 40dB, K_2 = 40dB, d_{\text{BS}} = 1000\text{m}, d_1 = 100\text{m}, \Psi_1 = 40^o, r_c = 700$, and $\theta_{HO} = 5^o$)

are shown by m and g in *Eq (6.13)* and *Eq (6.14)*, respectively. Point O is the position of MS where the received power from BS1 and BS2 gets equal (difference between the received powers is zero), which is

$$0 = P_{a,2} - P_{a,1} \qquad \textit{Eq (6.22)}$$

By setting the values of $P_{a,1}$ and $P_{a,2}$ as the power received at point O from BS1 and BS2, and rearranging *Eq (6.22)* for m, we get

$$m = \frac{-d_1^2 + d_2^2}{2(d_2 \cos(\Psi_2 - \theta_{\text{HO}}) + d_1 \cos(\Psi_1 + \theta_{\text{HO}}))} \qquad \textit{Eq (6.23)}$$

N is the point (Fig. 6.2) at which the difference between the received power from BS1 and BS2 gets equal to the predefined residual power ratio, q_2, which can be expressed as

$$q_2 = P_{a,2} - P_{a,1} \qquad \textit{Eq (6.24)}$$

After rearranging *Eq (6.24)* for g and doing tedious calculations (refer section A.2 in Appendix A), the simplified form can be expressed as

$$g = \frac{1}{10^{2q_2/K2}-1}\left(10^{2q_2/K_2}d_2\cos(\Psi_2-\theta_{\mathrm{HO}})+d_1\cos(\alpha_1+\theta_{\mathrm{HO}})\right.$$
$$-\frac{1}{2}\Big(-4\big(10^{2q_2/K_2}-1\big)\big(10^{2q_2/K_2}d_2^2-d_1^2\big)+4\big(10^{2q_2/k_2}d_2\cos(\Psi_2-\theta_{\mathrm{HO}})$$
$$\left.+d_1\cos(\Psi_1+\theta_{\mathrm{HO}})\ \big)^2\ \Big)^{1/2}\right) \qquad \textit{Eq (6.25)}$$

The distance, $(g-m)$, associated with the handover margin, τ_{marg}, is dependent upon the predefined residual power ratio, q_i. The time available to complete the handover procedure is the time taken by the MS to travel the distance, $(g-m)$, with a certain velocity. Therefore, the time margin that is available to perform the handover procedure is denoted by τ_{marg} and can be obtained from the following equation,

$$\tau_{\mathrm{marg}} = \frac{1}{v}\Big(g-m\Big) \qquad \textit{Eq (6.26)}$$

The required horizontal length of overlapped region between adjacent cells corresponding to a certain handover margin shown by d_τ in Fig. 6.2, can be found as

$$d_\tau \ = \ v\ \tau_{\mathrm{marg}}\ \cos(\theta_{\mathrm{HO}}) \qquad \textit{Eq (6.27)}$$

The maximum horizontal length of overlapped region along the line joining the BS1 and BS2 is shown by d_{OR} in Fig. 6.2, which can be written as,

$$\frac{d_{\mathrm{OR}}}{2} \;=\; v\ \tau_{\mathrm{marg}}\ \cos(\theta_{\mathrm{HO}})\Big|_{\Psi_1=0^o \text{ and } \theta_{\mathrm{HO}}=0^o} \qquad \textit{Eq (6.28)}$$

The radius of cell, r_c, can be expressed as a function of distance between the adjacent BSs, d_{BS}, and horizontal maximum length of overlapped region, d_{OR}, as

$$r_c = \frac{d_{\mathrm{BS}} + d_{\mathrm{OR}}}{2} \qquad \textit{Eq (6.29)}$$

by substituting *Eq (6.28)* in *Eq (6.29)*, we get

$$r_c = \frac{d_{\mathrm{BS}} \;+\; v\ \tau_{\mathrm{marg}}\ \cos(\theta_{\mathrm{HO}})}{2}\Bigg|_{\Psi_1=0^o \text{ and } \theta_{\mathrm{HO}}=0^o} \qquad \textit{Eq (6.30)}$$

The ratio between the length of overlapping region and radius of cell, $\delta_{\mathrm{RO}} = d_{\mathrm{OR}}/r_c$, required to achieve a certain handover margin, can thus be obtained by using the results in *Eq (6.31)* and *Eq (6.28)*, as

$$\delta_{\mathrm{RO}} = \frac{2\ v\ \tau_{\mathrm{marg}}\ \cos(\theta_{\mathrm{HO}})}{d_{\mathrm{BS}} \;+\; v\ \tau_{\mathrm{marg}}\ \cos(\theta_{\mathrm{HO}})}\Bigg|_{\Psi_1=0^o \text{ and } \theta_{\mathrm{HO}}=0^o} \qquad \textit{Eq (6.31)}$$

Three base-stations are considered for the simulation setup; as shown in Fig. 6.1. The measurements of wireless channels for frequency range between $0.5 - 15$ GHz correspond to channel characterizing parameter K_2 as between $15 - 50$ dB [53]. We assume a typical urban environment for which the value of K_2 can be taken as $40dB$ [76]. The distance among adjacent BSs and the radius of each cell are set as $d_{\mathrm{BS}} = 1000$m and $r_c = 700$m, respectively. The initial position of MS at an arbitrary time instant t is defined as, $d_1 = 100$m and $\Psi_1 = 40^o$. The initial position of MS along with its direction of motion together set the potential positions of MS where the handover should be triggered and accomplished. General scenarios for the motion of MS are considered, where the MS is neither moving in a circular

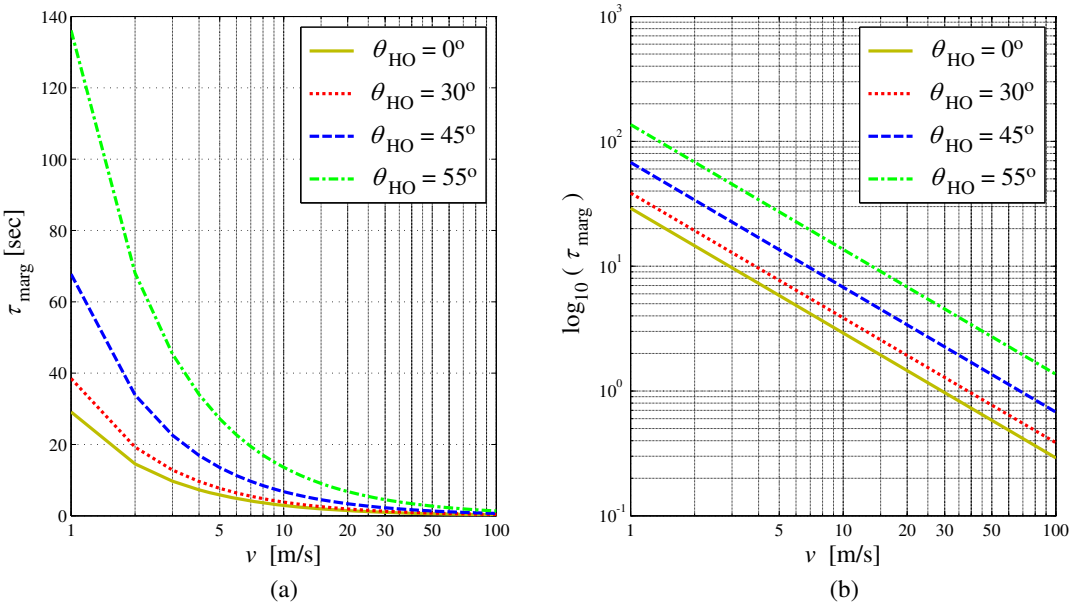

FIGURE 6.7: The handover margin, τ_{marg}, in correspondence with velocity, v, of MS for different angles of MS's motion, θ_{HO} by using the residual power ratio, ($q_2 = 6dB, d_{\text{BS}} = 1000\text{m}, d_1 = 100\text{m}, K_2 = 40dB, \Psi_1 = 40^o$, and $r_c = 700\text{m}$). (a) Shown on linear scale (along y-axis), (b) shown in logarithmic scale (along y-axis).

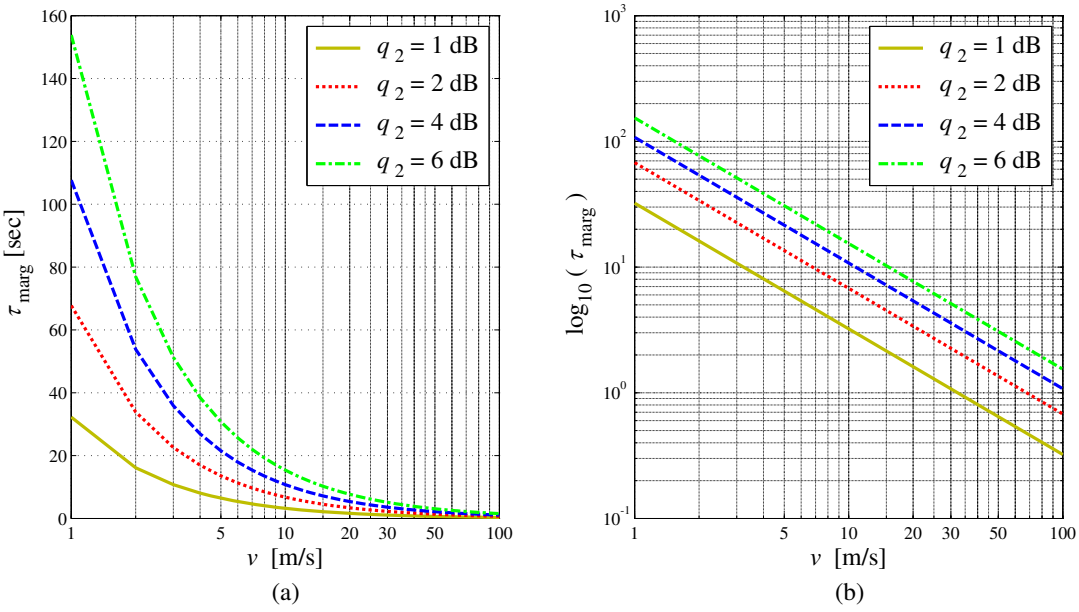

FIGURE 6.8: The handover time margin τ_{marg} in correspondence with velocity v of MS for different values of residual power ratio, ($\theta_{\text{HO}} = 45^o, d_{\text{BS}} = 1000\text{m}, d_1 = 100\text{m}, K_2 = 40dB, \Psi_1 = 40^o$, and $r_c = 700\text{m}$). (a) Shown on linear scale (along y-axis), (b) shown on logarithmic scale (along y-axis).

path with respect to BS nor along the line joining the two intersection points of the adjacent cells as shown in Fig. 6.3.

In Fig. 6.7, the effects of various directions of mobile motion on the handover margin w.r.t. the velocity v of MS are shown on both linear and logarithmic scales. For higher angles of θ_{HO} the MS moves away from both the BSs with a different rate, therefore it takes more distance to create the required difference, q_2, between the received powers, which further leads to increased handover margin. Whereas, in contrast to these results, the results shown in Fig. 6.5 have a converse behavior. In the approach used to obtain the plots of Fig. 6.5, the handover always accomplishes at the border of the serving cell. This is because, the cross-section distance of the overlapped region decreases with an increase in θ_{HO}; therefore the handover margin decreases accordingly.

The effects of residual power ratio on the handover margin τ_{marg} for different values of velocity v are shown in Fig. 6.8, where it is evident that, with an increase in the predefined residual power ratio, q_2, the time margin available to perform handover increases. Furthermore, the effects of K_2 (containing the effect of propagation environment) on handover margin, τ_{marg}, are shown in Fig. 6.9, where it can be observed that handover margin decreases significantly with an increase in K_2. In other words, for dense urban areas with higher propagation path loss exponent, the time margin available to perform the handover is less; therefore, quicker decision of handover is required to be made.

6.3 Summary

A geometrically based analysis has been presented to gauge the performance of handover schemes. Mathematical relationship of the handover margin with velocity of MS, direction of mobile motion, and propagation environment has been derived on the basis of both geometrical model and path loss propagation model. Relationship for the ratio between the radius of coverage area and the length of

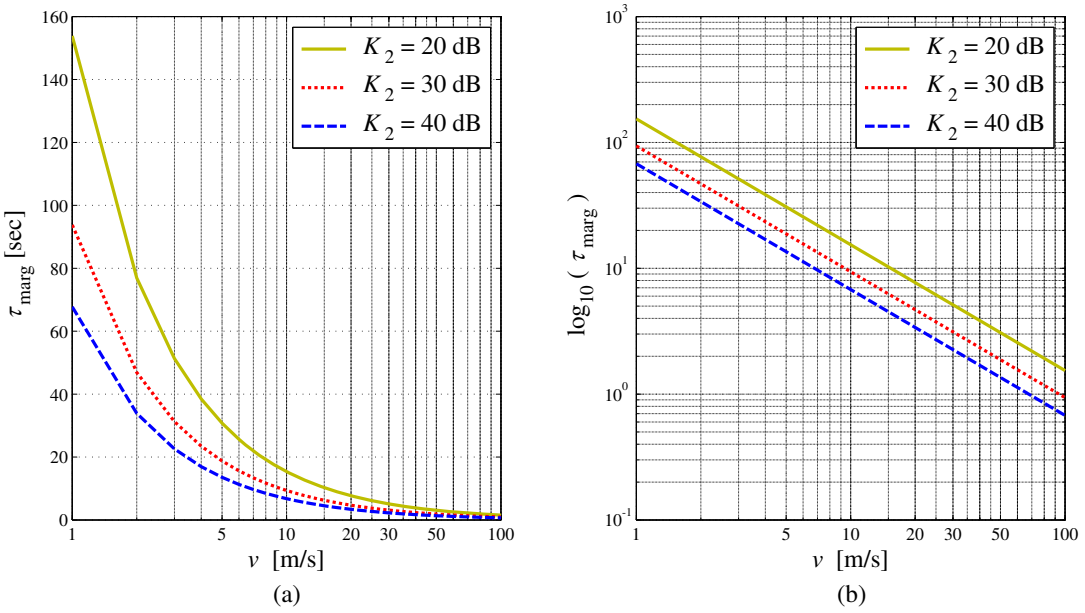

FIGURE 6.9: The effects of K_2 on handover margin τ_{marg} in correspondence with velocity v of MS for different values K_2, ($\theta_{\text{HO}} = 45^o, d_{\text{BS}} = 1000\text{m}, d_1 = 100\text{m}, q_2 = 2dB, \Psi_1 = 40^o$, and $r_c = 700\text{m}$). (a) Shown on linear scale (along y-axis), (b) shown on logarithmic scale (along y-axis).

overlapped region between adjacent cells has been derived, which guarantees to satisfy the required handover margin. The impact of velocity and direction of MS's motion on the handover margin has been analyzed. Moreover, the impact of propagation environment on the handover margin has also been analyzed. Where it has been observed that, handover margin decreases significantly with an increase in the path loss exponent. In dense urban areas with higher propagation path loss exponent, the time margin available to perform the handover is less; therefore, quicker decision of handover is required to be made.

Chapter 7

CONCLUSIONS AND FUTURE DIRECTIONS

This chapter presents a brief summary of the thesis in Section 7.1 and discusses future research directions in Section 7.2 on the basis of achieved results.

7.1 Summary and Conclusions

A generalized 3-D scattering model has been developed, which assumes a directional antenna with controllable azimuthal beam-width employed at an elevated BS. The scattering objects have been assumed to be confined within a semi-spheroid shaped region with its base centered at MS. The radius of semi-spheroid region is independently controllable along with its major and minor axes. Both uniform and Gaussian distribution functions have been considered to model the scattering objects. The directional antenna at BS results in the clipping of scattering region and only the illuminated scattering objects correspond to the arrival of waves at receiver. The effects of directional antenna at BS on the geometry of scattering region has thoroughly been investigated and various threshold angular parameters have been established to distinguished illuminated and eliminated scattering regions.

The spatial and temporal statistics of up and down radio communication links have been derived for the proposed 3-D propagation model for both uniform and Gaussian scatter densities. The effects of directional antenna has thoroughly been observed on the spatial and temporal statistics in correspondence with the azimuth and elevation angles. Closed-form expressions for the joint and the marginal PDFs of AoA both in azimuth and elevation planes have been derived by assuming the uniform as well as Gaussian distribution of scattering objects. Moreover, to demonstrate the validity of proposed model, the obtained theoretical results for spatial statistics at BS assuming Gaussian scatter density have been compared with measured data provided in the literature.

The developed 3-D scattering model has been shown to deduce some notable 2-D and 3-D scattering models that assume uniform distribution of scatterers around MS for macro-cell environment [13, 15, 22–24, 26].

Further, the impact of directional antenna and motion of MS has thoroughly been investigated on the statistic distribution of power and Doppler shift. A relationship for the distribution of Doppler spectrum and power over multipath waves with the beam-width of directional antenna has been derived for a 3-D mobile radio propagation environment. Closed-form expressions for trivariate PDFs of propagation path distance, power, and Doppler shift in correspondence with the beam-width of the directional antenna have been derived. Moreover, generalized expressions for the relation of elevation AoA with the power and Doppler shift have been presented. Further, to demonstrate the effects of directional antenna on the statistic distribution of Doppler power spectrum, the theoretical results obtained from the proposed analytical model along with the observations have been presented.

It has been observed that for the mobility of MS at all the directions, when a directional antenna with sharp beam is used at the BS, the spread in Doppler shift reduces significantly and the higher values of PDF of normalized Doppler shift lie close around the central frequency. It has been observed that, by increasing the elevation AoA β_m, the larger values of the PDF of normalized Doppler shift tend to decrease from their maximum when $|\gamma| = 1$ towards the central frequency on the axis of the normalized Doppler shift. This is, because, there is higher probability for the existence of less scatterers in horizontal plane for the higher values of elevation angle. Furthermore, it has been concluded that for all the beam-widths of directional antenna, the scatterers located vertically high correspond to significant reduction in Doppler shift. Therefore, it is essential to consider the propagation of multipath waves in 3-D space to determine the accurate channel characteristics, which further leads to the design of more precise and reliable communication links.

A geometrically based analysis has been presented to gauge the performance of handover schemes. Mathematical relationship of the handover margin with velocity of MS, direction of mobile motion, and propagation environment has been derived on the basis of both geometrical model and path loss propagation model. Relationship for the ratio between radius of coverage and overlapped region between adjacent cells has been derived, which guarantees to satisfy the required handover margin. The impact of velocity and direction of MS's motion on the handover margin has intensively been analyzed. Moreover, the impact of propagation environment on the handover margin has also been analyzed. Where it has been observed that, handover margin decreases significantly with an increase in the path loss exponent. It has been concluded that, in dense urban areas with higher propagation path loss exponent, the time margin available to perform the handover is less; therefore, quicker decision of handover is required to be made.

7.2 Future Work

The analytical results for characterization of angular and temporal statistics of multipath signals presented in this thesis are useful for the performance evaluation and system design of wireless cellular systems. Such statistics of the multipath waves in 3-D propagation environment is useful to evaluate the capabilities of beam oriented technologies. Moreover, these statistics are also necessary for avoiding antenna correlations in designing diversity techniques with improved diversity gain in MIMO systems.

The strategy of our future work is composed of the following three plans:

7.2.1 Plan 1: Shape Factors

The derived angular and temporal statistics for 3-D propagation environment can be used to derive their shape factors (which are, angular Spread, Angular Constriction, and direction of maximum fading), which can further be used to derive the second order statistics, like level crossing rate, average fade duration, spatial

correlation and coherence distance. Such study for the case of 2-D scattering models is presented in [1, 11, 12], *however, there is a scope to conduct such analysis for the case of 3-D propagation models.*

7.2.2 Plan 2: Accurate Scatter Density Function

Assuming a single bounce 3-D scattering model with spherical symmetric scatter density, we have derived angular and temporal statistics for both uniform and Gaussian scatter densities. However, in realistic 3-D propagation environments, the geometry of scattering region around the MS is not always symmetric. This plan of future work aims at numerical computation of accurate scatter density function for given angular (3-D AoA) and temporal (ToA) measurements. A relationship between numerical measurements of ToA or AoA and scatter density function can be derived. Such effort for the case of 2-D scattering environment has been made recently in [80]. Since, the use of 3-D propagation models is more realistic, *therefore, our proposed 3-D propagation model may be extended for the derivation of such relationship between the measurement data of AoA or ToA and the scatter density function.*

7.2.3 Plan 3: Geometrically Based Study of Handovers in Future Heterogenous Networks

In next generation networks, the handover of communication sessions can possibly be among heterogeneous cellular environments (e.g., from a serving BS with micro-cell scattering environment to a targeted BS with pico-cell scattering environment i.e., Wireless Local Area Networks (WLANs)). *Therefore, there is a scope to conduct a geometrically-based analysis that includes the impact of scattering environment and system heterogeneity on the handover procedure.*

Appendix A

MATHEMATICAL DERIVATIONS

A.1 Jacobian Transformations

The Jacobian transformation, $J\left(\mathrm{x_m}, \mathrm{y_m}, \mathrm{z_m}\right)$, given in *Eq (4.1)* can be found as,

$$J\left(\mathrm{x_m}, \mathrm{y_m}, \mathrm{z_m}\right) = \begin{vmatrix} \frac{\partial\ \mathrm{x_m}}{\partial\ r_m} & \frac{\partial\ \mathrm{x_m}}{\partial\ \phi_m} & \frac{\partial\ \mathrm{x_m}}{\partial\ \beta_m} \\ \frac{\partial\ \mathrm{y_m}}{\partial\ r_m} & \frac{\partial\ \mathrm{y_m}}{\partial\ \phi_m} & \frac{\partial\ \mathrm{y_m}}{\partial\ \beta_m} \\ \frac{\partial\ \mathrm{z_m}}{\partial\ r_m} & \frac{\partial\ \mathrm{z_m}}{\partial\ \phi_m} & \frac{\partial\ \mathrm{z_m}}{\partial\ \beta_m} \end{vmatrix}^{-1} \qquad \textit{Eq (A.1)}$$

The relationships for transformation between different coordinate systems can be expressed as follow,

$$\mathrm{x_m} = r_m \cos\beta_m \cos\phi_m \qquad \textit{Eq (A.2)}$$

$$\mathrm{y_m} = r_m \cos\beta_m \sin\phi_m \qquad \textit{Eq (A.3)}$$

$$\mathrm{z_m} = r_m \sin\beta_m \qquad \textit{Eq (A.4)}$$

After simplifications *Eq (A.1)* can be expressed as,

$$J\left(\mathrm{x_m}, \mathrm{y_m}, \mathrm{z_m}\right) = \begin{vmatrix} \cos\beta_m \cos\phi_m & -r_m \cos\beta_m \sin\phi_m & -r_m \sin\beta_m \cos\phi_m \\ \cos\beta_m \sin\phi_m & r_m \cos\beta_m \cos\phi_m & -r_m \sin\beta_m \sin\phi_m \\ \sin\beta_m & 0 & r_m \cos\beta_m \end{vmatrix}^{-1}$$

Eq (A.5)

$$\begin{aligned} &J(r_m, \phi_m, \beta_m) = \\ &\Big[(\cos\beta_m \cos\phi_m) \times [\ (r_m \cos\beta_m \cos\phi_m) \times (r_m \cos\beta_m) \\ &\qquad -(0) \times (-r_m \sin\beta_m \sin\phi_m)] \\ &\quad -(-r_m \cos\beta_m \sin\phi_m) \times [\ (\cos\beta_m \sin\phi_m) \times (r_m \cos\beta_m) \\ &\qquad -(\sin\beta_m) \times (-r_m \sin\beta_m \sin\phi_m)] \\ &\quad +(-r_m \sin\beta_m \cos\phi_m) \times [\ (\cos\beta_m \sin\phi_m) \times (0) \\ &\qquad -(\sin\beta_m) \times (r_m \cos\beta_m \cos\phi_m)] \Big]^{-1} \end{aligned}$$

Eq (A.6)

$$\begin{aligned} &J\left(\mathrm{x_m}, \mathrm{y_m}, \mathrm{z_m}\right) = \\ &\Big[(\cos\beta_m \cos\phi_m) \times [\ (r_m^2 \cos^2\beta_m \cos\phi_m)] \\ &\quad +(r_m \cos\beta_m \sin\phi_m) \times \big[\ (r_m \cos^2\beta_m \sin\phi_m) + (r_m \sin^2\beta_m \sin\phi_m)\big] \\ &\qquad +(r_m \sin\beta_m \cos\phi_m) \times [(r_m \sin\beta_m \cos\beta_m \cos\phi_m)] \Big]^{-1} \end{aligned}$$

Eq (A.7)

$$\begin{aligned} &J\left(\mathrm{x_m}, \mathrm{y_m}, \mathrm{z_m}\right) = \\ &\Big[(r_m^2 \cos^3\beta_m \cos^2\phi_m) + (r_m^2 \cos^3\beta_m \sin^2\phi_m) \\ &\qquad +(r_m^2 \sin^2\beta_m \sin^2\phi_m \cos\beta_m) + (r_m^2 \sin^2\beta_m \cos^2\phi_m \cos\beta_m)\Big]^{-1} \end{aligned}$$

Eq (A.8)

$$J\left(\mathrm{x_m}, \mathrm{y_m}, \mathrm{z_m}\right) = \left[r_m^2 \cos^3\beta_m(\cos^2\phi_m + \sin^2\phi_m) + r_m^2 \cos\beta_m \sin^2\beta_m(\cos^2\phi_m + \sin^2\phi_m)\right]^{-1}$$

Eq (A.9)

The simplified solution can be expressed as,

$$J\left(\mathrm{x_m}, \mathrm{y_m}, \mathrm{z_m}\right) = \frac{1}{r_m^2 \cos\beta_m} \qquad \textit{Eq (A.10)}$$

A.2 Handover Delay

The power level of received signals at MS from serving cell (i.e., BS1) and adjacent candidate cell (i.e., BS2) are

$$p_{r,1}(d_{1,n}) = K_1 - K_2 \log_{10}(d_{1,n}) \qquad \textit{Eq (A.11)}$$

$$p_{r,2}(d_{2,n}) = K_1 - K_2 \log_{10}(d_{2,n}) \qquad \textit{Eq (A.12)}$$

where, $d_{1,n}$ and $d_{2,n}$ are given in *Eq (6.8)* and *Eq (6.9)*, respectively. The residual power ratio of the i^{th} candidate BS can be found as

$$q_i = p_{a,i} - p_{a,1} \qquad \textit{Eq (A.13)}$$

By assuming $p_{a,i}$ as, $p_{a,i} \cong p_{r,i}$, *Eq (A.13)* can be rearranged as,

$$q_2 = \Big(K_1 - K_2 \log_{10}\Big(\sqrt{d_1^2 + g^2 + 2\ d_1\ g\ \cos(\pi - \Psi_1 - \theta_{HO})}\Big)\Big) - \Big(K_1 - K_2 \log_{10}\Big(\sqrt{d_2^2 + g^2 + 2\ d_2\ g\ \cos(\Psi_2 - \theta_{HO})}\Big)\Big) \qquad \textit{Eq (A.14)}$$

where, g is the distance traveled by MS with a certain velocity from its initial position 'R' to the point 'N' where it completes the handover (refer Fig. 6.2). The transition from $p_{a,i}$ to $p_{r,i}$ requires an addition of certain time delay τ_{avg} which depends upon the used averaging scheme. Such delay has been computed in literature [53]. After simplifications, the above equation can be rearranged as,

$$q_2 = \frac{K_2}{2}\Big(\log_{10}\big(d_2^2 + g^2 + 2\ d_2\ g\ \cos(\Psi_2 - \theta_{HO})\big) - \log_{10}\big(d_1^2 + g^2 + 2\ d_1\ g\ \cos(\Psi_1 + \theta_{HO})\big)\Big) \qquad \textit{Eq (A.15)}$$

By rearranging *Eq (A.15)* for g, the simplified solution can be expressed as,

$$g = \frac{1}{10^{2q_2/K2} - 1}\Bigg(10^{2q_2/K_2} d_2 \cos(\Psi_2 - \theta_{\text{HO}}) + d_1 \cos(\alpha_1 + \theta_{\text{HO}}) + \frac{1}{2}\Big(-4\big(10^{2q_2/K_2} - 1\big)\big(10^{2q_2/K_2} d_2^2 - d_1^2\big) + 4\big(10^{2q_2/k_2} d_2 \cos(\Psi_2 - \theta_{\text{HO}}) + d_1 \cos(\Psi_1 + \theta_{\text{HO}})\big)^2\Big)^{1/2}\Bigg) \qquad \textit{Eq (A.16)}$$

REFERENCES

[1] N. M. Khan, "Modeling and characterization of multipath fading channels in cellular mobile communication systems," Ph.D. dissertation, University of New South Wales, 2006.

[2] T. S. Rappaport, *Wireless communications: principles and practice.* Prentice Hall PTR, 1996, vol. 207.

[3] N. J. Boucher, *The cellular radio handbook: a reference for cellular system operation*, ser. Gestión Turística. Wiley, 2001. [Online]. Available: http://books.google.com.pk/books?id=iwpTAAAAMAAJ

[4] T. Farley, "Mobile telephone history," *Telektronikk*, vol. 101, no. 3, pp. 22–34, 2005.

[5] T. E. Bell, J. A. Adam, and S. J. Lowe, "Communications," *IEEE Spectrum*, vol. 33, no. 1, pp. 30–41, Jan. 1996.

[6] P. Stavroulakis, *Third generation mobile telecommunication systems: UMTS and IMT-2000*, ser. Engineering online library. Springer, 2001. [Online]. Available: http://books.google.com.pk/books?id=z39Bqp-0BgQC

[7] H. Kaaranen, *UMTS networks: architecture, mobility, and services.* J. Wiley, 2005. [Online]. Available: http://books.google.com.pk/books?id=cmserrFfemcC

[8] M. R. Karim and M. Sarraf, *W-CDMA and CDMA2000 for 3G mobile networks*, ser. McGraw-Hill telecom professional. McGraw-Hill, 2002. [Online]. Available: http://books.google.com.pk/books?id=4kk37Qm8OQwC

[9] M. Rumney, *LTE and the Evolution to 4G Wireless: Design and Measurement Challenges.* J. Wiley & Sons, 2009. [Online]. Available: http://books.google.com.pk/books?id=boePyryvxRAC

[10] S. Sesia, I. Toufik, and M. Baker, *LTE - The UMTS Long Term Evolution: From Theory to Practice.* J. Wiley & Sons, 2011. [Online]. Available: http://books.google.com.pk/books?id=beIaPXLzYKcC

[11] G. D. Durgin and T. S. Rappaport, "Effects of multipath angular spread on the spatial cross-correlation of received voltage envelopes," in *proc. of IEEE, 49th Veh. Technol. Conf.*, vol. 2, Jul. 1999, pp. 996–1000.

[12] ——, "Theory of multipath shape factors for small-scale fading wireless channels," *IEEE Trans. on Antennas and Propag.*, vol. 48, no. 5, pp. 682–693, May 2000.

[13] N. M. Khan, M. T. Simsim, and P. B. Rapajic, "A generalized model for the spatial characteristics of the cellular mobile channel," *IEEE Trans. on Veh. Technol.*, vol. 57, no. 1, pp. 22–37, Jan. 2008.

[14] J. C. Liberti and T. S. Rappaport, "A geometrically based model for line of sight multipath radio channels," in *proc. of IEEE, 46th Veh. Technol. Conf.*, vol. 2, Apr.-May 1996, pp. 844–848.

[15] R. B. Ertel and J. H. Reed, "Angle and time of arrival statistics for circular and elliptical scattering models," *IEEE J. on Selected Areas in Commun.*, vol. 17, no. 11, pp. 1829–1840, Nov. 1999.

[16] S. S. Mahmoud, F. S. Al-Qahtani, Z. M. Hussain, and A. Gopalakrishnan, "Spatial and temporal statistics for the geometrical-based hyperbolic macrocell channel model," *Digital Signal Process.*, vol. 18, no. 2, pp. 151–167, Mar. 2008.

[17] M. T. Simsim, N. M. Khan, R. Ramer, and P. B. Rapajic, "Time of arrival statistics in cellular environments," in *proc. of IEEE, 63rd Veh. Technol. Conf.*, vol. 6, May 2006, pp. 2666–2670.

[18] I. Jaafar, H. Boujemaa, and M. Siala, "Angle and time of arrival statistics for hollow-disc and elliptical scattering models," in *proc. of 2nd Int. Conf. on Signals, Circuits and Systems*, Nov. 2008, pp. 1–4.

[19] R. Janaswamy, "Angle and time of arrival statistics for the Gaussian scatter density model," *IEEE Trans. on Wireless Commun.*, vol. 1, no. 3, pp. 488–497, Jul. 2002.

[20] K. N. Le, "On angle-of-arrival and time-of-arrival statistics of geometric scattering channels," *IEEE Trans. on Veh. Technol.*, vol. 58, no. 8, pp. 4257–4264, Oct. 2009.

[21] S. Qu and T. Yeap, "A three-dimensional scattering model for fading channels in landmobile environment," *IEEE Trans. on Veh. Technol.*, vol. 48, no. 3, pp. 765–781, May 1999.

[22] R. Janaswamy, "Angle of arrival statistics for a 3-D spheroid model," *IEEE Trnas. on Veh. Technol.*, vol. 51, no. 5, pp. 1242–1247, Sep. 2002.

[23] A. Y. Olenko, K. T. Wong, S. A. Qasmi, and J. Ahmadi-Shokouh, "Analytically derived uplink/downlink ToA and 2-d DoA distributions with scatterers in a 3-D hemispheroid surrounding the mobile," *IEEE Trnas. on Antenna and Propag.*, vol. 54, no. 9, pp. 2446–2454, Sep. 2006.

[24] K. B. Baltzis and J. N. Sahalos, "A simple 3-D geometric channel model for macrocell mobile communication," *Wireless Pers. Commun.*, vol. 51, no. 2, pp. 329–347, Oct. 2009.

[25] M. Alsehaili, A. Sebak, and S. Noghanian, "A 3-D geometrically based ellipsoidal wireless channel model," in *proc. of 12th Int. Symp. on Antenna Technol. and Applied Electromagnetics*, Jul. 2006, pp. 407–410.

[26] P. Petrus, J. H. Reed, and T. S. Rappaport, "Geometrical-based statistical macrocell channel model for mobile environments," *IEEE Trans. on Commun.*, vol. 50, no. 3, pp. 495–502, Mar. 2002.

[27] M. P. Lotter and P. V. Rooyen, "Modeling spatial aspects of cellular CDMA/SDMA systems," *IEEE Commun. Lett.*, vol. 3, no. 5, pp. 128–131, May 1999.

[28] C. A. Lopez, D. H. Covarrubias, D. Munoz, and M. A. Panduro, "Statistical cellular Gaussian scatter density channel model employing a directional antenna for mobile environments," *AEU - Int. J. of Electronics and Commun.*, vol. 59, no. 3, pp. 195–199, Jun. 2005.

[29] B. H. Qureshi, S. Iqbal, and N. M. Khan, "Effect of directional antennas at both ends of the link on spatial characteristics of cellular and mobile channel," in *proc. of 5th IEEE Int. Conf. on Emerging Technol.*, Oct. 2009, pp. 87–93.

[30] S. Iqbal, B. H. Qureshi, and N. M. Khan, "Effect of directional antennas at both ends of the radio link on the Doppler power spectrum," in *IEEE 13th Int. Multitopic Conf.*, vol. 1, Dec. 2009, pp. 1–4.

[31] A. S. Glassner, *An Introduction to ray tracing*, ser. Morgan Kaufmann Series in Computer Graphics and Geometric Modeling. Academic Press, 1989. [Online]. Available: http://books.google.com.pk/books?id=YPblYyLqBM4C

[32] P. Beckmann and A. Spizzichino, "The scattering of electromagnetic waves from rough surfaces," *Norwood, MA, Artech House, Inc., 1987, 511 p.*, vol. 1, 1987, provided by the SAO/NASA Astrophysics Data System. [Online]. Available: http://adsabs.harvard.edu/abs/1987ah...book.....B

[33] L. Tsang, J. A. Kong, K. H. Ding, and C. O. Ao, *Scattering of Electromagnetic Waves*. Wiley Online Library, 2000. [Online]. Available: http://books.google.com.pk/books?id=sNiz4y9Ss8MC

[34] S. S. Mahmoud, Z. M. Hussain, and P. O'Shea, "Properties of the hyperbolic macrocell channel model: path power and Doppler shift statistics," in *proc. of Australian Telecommun. Networks and Applications Conf.,*, Dec. 2003.

[35] ——, "A geometrical-based microcell mobile radio channel model," *Wireless Networks*, vol. 12, no. 5, pp. 653–664, 2006.

[36] Q. Yao and M. Patzold, "Spatial-temporal characteristics of a halfspheroid model and its corresponding simulation model," in *proc. of IEEE Veh. Technol. Conf.*, vol. 1, 2004, pp. 147–151.

[37] A. Y. Olenko, K. T. Wong, and E. H.-O. Ng, "Analytically derived TOA-DOA statistics of uplink/downlink wireless multipaths arisen from scatterers on an hollow-disc around the mobile," *IEEE Antennas and Wireless Propag. Lett.*, vol. 2, pp. 345–348, 2003.

[38] S. J. Nawaz, B. H. Qureshi, N. M. Khan, and M. Abdel-Maguid, "Effect of directional antenna on the spatial characteristics of 3-D macrocell environment," in *proc. of 2nd Int. Conf. on Future Computer and Commun.*, vol. 1, May 2010, pp. 552–556.

[39] A. Y. Olenko, K. T. Wong, and S. A. Qasmi, "Distribution of bad urban uplink multipaths' arrival delay & azimuth-elevation arrival angles, with scatterers distributed cylindrically above the mobile," in *proc. of IEEE, Global Telecommun. Conf. (GLOBECOM'06).* IEEE, 2006, pp. 1–6.

[40] A. Y. Olenko, S. A. Qasmi, and K. T. Wong, "bad urban uplink multipaths distribution in azimuth-elevation DOA, with scatterers modeled as inside a cylinder above the mobile & as more sparse with height," in *proc. of IEEE, Region 10 Conf., TENCON.* IEEE, 2007, pp. 1–4.

[41] M. Alsehaili and A. R. S. S. Noghanian, "An improved 3-D geometric scattering channel model for wireless communication systems," in *proc. of Int. URSI Commission B - Electromagnetic Theory Symp.*, Jul. 2007, pp. 1–3.

[42] R. Ertel and J. H. Reed, "Impact of path-loss on the Doppler spectrum for the geometrically based single bounce vector channel models," in *proc. of 48th IEEE Veh. Technol. Conf.*, vol. 1, May 1998, pp. 586–590.

[43] S. J. Nawaz, B. H. Qureshi, and N. M. Khan, "Angle of arrival statistics for 3-D macrocell environment using directional antenna at BS," in *proc. of 13th IEEE Int. Multitopic Conf.*, Dec. 2009, pp. 1–5.

[44] S. Kong, "TOA and AOD statistics for down link Gaussian scatterer distribution model," *IEEE Trans. on Wireless Commun.*, vol. 8, no. 5, pp. 2609–2617, May 2009.

[45] S. J. Nawaz, M. N. Patwary, N. M. Khan, and H. Yu, "3-D Gaussian scatter density propagation model employing a directional antenna at BS," in *proc. of Adv. satellite multimedia systems conf. and the 11th signal Process. for space commun. workshop*, Sep. 2010, pp. 395–400.

[46] S. S. Mahmoud, Z. M. Hussain, and P. O'Shea, "A space-time model for mobile radio channel with hyperbolically distributed scatterers," *IEEE Antennas and Wireless Propag. Letters*, vol. 1, pp. 211–214, 2002.

[47] M. Castrellon, D. Munoz, C. Vargas, C. A. Lopez, and D. Covarrubias, "Doppler spread for Gaussian scatter density environments employing smart antennas," *AEU - Int. J. of Electronics and Commun.*, vol. 61, no. 9, pp. 631–636, Oct. 2007.

[48] S. J. Nawaz, B. H. Qureshi, and N. M. Khan, "A generalized 3-D scattering model for macrocell environment with directional antenna at BS," *IEEE Trans. on Veh. Technol.*, vol. 59, no. 7, pp. 3193–3204, Sep. 2010.

[49] R. J. Piechocki, G. V. Tsoulos, and J. P. McGeehan, "Simple general formula for PDF of angle of arrival in large cell operational environments," *IEE Electron. Lett.*, vol. 34, no. 18, pp. 1784–1785, Sep. 1998.

[50] W. C. Jakes, *Microwave Mobile Communications*. New York: Wiley, 1974. [Online]. Available: http://books.google.com.pk/books?id=mfKgSgAACAAJ

[51] R. H. Clarke, "A statistical theory of mobile radio reception," *Bell Syst. Technol. J.*, vol. 47, no. 6, pp. 957–1000, Jul. 1968.

[52] S. Qu, "An analysis of probability distribution of Doppler shift in three-dimensional mobile radio environments," *IEEE Trans. on Veh. Technol.*, vol. 58, no. 4, pp. 1634–1639, May 2009.

[53] M. Emmelmann, "Influence of velocity on the handover delay associated with a radio-signal-measurement-based handover decision," Telecommunication Networks Group, Technical University Berlin, Technical Report TKN-05-003 Rev. 2, Apr. 2005.

[54] M. Austin and G. Stuber, "Velocity adaptive handoff algorithms for microcellular systems," *IEEE Trans. Veh. Technol.*, vol. 43, no. 3, pp. 549–561, Apr. 1994.

[55] M. Zonoozi and P. Dassanayake, "Handover delay in cellular systems," in *proc. of, IEEE Int. Conf. on Personal Wireless Commun.*, Dec. 1997, pp. 24–27.

[56] A. Murase, I. Symington, and E. Green, "Handover criterion for marcro and microcellular systems," in *proc. of, IEEE Veh. Technol. Conf.*, May 1991, pp. 542–530.

[57] H. M. Altwelib, "Vertical handover scheme for next generation mobile networks," Ph.D. dissertation, Faculty of Engineering, Electrical and a Computer Department, University of AL-Mergib, May 2007.

[58] B. Liu, J. Wang, and J. Li, "A joint vertical handover technique for heterogeneous wireless networks," in *proc. of IEEE, Int. Conf. on Comp. Science Education*, vol. 1, Jul. 2009, pp. 227–232.

[59] S. Lee, K. Sriram, K. Kim, Y. H. Kim, and N. Golmie, "Vertical handoff decision algorithms for providing optimized performance in heterogeneous wireless networks," *IEEE Trans. Veh. Technol.*, vol. 58, no. 2, pp. 865–881, Feb. 2009.

[60] R. Kumar and B. Singh, "Comparison of vertical handover mechanisms using generic QoS trigger for next generation network," *Int. J. of Next-Generation Networks*, vol. 2, no. 3, pp. 80–97, Sep. 2010.

[61] D. Sarddar, T. Jana, S. K. Saha, J. Banerjee, U. Biswas, and M. K. Naskar, "Minimization of handoff failure probability for next-generation wireless systems," *Int. J. of Next-Generation Networks*, vol. 2, no. 2, pp. 36–51, Jun. 2010.

[62] J. Hämäläinen, "Optimizing handover performance in LTE networks containing relays," Master's thesis, School of Electrical Engineering, Aalto University, 2011.

[63] M. Emmelmann, "Influence of velocity on the handover delay associated with a radio-signal-measurement-based handover decision," in *proc. of, IEEE Veh. Technol. Conf.*, vol. 4, Jan. 2005, pp. 2282–2286.

[64] S. S. Mahmoud, Z. M. Hussain, and P. O'Shea, "Doppler spectrum analysis for the hyperbolic macrocell channel model," in *proc. of Int. Conf. on Electronics, Control and Signal Process.* World Scientific and Engineering Academy and Society (WSEAS), 2003, pp. 1–7.

[65] A. J. Berni, "Angle-of-arrival estimation using an adaptive antenna array," *IEEE Trans. on Aerospace and Electronic Systems*, vol. 11, no. 2, pp. 278–284, Mar. 1975.

[66] S. Applebaum, "Adaptive arrays," *IEEE Trans. on Antennas and Propag.*, vol. 24, no. 5, pp. 585–598, Sep. 1976.

[67] J. Laurila, K. Kalliola, M. Toeltsch, K. Hugl, P. Vainikainen, and E. Bonek, "Wideband 3-D characterization of mobile radio channels in urban environment," *IEEE Trans. on Antennas and Propag.*, vol. 50, no. 2, pp. 233–243, Feb. 2002.

[68] N. Blaunstein, M. Toeltsch, C. G. Christodoulou, J. Laurila, Tsalolihin, E. Bonek, P. Vainikainen, N. Tsouri, K. Kalliola, and H. Laitinen, "Azimuth, elevation, and time-delay distributions in wireless communication channels," *IEEE Antennas and Propag. Magazine*, vol. 48, no. 1, pp. 160–167, Feb. 2006.

[69] M. Toeltsch, J. Laurila, K. Kalliola, A. F. Molisch, P. Vainikainen, and E. Bonek, "Statistical characterization of urban spatial radio channels," *IEEE J. on Selected Areas in Commun.*, vol. 20, no. 3, pp. 539 –549, Apr. 2002.

[70] K. I. Pedersen, P. E. Mogensen, and B. H. Fleury, "A stochastic model of the temporal and azimuthal dispersion seen at the base station in outdoor propagation environments," *IEEE Trans. on Veh. Technol.*, vol. 49, no. 2, pp. 437–447, Mar. 2000.

[71] S. J. Nawaz, N. M. Khan, M. N. Patwary, and M. Moniri, "Effect of directional antenna on the Doppler spectrum in 3-D mobile radio propagation environment," *IEEE Trans. on Veh. Technol.*, vol. 60, no. 7, pp. 2895–2903, Sep. 2011.

[72] Q. A. Zeng and D. P. Agrawal, "Handoff in wireless mobile networks," *Handbook of wireless networks and mobile computing*, pp. 1–25, 2002.

[73] M. Emmelmann, "Influence of velocity on the handover delay associated with a radio-signal-measurement-based handover decision," in *proc. of IEEE, 62nd Veh. Technol. Conf.*, vol. 4, Jan. 2005, pp. 2282–2286.

[74] N. D. Tripathi, J. H. Reed, and H. F. VanLandinoham, "Handoff in cellular systems," *IEEE Personal Commun.*, vol. 5, no. 6, pp. 26–37, Dec. 1998.

[75] S. Qureshi, S. J. Nawaz, M. Patwary, M. Abdel-Maguid, and A. Kamar, "The impact of propagation environment and velocity on the handover performance of LTE systems," in *proc. of 2010 Int. Conf. on Wireless Commun. and Signal Processing*, Oct. 2010, pp. 1–5.

[76] J. B. Andersen, T. S. Rappaport, and S. Yoshida, "Propagation measurements and models for wireless communications channels," *IEEE Commun. Magazine*, vol. 33, no. 1, pp. 42–49, Jan. 1995.

[77] A. Aguiar and J. Gross, "Wireless channel models," Technical University of Berlin - Telecommunication Networks Group, Tech. Rep. TKN-03-007, Tech. Rep., Apr. 2003.

[78] N. Zheng and J. Wigard, "On the performance of integrator handover algorithm in LTE networks," in *proc. of IEEE, 68th Veh. Technol. Conf.*, Oct. 2008, pp. 1–5.

[79] M. Anas, F. D. Calabrese, P. E. Mogensen, C. Rosa, and K. I. Pedersen, "Performance evaluation of received signal strength based hard handover for UTRAN LTE," in *proc. of IEEE 65th Veh. Technol. Conf.*, May. 2007, pp. 1046–1050.

[80] J. Hamalainen, S. Savolainen, R. Wichman, K. Ruotsalainen, and J. Ylitalo, "On the solution of scatter density in geometry-based channel models," *IEEE Trans. on Wireless Commun.*, vol. 6, no. 3, pp. 1054–1062, Mar. 2007.